Isogeometric Finite Element Code Development for Analysis of Laminated Composites Structures

Hitesh Kapoor

Dissertation submitted to the Faculty of the

Virginia Polytechnic Institute and State University

in partial fulfillment of the requirements for the degree of

Doctor of Philosophy

in

Aerospace Engineering

Rakesh K. Kapania, Chair

Stephen B. Clay

Michael K. Philen

Romesh C. Batra

$30^{th} January, 2013$

Blacksburg, Virginia

Keywords: Nurbs Isogeometric analysis, k-refinement procedure, shear-deformable plates and beams, nonlinear analysis, interlaminar stress analysis, dynamic and eigenvalue analysis, a plate with a hole

Isogeometric Finite Element Code Development for Analysis of Laminated Composites Structures

Hitesh Kapoor

(ABSTRACT)

This research endeavor develops Isogeometric approach for analysis of composite structures and take advantage of higher order continuity, smoothness and variation diminishing property of Nurbs basis for stress analysis of composite and sandwich beams and plates. This research also computes stress concentration factor in a composite plate with a hole.

Nurbs Isogeometric nonlinear/linear finite element code is developed for static and dynamic analysis of laminated composite plates. Nurbs linear, quadratic, higher-order and k-refined elements in Isogeometric framework are constructed using various refinement procedures and validated with numerical testing. Nurbs post-processor is developed for in-plane and interlaminar stress calculation in laminated composite and sandwich plates. Nurbs post-processor is found to be superior than regular finite element and in good agreement with the literature. Nurbs Isgoemetric analysis is used for stress analysis of laminated composite plate with open-hole. Stress concentration factor is computed along the hole edge and good agreement is obtained with the literature. Nurbs Isogeometric finite element code for free-vibration and linear dynamics analysis of laminated composite plates also obtain good agreement with the literature.

Contents

List of Figures

List of Tables

Chapter 1

Introduction

1.1 Finite element and Isogeometric Analysis

1.1.1 Finite Element Analysis

Finite element methods, in general, use a variational formulation where trial and weight functions are defined by their basis functions. These basis functions are used for local representation of the field variables and finite element divide the domain into simple spaces. Most widely used finite element, the linear triangle, was formulated by Courant [1] in 1943. Similarly, the bi-linear quadrilateral was proposed by Zienkiewicz [2] and Taig [3]. Zienkiewicz et al. [4] developed an eight node serendipity quadrilateral element. Thin plate and shell bending analysis require C_1-continuous interpolation scheme due to square integrability of generalized second order derivatives. Reissener-Mindlin bending element requires only C_0

continuity and therefore, circumvents the problem in thin plate and bending analysis.

CAD based functions are increasingly used for solving mechanics problems. They offer great advantage over the regular finite element due to their piecewise form, smoothness and higher-order continuity. Besides that, these functions offer computational efficiency, good accuracy and convergence characteristics. CAE industry widely uses Nurbs (Non-uniform rational B-splines) to describe the smooth lines and surfaces. The curve or surface generated using Nurbs depends on control points, which do not belong to the curve or surface, and weight functions. The complexity of shape defines the number of control points required for exact representation of the geometry. On the other hand, the beam, plate or shell analysis based on the finite element discretization involve nodes whose number also depend on the complexity of structure. CAD basis functions **like** Nurbs, Splines, Bezier curves, if applied directly for beam, plate and shell analysis, are advantageous from the point of view that complex shapes require less number of control points.

B-splines were first introduced by Schoenberg [5] in order to develop piecewise polynomials with smoothness properties. De Boor [6] introduced a stable recursion formula for evaluating B-splines basis and their derivatives. Gontier and Vollmer [7] used Bezier basis functions for nonlinear analysis of planar beams. They showed that a fewer number of control points were required for nonlinear analysis of straight beams than required in finite element analysis. Kagan, Fisher and Bar [8] developed B-spline finite element analysis and integrated with geometric design. Same authors [9] included adaptive refinement like hp and h-refinement techniques in the their finite element code. Ganapathi et al. [10] developed a shear flexible

curved B-spline beam element. They used a field consistency approach (i.e. consistency of membrane/shear strain fields to obtain the optimal membrane/shear strain functions to eliminate the shear-locking phenomenon.

1.1.2 Meshless Methods

The finite element method is the most widely used method for solving complex problems. It offers versatility in solving problems with complex geometries where discretization error can be reduced by decreasing the element size. However, the lower order polynomial approximation still leads to inaccuracies in geometric representation and mesh generation results in higher computational cost. Besides, finite element method has difficulties in solving problems involving large deformation with severe element distortions, problems involving crack growth where arbitrary and complex paths do not coincide with the original element interfaces and problems involving material fragmentation. And, beam, plate and shell analysis require higher-order continuity at the inter-element boundary. Therefore, an alternative, mesh-free approach, seems to be an interesting choice. Meshfree methods are advantageous from the point of view that they do not require topological generation and provide smooth approximation over the domain. However, high computational cost of meshfree method is contributed to the interpolation and numerical integration. Various meshfree methods have been developed in recent past, namely, reproducing kernel particle method (RKPM)[11], meshless local Petrov-Galerkin method (MLPG) [12, 13], partition of unity method (PUM) [14, 15], element-free Galerkin method (EFG) [16, 17, 18], and point interpolation method

[19].

1.1.3 Isogeometric Analysis

In-spite of the extensive use of finite element methods, the barriers between engineering design and analysis still exist and the way to bridge the gap is to reconstitute the entire process. The geometric approximations in finite element could lead to significant errors and difficulties, for example, in case of plate with the holes and sharp corners. In order to improve upon geometry discretization errors is to use Isogeometric analysis approach introduced by T. J. R. Hughes. There are several CAD functions which can be used for CAD representation of analysis module. Of most widely used CAD basis in engineering design process are Nurbs as presented by Piegle and Tiller [20], Farin [21], Cohen et al. [22] and Rogers [23]. Nurbs represent a billion dollar CAE industry and are useful for analysis purposes because they possess useful mathematical property of refinement through knot insertion and variational diminishing property of convex hull. There are other computational geometry technologies that can be utilized as the basis for Isogeometric analysis such as sub-division surface by Peters [24] and Warren [25], Gordon patches [26], Greogory patch [27], S-patch [28] and A-patch [29] etc.

Hughes, Cottrell and Bzilevs [30] introduced the idea of Isogeometric analysis using Nurbs. They used Nurbs to exactly represent the CAD geometry and then, constructed a coarse mesh for the analysis. The idea behind Isogeometric analysis is to model the geometry ex-

actly which also serves the basis for the solution space i.e. invoking isoparametric concept. Similarly, Hughes et al. studied structural dynamics and wave propagation [31] and fluid structure interaction [32] using Isogeometric analysis. Cottrell et al. [33] studied vibration problem using Isogeometric analysis. Vuong et al. [34] developed a matlab code for Isogeometric analysis.

1.1.4 Laminated Composite Plate Theories

Advance multi-layered composite and sandwich plate/shell structures are being increasingly used in aerospace, shipbuilding, bridge and other industries. These structures have smaller thickness as compared to other dimensions and therefore, are often subjected to large deformation behavior under external loads. For accurate prediction of large displacement behavior, geometric nonlinear analysis is very important and development of computationally efficient geometric nonlinear finite element code for composite plates has been a topic of considerable interest. The plate theories for laminated composites can be categorized into equivalent single-layer theories (ELS) and layerwise theories. Equivalent single layer theories namely, classical, first-order and higher-order shear deformation theories, are derived from their 3D counterpart (i.e. layerwise and 3D elasticity) by making appropriate assumptions to the state of strain/stress in the thickness direction, reducing 3D continuum problem to a 2D problem.

Several articles are available in literature on shear deformation theories. Reissner-Mindlin

theory [35]-[37] (first-order shear deformation theory) assumes constant state of through the thickness strain and requires only C_0 interpolation functions to satisfy the continuity requirement. This theory was further extended for anisotropic plates by Whitney and Pagano [38]. Urthaler and Reddy [39] developed a mixed finite element for bending analysis of laminated composite plates using FSDT. They treated bending moment as a field variable along with displacement and rotation.

In higher-order shear deformation theories (HSDT), Putcha and Reddy [40] developed a mixed finite element approach with 9-node Lagrangian(L) quadrilateral element. Kant and Kommineni(1992) [41] developed refined HSDT with 9-node quadrilateral(L) element for linear and nonlinear finite element analysis of laminated composite and sandwich plates. Polit and Touratier [42] studied large deflection behavior using triangular element. Comparing higher-order theories and FSDT, higher-order plate theories enhances the accuracy of the solution slightly but are computationally more expensive, especially for nonlinear analysis and require C_1 continuity. Robbins and Reddy [43] reviewed various ELS and layerwise theories for laminated composite plates. On the other hand, FSDT has often been used due to its simplicity and provides best compromise between economy and accuracy in predicting the response of thin to moderately thick laminates [44]-[45].

1.1.5 Shear-Locking and Hourglass Stabilization

During the last few decades, many researchers have made significant contribution to the development of efficient lower order finite elements based on FSDT. Lower order elements suffer from shear locking problems as thickness to span ratio becomes too small. Zienkiewicz et al. [46] and Hughes et al. [47] used reduced or selective integration techniques to solve the shear locking problem. MacNeal [48], first, developed assumed strain method where he computed shear strain using kinematic variables at discrete collocation points of the element other than nodes. Modified versions of this method were successfully proposed by various researchers such as Bathe and Dvorkin [49], discrete shear elements [50] and linked interpolation elements by Zienkewicz et al. [51]. Braess, Ming and Shi [52] used enhanced assumed strain method to counter shear-locking phenomenon.

Discrete Shear Gap (DSG) method improves shear locking behavior by invoking Kirchhoff constraints on the element nodes. Echter and Bischoff [53] studied locking and unlocking of Nurbs finite element using discrete shear gap (DSG) method. Zhang and Kim [54] proposed a locking-free quadrilateral plate element for geometric nonlinear analysis of laminated composite plate. Similarly, Minighini, Tullini and Laudiero [55] developed a locking-free finite element for shear deformable orthotropic thin-walled beams. Nguyen et al. [56] developed a smoothed finite element for plate analysis. They incorporated strain smoothing stabilzation to develop a locking-free plate element. Cai et al. [57] developed a new shear locking-free triangular plate element with 6 extra degrees of freedom for linear problems. The additional degrees of freedom account for rotations caused by transverse shear deformation. Their el-

ement removed shear locking without extra numerical efforts such as reduced integration, assumed strain/stress or need for stabilization of zero energy modes.

Shear locking is accompanied with hourglass instability due to reduced integration, thus, requires stabilization control [58], [59] and [60]. Flanagan and Belytchsko [61] formulated hourglass control for reduced integration plate element and Tessler and Hughes [62] derived a plate element which performed well without stabilization. Reddy and Phan [63]'s special third order theory (STTR) was used for developing displacement based finite element and similarly, Ren and Hinton [64] developed a third order plate theory but these required C_1 continuity for transverse displacement. Codina [65] and Lyly [66] developed a stable first-order shear deformable plate finite element which was insensitive to mesh distortion.

1.1.6 Interlaminar Stress Calculations

It is a well known fact that composites are prone to damage under low transverse loads due to comparatively low transverse modulus and have higher probability of failure. The failure or damage is generally, initiated due to a variety of failure modes like delamination, matrix cracking, fiber failure etc; delamination being the primary mode of failure. Delamination is initiated when interlaminar stresses attain maximum interfacial strength. Therefore, predicting through-the-thickness stresses accurately is essential. This requires calculating higher-order derivatives of in-plane stresses accurately which in turn requires higher-order displacement derivatives. Lagrange polynomial start to oscillate as the order of polynomial

is increased (Gibbs phenomenon), therefore, are not adequate to calculate transverse stresses accurately and efficiently.

The first order shear deformation theory with the use of constitutive relation produces highly inaccurate interlaminar stresses exhibiting non-physical discontinuity at the ply interface of composite laminate. Accuracy of interlaminar stresses, using 3D equilibrium equations, in the context of finite element analysis depends upon the computation of higher order in-plane strain gradients which is generally poor as Lagrange polynomial gradient oscillates. Tessler [67] developed smoothing variational formulation which combined discrete least square and penalty constraints functional in a single variational form and recovered the stress gradients more accurately. Reddy [68] calculated the transverse shear stresses using the derivative of in-plane stresses that were obtained by differentiating the interpolation functions in finite element approximation. In order to accurately predict delamination, the interlaminar normal stress is as important as the shear stress. The computation of interlaminar normal stress requires an additional derivative of the basis function. These higher-order derivatives are not obtained directly in the finite element code. Byun and Kapania [69] developed a post-processing technique to overcome this drawback. They interpolated the finite element displacement data using polynomial functions like Chebyshev and orthogonal polynomials in a global domain. Use of Chebyshev polynomials require nodal displacement data to be available at some specific points *i.e.* Chebyshev points and can not interpolate the boundary edge nodal data while orthogonal polynomials use the arbitrarily distributed data points but are more difficult to obtain. Lee and Lee [70] introduced the non-iterative post processing

procedure for the recovery of transverse stresses. They followed the equilibrium based stress recovery method, using the one dimensional, least square finite element in the thickness direction.

Park and Kim [71] presented a predictor-corrector post-processing procedure for the accurate recovery of stresses and displacement in the multi-layered composite panels. The predictor only predicts the transverse shear stress while the corrector method enhances the accuracy of the displacement, in-plane and transverse normal stress in the thickness direction using the results of the predictor and finite element analysis. Park, Park, and Kim [72], later, used the nonlinear predictor-corrector method to obtain the stresses and displacement in composite panels in geometrically nonlinear formulation. Noor, Kim, and Peters [73] developed a computational procedure to get the transverse shear stresses in multi-layered composite panels. They first used the super convergent recovery technique to evaluate the in-plane stresses and then, used the piecewise integration in the thickness direction to obtain the interlaminar stresses.

Matsunaga [74] analyzed the displacement and stresses in laminated beams using global higher-order beam theory. Author expanded the displacement field variables with power series of z-coordinate. Makeev and Armanios [75] presented an iterative method to approximate analytical solution of elasticity problems in composite laminates. Rolfes and Rohwer [76] developed a method for calculating the improved transverse shear stresses in laminated composites using first-order shear-deformation theory. Kant and Manjunatha [77] developed numerical algorithms for accurate calculations of transverse stresses using higher-order shear-

deformation theories. They used direct integration, finite difference and exact surface fitting approach. Recently, Kant et al. [78] proposed a semi analytical model for the accurate estimation of stresses and displacement in composite and sandwich structures. The two-point boundary value problem governed by a set of linear first order differential equations through the thickness is solved using fourth-order Runge-Kutta method. Nosier and Bahrami [79] developed the analytical solution to study the edge effects in anti-symmetric angle-ply laminates using first order shear deformation and Reddy's layerwise theory. Senthil and Batra [80] discussed the analytical solution for thick laminated plates under sinusoidal loads. . [78] proposed a semi analytical model for the accurate estimation of stresses and displacement in composite and sandwich structures. The two-point boundary value problem governed by a set of linear first order differential equations through the thickness is solved using fourth-order Runge-Kutta method. Nosier and Bahrami [79] developed the analytical solution to study the edge effects in anti-symmetric angle-ply laminates using first order shear deformation and Reddy's layerwise theory. Senthil and Batra [80] discussed the analytical solution for thick laminated plates under sinusoidal loads.

Stress recovery is highly dependent on the structure of a particular element and on the formulation used in deriving elements. Stress recovery methods include interpolation-extrapolation from super-convergent points [81], L_2 projection [82], stress smoothing [83] and integral stress techniques [84]. Zienkeiwicz and Zhu [85] developed an efficient post-processing technique in terms of super-convergent patch recovery (SPR) procedure. A modified version of this technique was developed to obtain in-plane stresses at nodes and interlaminar stresses

using equilibrium equations [86]. Stress recovery procedures suffer from extraneous stress oscillations [87].

1.1.7 Free Edge Stress Calculations

Developing methods for analysis of composite laminates with curvilinear edges such as cut-outs is a significantly important research practice. Almost every aircraft structure contains stress concentration regions such as stiffeners and holes. Rivets and holes are basically part of structural joints. In laminated composites structures, presence of a hole introduces significant stress gradients in the vicinity of the hole, in addition to composite being more susceptible to failure due to low transverse modulus, inhomogeneity, and anisotropy. Many researchers have studied stress singularity problems in composite plate with a hole using different techniques such as, boundary layer method [88]-[89], anisotropic elasticity solution [90], linear finite element method [91], and spline variational method [93], 3D discrete layer FEM [92]-[94]. Atluri et al. [92] developed a special hole element for prediction of stress concentration around a hole in composite plate under in-plane load. Iarve [93] used spline variational three dimensional method for stress analysis in composite plate with open hole. Raju and Crews [94] performed three dimensional finite element analysis at hole edges in $(0/90)_s$ and $(-45/45)_s$ laminates. They used 20-node isoparametric brick element with highly refined mesh in the vicinity of a hole with approximately $20,000$ dofs. Folias [95] obtained a local asymptotic solution for three dimensional stress field in the vicinity of free edge of a hole. Bar-Yoseph and Avrashi [96] developed a sub-structuring approach around

the hole to capture the complete stress field. Pan et al. [97] performed stress analysis around a hole in composite plate under in-plane loading using 3D boundary element method.

1.1.8 Free Vibration and Linear Dynamics

Natural frequency determination play an important role in the design of structures in aerospace engineering applications. A dynamic study of these structures is essential in assessing their full potential. Vibration characteristics of laminated plates have been studied extensively in past and finite element method has been used to study vibration problem. Bert and Mohammad [99],[100] provide extensive literature on modal analysis of laminated composite plates. Song and Waas [101] conducted free vibration and buckling analysis by means of higher order beam model. In recent years, mesh-free methods have become an alternative for vibration analysis including element-free Galerkin method [102], the moving least square differential quadrature method [103] and the radial basis function method [104]. Liu et al. [105]-[106] proposed a new smoothed finite element method where strain smoothing technique of stabilized conforming nodal integration mesh-free method was incorporated into existing FEM for 2D elastic problems. Kapania and Raciti [107] did literature survey for the shear-deformation theories and buckling of laminated composite beams and plates. They [108], also, reviewed advances in the vibration and wave propagation analysis of laminated beams and plates.

Chapter 2

Interlaminar Stress Calculation in Composite and Sandwich Beams

This chapter details the development of Nurbs based element-free Galerkin method which utilizes non-oscillatory nature of higher-order Nurbs basis function and its derivatives to compute interlaminar normal stress in composite and sandwich beams, accurately and efficiently. This avoids the extra step in post-processing, generally, required in regular finite element formulation. Element-free Galerkin formulation is derived for the first order shear deformable multi-layered composite and sandwich beams. Nurbs basis are derived using recursion formulation. The displacement and its higher derivatives are computed and compared with the analytical-exact solution. Nurbs formulation used here is also compared with higher order B-spline basis. It is seen that shear deformable beam developed using Nurbs basis function is more efficient than the beam developed using older version of B-spline ba-

sis. Interlaminar shear and normal stresses are computed directly without the extra step required in post-processing. Various numerical examples are tested and validated with the analytical solution.

The chapter is organized as follows. Firstly, the theoretical formulation of Nurbs beam Galerkin element-free/finite element formulation is derived. Next, transverse/interlaminar stresses are computed. Code developed is validated with composite and sandwich beams analysis.

2.1 Theoretical Formulation

A laminated composite beam consisting of K layers with length L and rectangular cross-section of width B and depth H is considered here as shown in the Figure 2.1. The theoretical formulation for the *first-order shear-deformable composite beam* is obtained by condensing the *first-order shear-deformable plate theory* in the y-coordinate. It is assumed that the width of the laminated plate is small compared to the length and the laminate scheme, and the loading are such that the displacement is only a function of x-axis.

2.1.1 Displacement and strain field

In the *first-order shear-deformation plate theory*, the kirchhoff assumption that the transverse normal remain perpendicular to the mid-surface after deformation is relaxed. And, the

displacement field is given by

$$\begin{aligned} U(x,y,z) &= u_o(x,y) + z\phi_x(x,y) \\ V(x,y,z) &= v_o(x,y) + z\phi_y(x,y) \\ W(x,y,z) &= w_o(x,y) \end{aligned} \tag{2.1}$$

where $u_o, v_o, w_o, \phi_x, \phi_y$ are the mid-plane axial, lateral and transverse displacement and the rotation of transverse normal about the y and x-axis respectively.

The strain field is given as

$$\begin{Bmatrix} \epsilon_{xx} \\ \epsilon_{yy} \\ \gamma_{yz} \\ \gamma_{xz} \\ \gamma_{xy} \end{Bmatrix} = \begin{Bmatrix} \epsilon^o_{xx} \\ \epsilon^o_{yy} \\ \gamma^o_{yz} \\ \gamma^o_{xz} \\ \gamma^o_{xy} \end{Bmatrix} + z \begin{Bmatrix} \kappa^o_{xx} \\ \kappa^o_{yy} \\ \gamma^1_{yz} \\ \gamma^1_{xz} \\ \kappa^o_{xy} \end{Bmatrix} \tag{2.2}$$

where

$$\begin{Bmatrix} \epsilon^o_{xx} \\ \epsilon^o_{yy} \\ \gamma^o_{yz} \\ \gamma^o_{xz} \\ \gamma^o_{xy} \end{Bmatrix} = \begin{Bmatrix} \frac{\partial u_0}{\partial x} \\ \frac{\partial v_0}{\partial y} \\ \frac{\partial w_0}{\partial y} + \phi_y \\ \frac{\partial w_0}{\partial x} + \phi_x \\ \frac{\partial u_0}{\partial y} + \frac{\partial v_0}{\partial x} \end{Bmatrix}, \quad \begin{Bmatrix} \kappa^o_{xx} \\ \kappa^o_{yy} \\ \gamma^1_{yz} \\ \gamma^1_{xz} \\ \kappa^o_{xy} \end{Bmatrix} = \begin{Bmatrix} \frac{\partial \phi_x}{\partial x} \\ \frac{\partial \phi_x}{\partial y} \\ 0 \\ 0 \\ \frac{\partial \phi_x}{\partial y} + \frac{\partial \phi_y}{\partial x} \end{Bmatrix} \tag{2.3}$$

2.1.2 Constitutive Model

The constitutive relation for the k^{th} lamina in the laminate co-ordinate system can be written as;

$$\begin{Bmatrix} \sigma_{xx} \\ \sigma_{xy} \\ \sigma_{yy} \end{Bmatrix}^{(k)} = \begin{bmatrix} \overline{Q}_{11} & \overline{Q}_{12} & \overline{Q}_{16} \\ \overline{Q}_{12} & \overline{Q}_{22} & \overline{Q}_{26} \\ \overline{Q}_{16} & \overline{Q}_{26} & \overline{Q}_{66} \end{bmatrix} \begin{Bmatrix} \epsilon_{xx} \\ \epsilon_{yy} \\ \epsilon_{xy} \end{Bmatrix}^{(k)} \tag{2.4}$$

$$\begin{Bmatrix} \sigma_{yz} \\ \sigma_{xz} \end{Bmatrix}^{(k)} = \begin{bmatrix} \overline{Q}_{44} & \overline{Q}_{45} \\ \overline{Q}_{45} & \overline{Q}_{55} \end{bmatrix} \begin{Bmatrix} \gamma_{yz} \\ \gamma_{xz} \end{Bmatrix}^{(k)} \tag{2.5}$$

Where $\overline{Q}_{ij}$s are the transformed plane-stress reduced stiffnesses.

2.1.3 Laminate Constitutive equations

Laminate constitutive equations for a laminated composite are obtained by integrating the stresses through the laminate thickness. The resulting force ($N's$) and the moment ($M's$) resultants are written in the matrix form as given below.

$$\begin{Bmatrix} N_x \\ N_y \\ N_{xy} \\ M_x \\ M_y \\ M_{xy} \end{Bmatrix} = \begin{bmatrix} A_{11} & A_{12} & A_{16} & B_{11} & B_{12} & B_{16} \\ A_{12} & A_{22} & A_{26} & B_{12} & B_{22} & B_{26} \\ A_{16} & A_{26} & A_{66} & B_{16} & B_{26} & B_{66} \\ B_{11} & B_{12} & B_{16} & D_{11} & D_{12} & D_{16} \\ B_{12} & B_{22} & B_{26} & D_{12} & D_{22} & D_{26} \\ B_{16} & B_{26} & B_{66} & D_{16} & D_{26} & D_{66} \end{bmatrix} \begin{Bmatrix} \epsilon_x^o \\ \epsilon_y^o \\ \gamma_{xy}^o \\ \kappa_x^o \\ \kappa_y^o \\ \kappa_{xy}^o \end{Bmatrix} \tag{2.6}$$

$$\begin{Bmatrix} Q_y \\ Q_x \end{Bmatrix} = K \begin{bmatrix} A_{44} & A_{45} \\ A_{45} & A_{55} \end{bmatrix} \begin{Bmatrix} \gamma_{yz}^o \\ \gamma_{xz}^o \end{Bmatrix} \tag{2.7}$$

Here, A_{ij}, B_{ij} and D_{ij}'s are the extensional, bending-extensional and bending stiffness elements of a laminate.

Symmetric Laminate Composite Beam

Considering bending only problem in a symmetric laminate and negligible bending-extensional stiffness i.e. $[B] = 0$, the problem is reduced to pure bending of symmetric laminated beam. Thus, the inverse form of resulting laminate constitutive equations are written as,

$$\begin{Bmatrix} \kappa_x^o \\ \kappa_y^o \\ \kappa_{xy}^o \end{Bmatrix} = \begin{bmatrix} D_{11}^* & D_{12}^* & D_{16}^* \\ D_{12}^* & D_{22}^* & D_{26}^* \\ D_{16}^* & D_{26}^* & D_{66}^* \end{bmatrix} \begin{Bmatrix} M_{xx} \\ 0 \\ 0 \end{Bmatrix} \tag{2.8}$$

$$\left\{ \gamma_{xz}^{o} \right\} = \frac{1}{K} \left[A_{55}^{*} \right] \left\{ Q_x \right\} \tag{2.9}$$

where

$$\begin{aligned} D_{11}^{*} &= \left(D_{22}D_{66} - D_{26}D_{26}\right)/D^{*} \\ D_{12}^{*} &= \left(D_{16}D_{26} - D_{12}D_{66}\right)/D^{*} \\ D_{16}^{*} &= \left(D_{12}D_{26} - D_{22}D_{16}\right)/D^{*} \\ D^{*} &= D_{11}D_1 + D_{12}D_2 + D_{16}D_3 \\ D_1 &= D_{22}D_{66} - D_{26}D_{26} \\ D_2 &= D_{16}D_{26} - D_{12}D_{66} \\ D_3 &= D_{12}D_{26} - D_{22}D_{16} \end{aligned} \tag{2.10}$$

$$A_{44}^{*} = \frac{A_{55}}{A},\ A_{55}^{*} = \frac{A_{44}}{A},\ A_{45}^{*} = \frac{A_{45}}{A},\ A = A_{44}A_{55} - A_{45}A_{45} \tag{2.11}$$

D_{ij}^{*}s denote the elements of the inverse of [D] matrix and A_{ij}^{*}s denote the elements of inverse of [A] matrix.

2.1.4 Higher Order Compact B-spline Beam

A B-spline beam consists of m sections with each section of equal length h. The displacement w and the rotation ϕ are represented by B-spline basis function and are defined as,

$$w = \sum_{i=-2}^{m+2} \alpha_i \varphi_i^k, \phi = \sum_{i=-2}^{m+2} \beta_i \varphi_i^j \tag{2.12}$$

where φ_i^k and φ_i^j are the local B-spline basis for transverse displacement and rotation representation of order k and j respectively. Here, we are using local b_5-spline (quintic) basis which has non-zero values over 6 consecutive sections, with the section-knot x_i as the center. The values of k and j are the same *i.e.* b_5-spline. The local b_5-spline basis over these intervals are defined in the compact form as follows,

$$\varphi_i^k = \begin{cases} 0 & x < x_{i-3} \\ (x - x_{i-3})^5 & x_{i-3} < x < x_{i-2} \\ h^5 + 5h^4 (x - x_{i-2}) + 10h^3 (x - x_{i-2})^2 & \\ +10h^2 (x - x_{i-2})^3 + 5h (x - x_{i-2})^4 - 5 (x - x_{i-2})^5 & x_{i-2} < x < x_{i-1} \\ 26h^5 + 50h^4 (x - x_{i-1}) + 20h^3 (x - x_{i-1})^2 & \\ -20h^2 (x - x_{i-1})^3 - 20h (x - x_{i-1})^4 + 10 (x - x_{i-1})^5 & x_{i-1} < x < x_i \\ 26h^5 + 50h^4 (x_{i+1} - x) + 20h^3 (x_{i+1} - x)^2 & \\ -20h^2 (x_{i+1} - x)^3 - 20h (x_{i+1} - x)^4 + 10 (x_{i+1} - x)^5 & x_i < x < x_{i+1} \\ h^5 + 5h^4 (x_{i+2} - x) + 10h^3 (x_{i+2} - x)^2 & \\ +10h^2 (x_{i+2} - x)^3 + 5h (x_{i+2} - x)^4 - 5 (x_{i+2} - x)^5 & x_{i+1} < x < x_{i+2} \\ (x_{i+3} - x)^5 & x_{i+2} < x < x_{i+3} \\ 0 & x > x_{i+3} \end{cases} \tag{2.13}$$

where α_i and β_i are the spline parameters. In this formulation, the displacement and rotation which are present only at the boundaries can be expressed in terms of the spline parameters as

$$\begin{aligned} w_0 &= (\alpha_{-2} + 26\alpha_{-1} + 66\alpha_0 + 26\alpha_1 + \alpha_2) \\ w_m &= (\alpha_{m-2} + 26\alpha_{m-1} + 66\alpha_m + 26\alpha_{m+1} + \alpha_{m+2}) \\ w_0' &= -\tfrac{5}{d}\,(\alpha_{-2} + 10\alpha_{-1} - 10\alpha_1 - 5\alpha_2) \\ w_m' &= -\tfrac{5}{d}\,(\alpha_{m-2} + 10\alpha_{m-1} - 10\alpha_{m+1} - 5\alpha_{m+2}) \end{aligned} \tag{2.14}$$

Since, the domain is divided into m sections, there are $[2 \times (m+5))]$ B-spline parameters which represent displacement (w) and rotation (ϕ_x) function. The spline parameters $\alpha_{-2}, \alpha_{-1}, \alpha_{m+1}, \alpha_{m+2}$ lying outside the domain are replaced by $w_0, w_0^{'}, w_m, w_m^{'}$ and same applies for the *rotation vector*. In all, there are $[2 \times (m+1))]$ interior spline parameters within the domain. This results in an element-free Galerkin formulation *i.e.* an approximation or interpolation scheme is constructed entirely from the spline parameters. One of the advantages of meshfree formulation is that it does not require element connectivity.

Gauss-quadrature rule is applied for the numerical integration. In this formulation, the number of integration points are allowed to vary with the number of spline parameters used and require testing for the optimal solution.

The generalized vector in terms of physical co-ordinates at the boundary and interior splines, can be written as

$$\delta_{ph} = \{w_o \; w_o' \; \alpha_o \; \alpha_1 \; ..... \; \alpha_m \; w_m \; w_m'\} \tag{2.15}$$

And, the transformation is obtained using a transformation matrix T as follows,

$$\delta_{ph} = T\delta_{sp} \tag{2.16}$$

The transformation matrix for the boundary terms consists of coefficients of spline-parameters given in the equation no. (2.14).

2.1.5 Nurbs Beam Galerkin Formulation

For shear-deformable beam, the displacement fields, w and ϕ are defined as,

$$w = \sum_{i=1}^{CP} R_i^p w_i \qquad \phi = \sum_{i=1}^{CP} R_i^p \phi_i \tag{2.17}$$

where R_i^ps are the Nurbs basis functions of order p, and CP is the number of control points.

B-spline Basis

A knot vector in one dimension is a set of co-ordinates in the parametric space, written as $\Xi = \{\xi_1, \xi_2, ..., \xi_{n+p+1}\}$, where ξ_i is the i^{th} knot, i is the knot index where $i = 1, 2, ..., n + p + 1$, p is the order of the polynomial and n is the number of basis functions. The order of the polynomial, $p = 0, 1, 2, 3....$, refers to the constant, linear, quadratic, cubic piecewise polynomials, respectively. The knots in the parametric space are either equally-spaced or unequally-spaced and the knot vectors are termed as *uniform* or *non-uniform*, respectively.

If more than one knot is located at the same parametric co-ordinate, these are termed as repeated knots. For open knot vector, first and last knots are repeated $p+1$ times. Basis function formed using the open knot vector are interpolatory at the beginning and end of the parametric space interval, $[\xi_1, \xi_{n+p+1}]$. This distinguishes the knots from the nodes in the finite element analysis. In this formulation, open knot vector is used to define the Nurbs basis functions.

B-spline basis functions are defined recursively starting with piecewise constants ($p = 0$).

$$N_i^p(\xi) = \begin{cases} 1 & if\ \xi_i \leq \xi < \xi_{i+1}, \\ 0 & otherwise \end{cases} \tag{2.18}$$

For $p = 1, 2, 3, ...$, basis functions are defined by

$$N_i^p(\xi) = \frac{\xi - \xi_i}{\xi_{i+p} - \xi_i} N_i^{p-1}(\xi) + \frac{\xi_{i+p+1} - \xi}{\xi_{i+p+1} - \xi_{i+1}} N_{i+1}^{p-1}(\xi) \tag{2.19}$$

Rational Basis

The rational basis functions are constructed from the B-spline basis as follows,

$$R_i^p(\xi) = \frac{N_i^p(\xi) W_i}{\sum_{i=1}^{CP} N_i^p(\xi) W_i} \tag{2.20}$$

and, the Nurbs curve can be written as,

$$C(\xi) = \sum_{i=1}^{CP} R_i^p(\xi) B_i \tag{2.21}$$

where W_is are the weights associated with it. Weights are the vertical coordinate of control points and B_is are the set of control points.

Some of the important properties of Nurbs are as follows[30] :

1) Nurbs basis functions form a partition of unity.

2) The continuity and support of the Nurbs basis function are the same as those of b-splines.

3) If the weights are equal to 1, Nurbs becomes B-spline.

Figure 2.2 shows the cubic, non-uniform Nurbs basis function for a given knot vector. Nurbs Basis functions are interpolatory at the end knots, i.e. where the knots are repeated. The derivation of weak formulation using Galerkin method is given in the appendix A and B. The refinement process are briefly discussed in the Appendix C.

Substituting the representations for the field variables in the weak formulation, the governing equation is obtained as follows,

$$[[K_b] + [K_{sh}]] \{\delta\} = \{F\} \tag{2.22}$$

where $[K_b]$ and $[K_{sh}]$ are the bending and shear stiffness matrices respectively; and $\{F\}$ is

the consistent load vector.

$$K_b = E^c_{xx} I \begin{bmatrix} 0 & 0 \\ 0 & K^2 \end{bmatrix} \tag{2.23}$$

$$K_{sh} = k_{sh} G^c_{xz} A \begin{bmatrix} K^2 & K^{1^T} \\ K^1 & K^0 \end{bmatrix} \tag{2.24}$$

$$\begin{aligned} K^0_{ij} &= \int_0^L \overline{R}^{pT}_i(x) \overline{R}^p_j(x) dx \\ K^1_{ij} &= \int_0^L \overline{R}^{pT}_i(x) \overline{R}^{p\prime}_j(x) dx \\ K^2_{ij} &= \int_0^L \overline{R}^{\prime T}_i(x) \overline{R}^{\prime}_j(x) dx \\ F^1_i &= \int_0^L \overline{R}^T_i(x) q dx \end{aligned} \tag{2.25}$$

The total number of degrees of freedom are equal to $d * (m - p - 1)$, where d is the number of displacement field variables, m is the length of the knot vector and p is the order of the polynomial.

This naturally results in element-free Galerkin formulation i.e. an approximation scheme is constructed entirely from the nodes. Discretization can be performed by increasing the number of nodes or control points and it is adaptive in nature. Gauss-Quadrature rule is used for the integration purposes. The number of Gauss points depend on the number of control points used to discretize the domain and require numerical testing for optimal number of Gauss-integration points. The boundary conditions are naturally satisfied and required no additional step.

2.2 Calculation of Interlaminar Stresses

The evaluation of transverse stresses τ_{xz} and σ_{zz} from the stress-strain constitutive relations lead to the discontinuity at the interface of the two adjacent layers of the laminate and thus, violates the equilibrium conditions. The three-dimensional analysis is very complex due to the variation in the constitutive laws in the thickness direction and the continuity requirements of transverse stresses and displacement across the interface. Therefore, the reduced 3D elasticity equilibrium equations are used to calculate the transverse stresses in the k^{th} lamina and the equations are given as,

$$\sigma^k_{xx,x} + \tau^k_{xz,z} = 0 \tag{2.26}$$

$$\tau^k_{xz,x} + \sigma^k_{zz,z} = 0 \tag{2.27}$$

Here, the stresses are calculated using the direct integration method. Since, we are looking into the 1D beam analysis, the equilibrium equations can be rearranged as follows,

$$\tau^k_{xz,z} = -\sigma^k_{xx,x} \tag{2.28}$$

$$\sigma^k_{zz,z} = -\tau^k_{xz,x} \tag{2.29}$$

from which the transverse/interlaminar stresses through the thickness can be evaluated. It can be seen that the equation for transverse shear stress, τ_{xz}, is a first-order equation. Since,

in general, the transverse shear stresses are known at the top and bottom of the laminate, one can only obtain a non-unique solution as both the traction boundary conditions can not be enforced simultaneously. However, for the transverse normal stresses, a second-order equation is derived and requires double integration through the thickness. Two constants can be evaluated from the traction boundary conditions at the top and bottom of the laminate[77].

The 3D equilibrium equations for transverse stress calculations are as follows,

$$\tau_{xz}^{k} = \int_{z_i}^{z_{i+1}} \left(\sigma_{xx,x}^{k}\right) dz + H^{k}(x) \tag{2.30}$$

$$\sigma_{zz}^{k}|_{k+1} = \sum_{i=1}^{k} \int_{z_i}^{z_{i+1}} \left(\int_{z} \sigma_{xx,xx}\ dz \right) dz + zG_1 + G_2 \tag{2.31}$$

where H^k, G_1 and G_2 are the constants of integration.

2.3 Numerical Examples

In this section, numerical examples of composite and sandwich beam under transverse uniformly distributed load for different boundary conditions are presented. The higher-order derivatives and transverse stresses are calculated for different cases and compared with the analytical exact solution. The material properties used here are given in Table 1.1. The transverse stresses calculated for various numerical examples are normalized using the following notation.

$$s = L/H,\ \overline{\sigma}_{xx} = \sigma_{xx}/(qs^2),\ \overline{\tau}_{xz} = \tau_{xz}/(qs),\ \overline{\sigma}_{zz} = \sigma_{zz}/q$$

Table 2.1: Material Properties for Composite and Sandwich Structures

Name	Property		
Face Sheet	$E_1 = 172.4$ GPa	$\nu_{12} = 0.25$	$G_{12} = 3.45$ GPa
(Composite)	$E_2 = 172.4$ GPa	$\nu_{13} = 0.25$	$G_{13} = 3.45$ GPa
	$E_3 = 6.890$ GPa	$\nu_{23} = 0.25$	$G_{23} = 1.378$ GPa
Core sheet	$E_1 = 0.276$ GPa	$\nu_{12} = 0.25$	$G_{12} = 0.1104$ GPa
(Sandwich)	$E_2 = 0.276$ GPa	$\nu_{13} = 0.25$	$G_{13} = 0.414$ GPa
	$E_3 = 3.450$ GPa	$\nu_{23} = 0.25$	$G_{23} = 0.414$ GPa

2.3.1 Cantilever Beam and Derivative Analysis

A 3 layer cross-ply [0 90 0] composite beam under uniformly distributed load is considered here. The displacement and its higher-order derivatives are calculated and compared with the exact solution[116]. It is observed that 4^{th} order Nurbs shear-deformable beam, with 10 degrees of freedom and 4 integration point over the whole domain, computes the higher order derivatives of displacement accurately within the domain and at the boundary as compared with the analytical-exact solution. The number of integration points over the domain were chosen in such a way so as to match the displacement profile with the analytical-exact solution. Compact B-spline formulation required 52 degrees of freedom and 25 integration points over the entire domain to compute the higher order displacement derivative. Figures 2.3- 2.4 compares the displacement and higher-order derivative of displacement for Nurbs Compos-

ite beam with the analytical-exact solution and higher order compact B-spline(HOCBS) formulation.

2.3.2 Simply-Supported Beam and Derivative Analysis

A 3 layer cross-ply [0900] composite beam under uniformly distributed load is considered. The displacement and its derivatives are compared with the closed form / analytical exact solution and compact B-spline formulation. It is observed that the 4^{th} order Nurbs basis, with 10 degrees of freedom and 5 integration point over the whole domain, computes higher order derivatives of displacement accurately within the domain and at the boundary as compared with the analytical-exact solution. B-spline formulation again required more number of B-spline parameters and integration points i.e. 50 degrees of freedom with 24 integration points were required for the same analysis. Figures 2.5- 2.6 compares the displacement and its higher-order derivatives for Nurbs basis as compared with the analytical-exact solution and higher order compact B-spline (HOBS) formulation.

2.3.3 Simply-Supported Cross-ply Beam

A three-layered cross-ply [0 90 0], simply supported, laminated composite beam with aspect ratio, $s = 4$ under uniformly distributed load is considered. Nurbs based shear-deformable beam formulation is used for the computation of interlaminar stress. Material properties are given in Table 2.1. The transverse shear and normal stresses are computed from the

second derivative of in-plane stress by through the thickness integrating of 3D equilibrium equations. Normalized transverse stresses are computed and validated with the analytical-exact solution. Figures 2.7- 2.8 show the variation of normalized transverse stresses in a 3-layer cross-ply [0 90 0] composite beam.

2.3.4 Simply-Supported Sandwich Beam

A sandwich beam [45 -45 *core* -45 45] with aspect ratio, $s = 4$, under simply-supported boundary condition, subjected to uniform distributed load is considered. Material properties used are given in Table 2.1. The thickness of the face sheet is taken to be $1/8^{th}$ of the core thickness. The transverse shear and normal stresses are obtained from in-plane stress derivative by integrating the equilibrium equations through the thickness. Normalized transverse stress are computed and validated with the analytical-exact solution. Figures 2.9- 2.10 show the variation of normalized transverse stresses in a sandwich beam under uniformly distributed load.

2.3.5 Four-layer Cross-ply Composite Beam

A four-layered symmetric cross-ply [0 90 90 0] laminated composite beam with aspect ratio, $s = 4$, simply supported and subjected to uniform distributed load is considered. Material properties are given in Table 2.1. The transverse shear and normal stresses are obtained from the second derivative of in-plane stress by integrating the equilibrium equations through

the thickness. Normalized transverse stress results are validated with the analytical-exact solution[116]. Figures 2.11- 2.12 show the variation of normalized transverse stresses in a four-layer cross-ply laminated composite beam.

2.4 Conclusion

A variable-order Nurbs shear-deformable laminated composite element-free beam formulation is developed. The displacement and interlaminar stresses are computed for composite and sandwich beams under transverse loads. Nurbs beam required less number of control points to obtain the higher order derivatives of displacement and is found to be more efficient than the B-spline formulation. The higher-order derivative required for computing transverse/interlaminar normal stress is obtained directly *i.e.* without using an extra step in post-processing, necessitated in the finite element formulation. This is attributed to higher order continuity and smoothness properties of Nurbs basis due to stable recursion algorithm. The present computational analysis is more rigorous as the loading is uniformly distributed over the domain of the beam. Higher-order displacement derivatives and interlaminar stresses are accurately and efficiently computed and compared with the closed-form solution.

2.5 Appendix

2.5.1 Governing Equations

The special case of principle of virtual displacement that deals with linear as well as non-linear elastic bodies is known as principle of minimum total potential energy. The principle of minimum total potential energy is used to derive the governing equations for *first-order shear deformable composite beam*. The principle states that under equilibrium conditions, the first variation of the total potential energy i.e. the sum of the strain energy and the potential of the applied loads is zero *i.e.*

$$\delta\left(U+V\right)=\delta U+\delta V=0 \tag{2.32}$$

$$\delta U=\int_0^L\int_A\left[\sigma_{xx}\ \delta\epsilon_{xx}+\sigma_{xz}\delta\gamma_{xz}\right]dAdx \tag{2.33}$$

$$\delta V=-\int_0^L q\ \delta w_0\ dx \tag{2.34}$$

where q is the distributed load at the top surface ($z=-h/2$) of the laminate. Integrating over the area,

$$\int_0^L\left(M_{xx}\delta\epsilon_{xx}^1+Q_x\delta\gamma_{xz}^0-q\delta w_0\right)dx=0 \tag{2.35}$$

Integrating over the parts,

$$\int_0^L\left\{\left(-M_{xx,x}+Q_x\right)\delta\phi+\left(-q-Q_{x,x}\right)\delta w_o\right\}dx+\left\{M_{xx}\delta\phi+Q_x\delta w_o\right\}\mid_0^L=0 \tag{2.36}$$

Thus, the Euler-Lagrange equations are,

$$\delta w_o : Q_{x,x} + q = 0 \tag{2.37}$$

$$\delta \phi : M_{xx,x} - Q_x = 0 \tag{2.38}$$

Where, w_o and ϕ are the primary variables and M_{xx} and Q_x are the secondary variables. The governing equation of motion in terms of displacement variables can be written as,

$$k_{sh} G^c_{xz} A \left(\frac{\partial^2 w_o}{\partial x^2} + \frac{\partial \phi_x}{\partial x} \right) + q = 0 \tag{2.39}$$

$$E^c_{xx} I_{yy} \frac{\partial^2 \phi_x}{\partial x^2} - k_{sh} G^c_{xz} A \left(\frac{\partial w_o}{\partial x} + \phi_x \right) = 0 \tag{2.40}$$

where, $E^c_{xx} I_{yy} = \frac{12}{D^*_{11} H^3}, G^c_{xz} A = \frac{1}{A^*_{55} H}$ are the equivalent moduli for the composite beam, $A = BH$, is the area of cross-section and k_{sh} is the shear-correction factor.

2.5.2 Weighted Residual-Galerkin Method

The weak formulation for the strong form of governing equations is derived by using the weighted residual-Galerkin method. Here, -w_1 and -w_2 are the weight functions which reduce the order of the equations resulting in a weak formulation. Multiplying equations (34) & (35) with weight functions and integrating over the element domain Ω_e, we obtain the following form,

$$\int_{x_A}^{x_B} -w_1 \left\{ k_{sh} G^c_{xz} A \left(w_{o,xx} + \phi_{x,x} \right) + \hat{q} \right\} = 0 \tag{2.41}$$

$$\int_{x_A}^{x_B} -w_2 \left[E^c_{xx} I_{yy} \phi_{x,xx} - k_{sh} G^c_{xz} A \left(w_{o,x} + \phi_x\right)\right] = 0 \tag{2.42}$$

Integrating by parts once, we obtain

$$\int_{x_A}^{x_B} \left[w_{1,x} \left\{k_{sh} G^c_{xz} A \left(w_{o,x} + \phi_x\right)\right\} - w_1 \hat{q}\right] dx - w_1(x_A) Q^e_1 \tag{2.43}$$

$$-w_1(x_B) Q^e_3 = 0$$

$$\int_{x_A}^{x_B} \left[w_{2,x} \left(E^c_{xx} I_{yy} \phi_{x,x}\right) + w_2 k_{sh} G^c_{xz} A \left(w_{,x} + \phi_x\right)\right] dx - w_2(x_A) Q^e_2 \tag{2.44}$$

$$-w_2(x_B) Q^e_4 = 0$$

$$\tag{2.45}$$

where

$$Q^e_1 = -\left[k_{sh} G^c_{xz} A \left(\phi_x + w_{,x}\right)\right]|_{x_A}, Q^e_3 = \left[k_{sh} G^c_{xz} A \left(\phi_x + w_{,x}\right)\right]|_{x_B} \tag{2.46}$$

$$Q^e_2 = -\left(E^c_{xx} \phi_{x,x}\right)|_{x_A}, Q^e_4 = \left(E^c_{xx} \phi_{x,x}\right)|_{x_B} \tag{2.47}$$

For the Galerkin method, $w_i = \varphi_i$ *i.e.* weight/trial functions are replaced by the same basis function as used to define the displacement and rotation fields. In our case, $x_A = 0, x_B = L$.

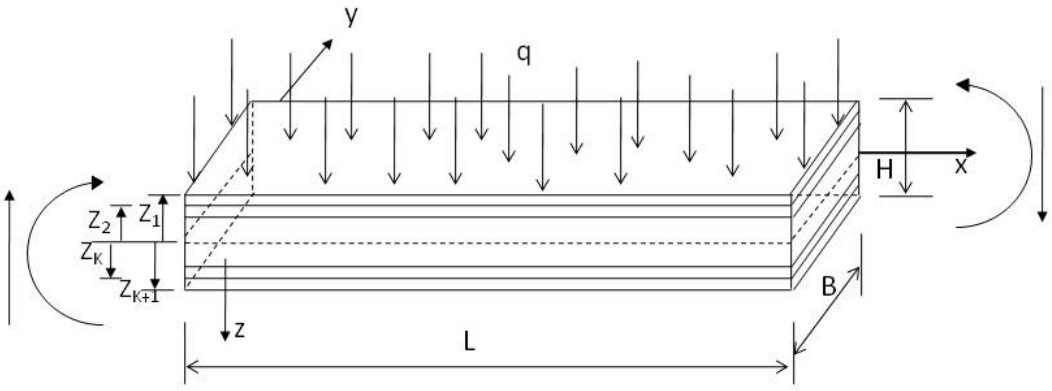

Figure 2.1: Composite beam under uniformly distributed load and sign convention

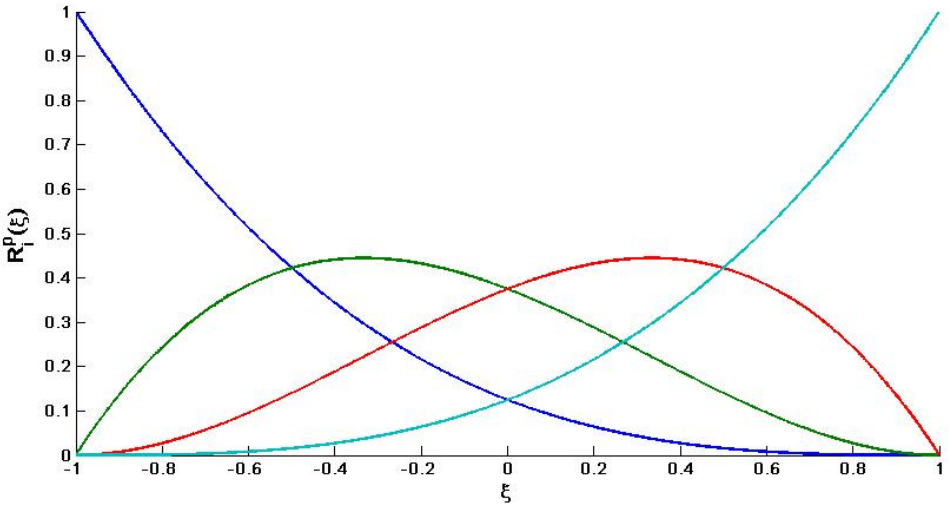

Figure 2.2: Cubic Nurbs basis functions for open, non-uniform knot vector

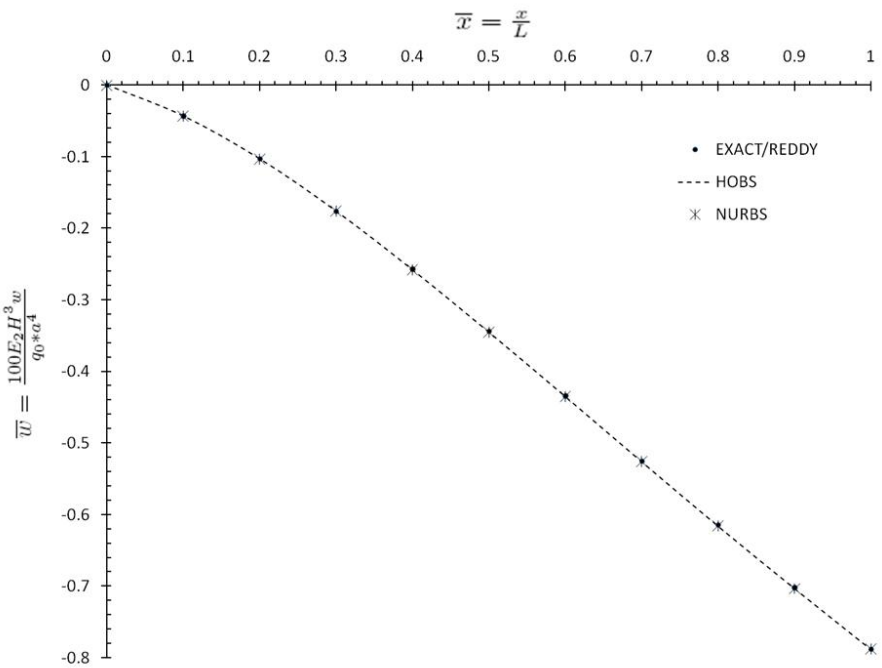

Figure 2.3: Normalized displacement profile of a cantilever composite beam under uniform distributed load

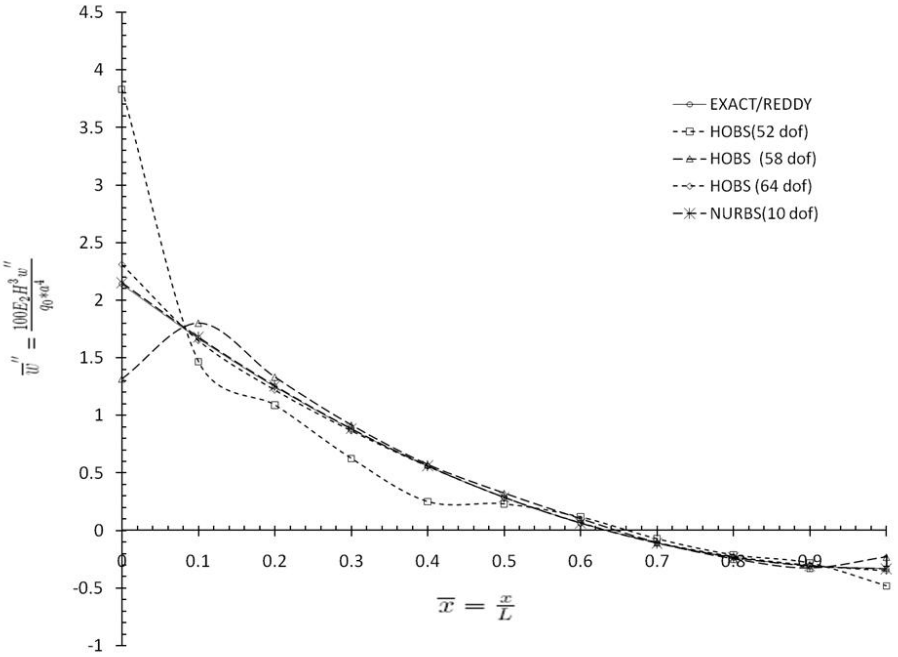

Figure 2.4: Normalized second derivative of displacement of a cantilever composite beam under uniform distributed load

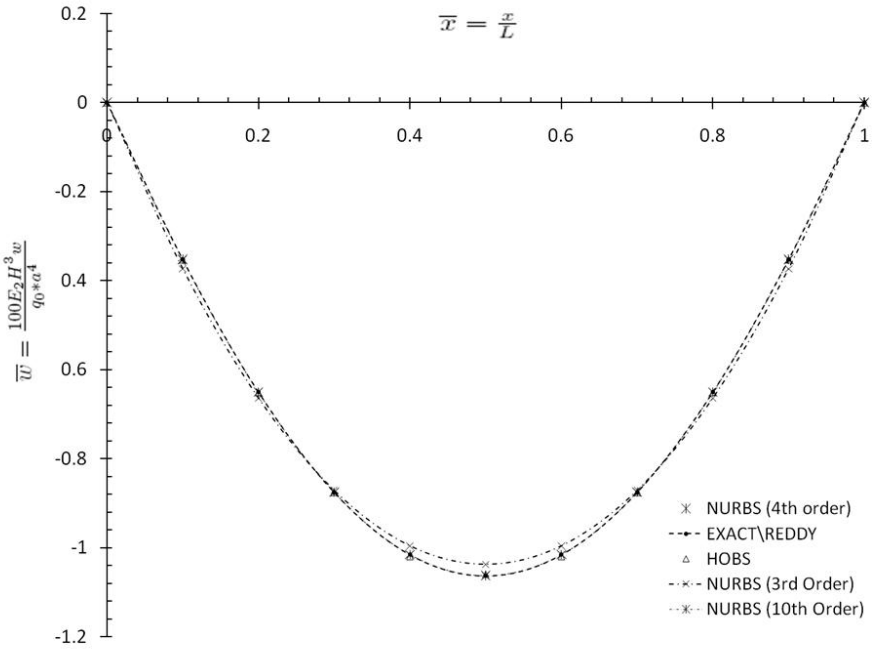

Figure 2.5: Normalized displacement profile over the length of a simply supported composite beam under uniform distributed load

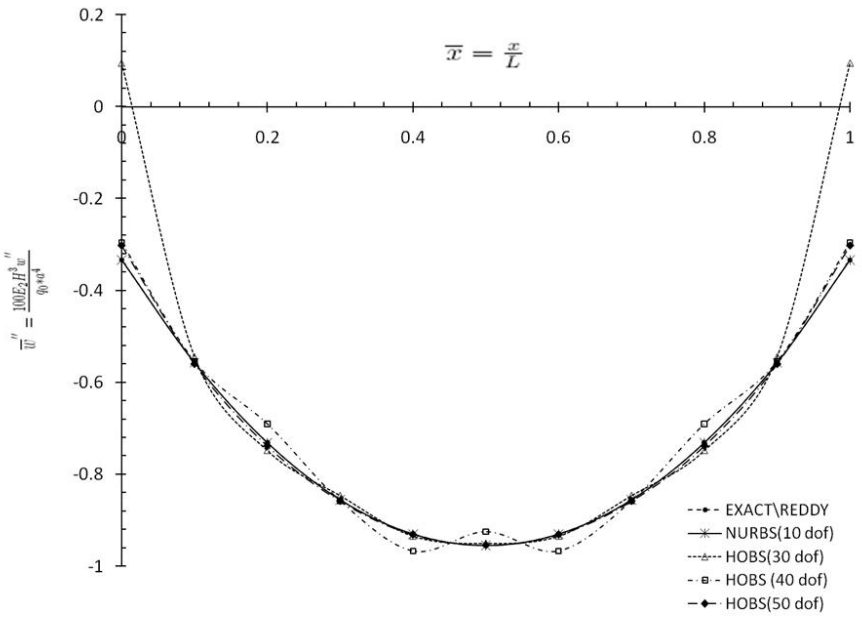

Figure 2.6: Normalized second derivative of displacement of a simply supported composite beam under uniform distributed load

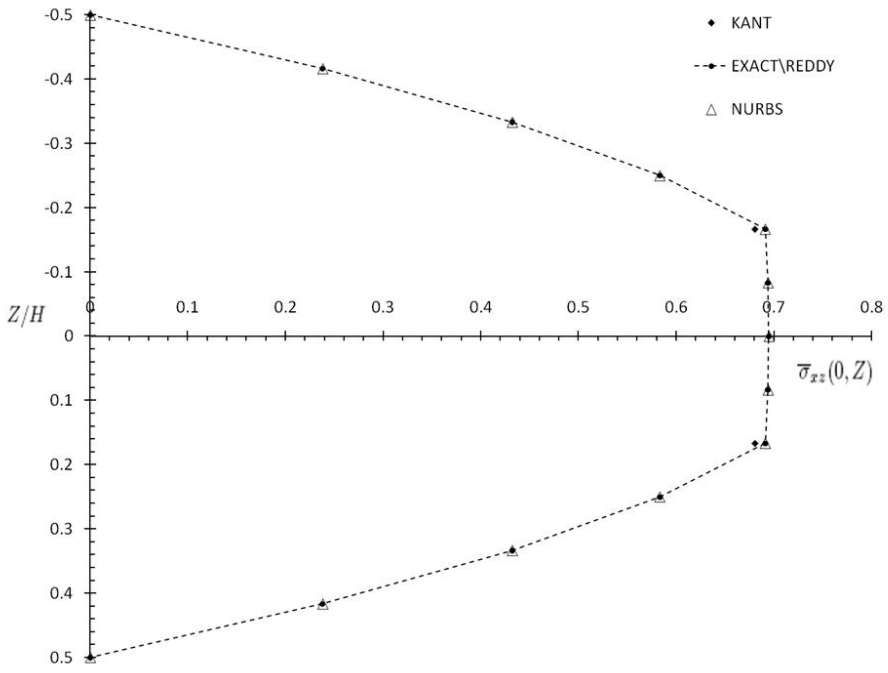

Figure 2.7: Variation of normalized transverse shear stress through the thickness in a cross-ply [0 90 0] laminate composite beam under uniform distributed load

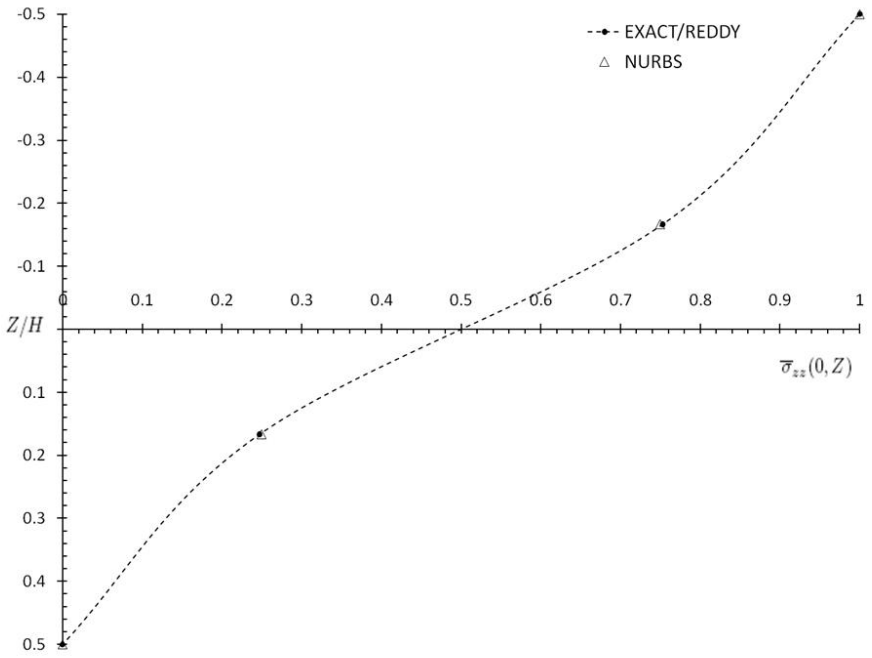

Figure 2.8: Variation of normalized transverse normal stress through the thickness in a cross-ply [0 90 0] laminate composite beam under uniform distributed load

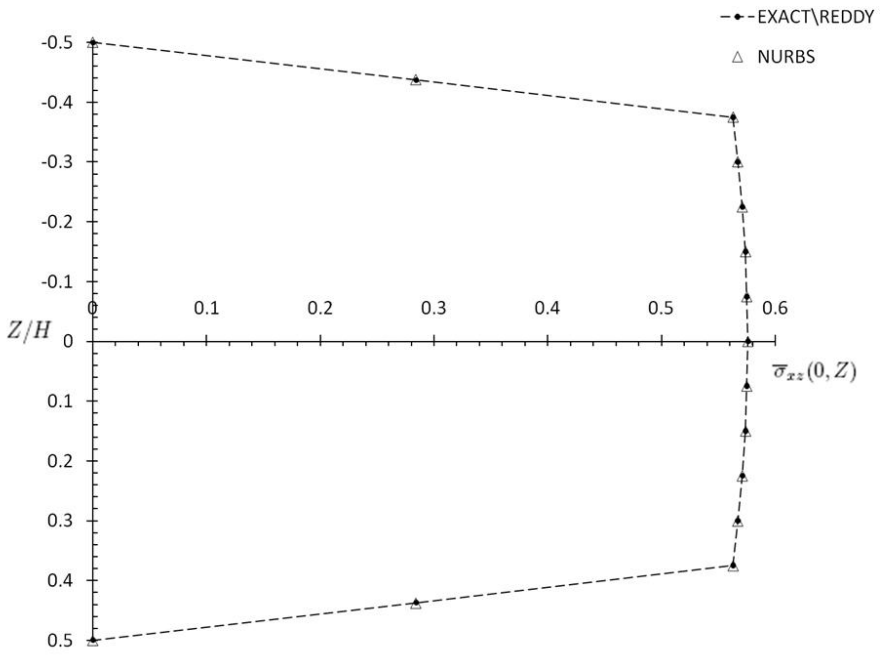

Figure 2.9: Variation of normalized transverse shear stress through the thickness in a sandwich beam [45 -45 core -45 45] under uniform distributed load

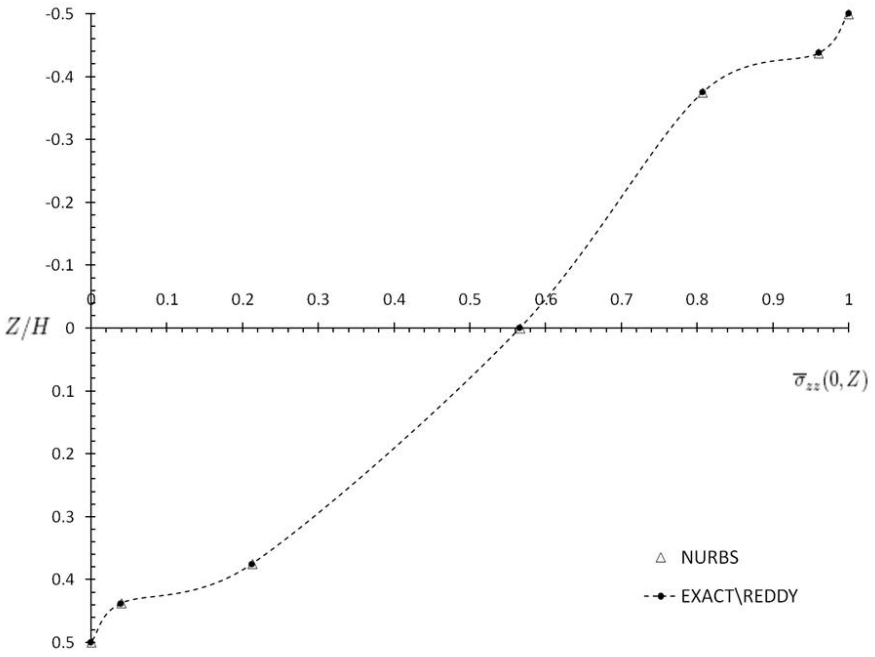

Figure 2.10: Variation of normalized transverse normal stress in a sandwich beam [45 -45 core -45 45] under uniform distributed load

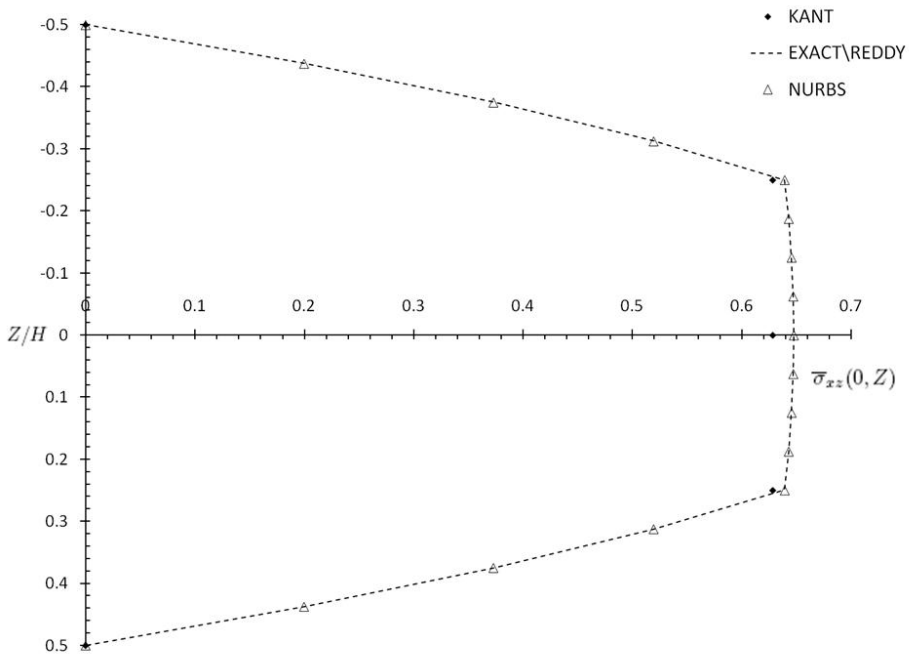

Figure 2.11: Variation of normalized transverse shear stress in a 4 layer cross-ply [0 90 90 0] composite beam under uniform distributed load

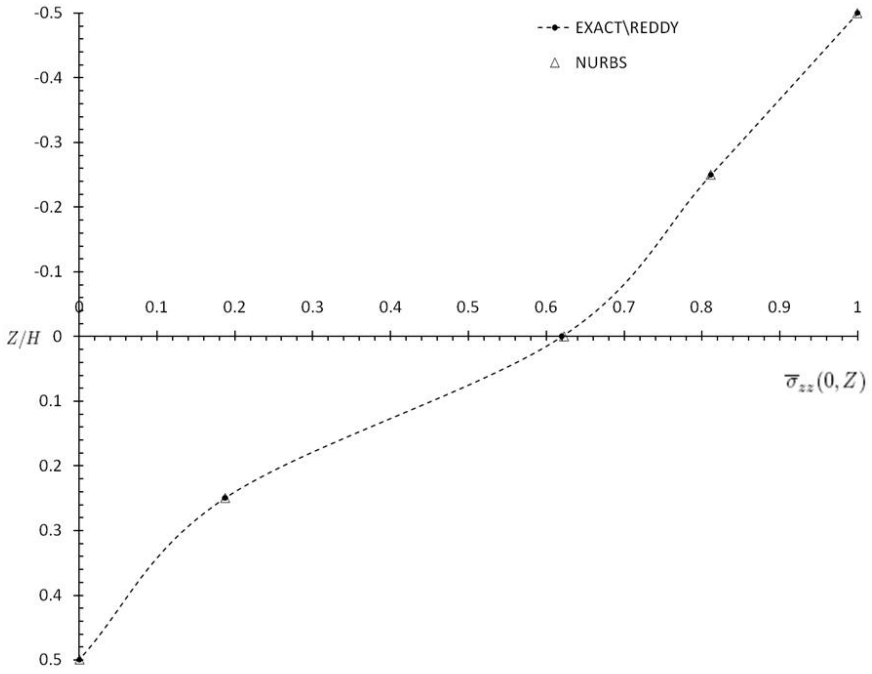

Figure 2.12: Variation of normalized transverse normal stress in a 4 layer cross-ply [0 90 90 0] composite beam under uniform distributed load

Chapter 3

Geometrically Nonlinear Nurbs Isogeometric Finite Element Analysis of Laminated Composite Plate

This research present the development of geometrically nonlinear Nurbs Isogeometric finite element analysis of laminated composite plates. First-order, shear-deformable laminate composite plate theory is utilized in deriving the governing equations using a variational formulation. Geometric nonlinearity is accounted for in Von-Karman sense. Nurbs quadratic and higher-order elements are constructed where k-refinement has no analogous in regular finite element. Isotropic, orthotropic and laminated composite plates are studied for various boundary conditions, length to thickness ratios and ply-angles. The computed center

direction is found to be in an excellent agreement with the literature and required fewer degrees of freedom/control point when compared with regular finite element analysis. For thin plate analysis, k-refined, quadratic Nurbs element is found to remedy the shear locking problem, i.e. it eliminated the need for reduced integration of transverse shear stifiness terms. k-refined quadratic Nurbs element also provided stable nonlinear deflection (hourglass instability) for distorted quadrilateral meshes. This research presents the development of Nurbs Isogeometric finite element where k-refined Nurbs element eliminates the need for extra step required in developing locking-free and stable shear-deformable plate elements.

3.1 Theoretical Formulation

3.1.1 First-order shear deformation plate theory (FSDT)

Displacement and strain field

The origin of the material coordinate system is considered to be the mid-plane of the laminate and the Kirchhoff assumption, that the transverse normal remain perpendicular to the mid-surface after deformation, is relaxed. Figure 3.1shows the coordinate system and layer numbering of a laminated composite plate. The displacement field is defined as,

$$u(x, y, z) = u_0(x, y) + z\phi_x(x, y)$$

$$v(x, y, z) = v_0(x, y) + z\phi_y(x, y) \tag{3.1}$$

$$w(x, y, z) = w_0(x, y)$$

where u_0, v_0, w_0 are the displacement along the x, y and z-axis and ϕ_x, ϕ_y are the rotation of transverse normal of the mid-plane about the y and x-axis respectively. Figure 3.2 shows the undeformed and deformed configuration of first order shear-deformable laminated composite plate.

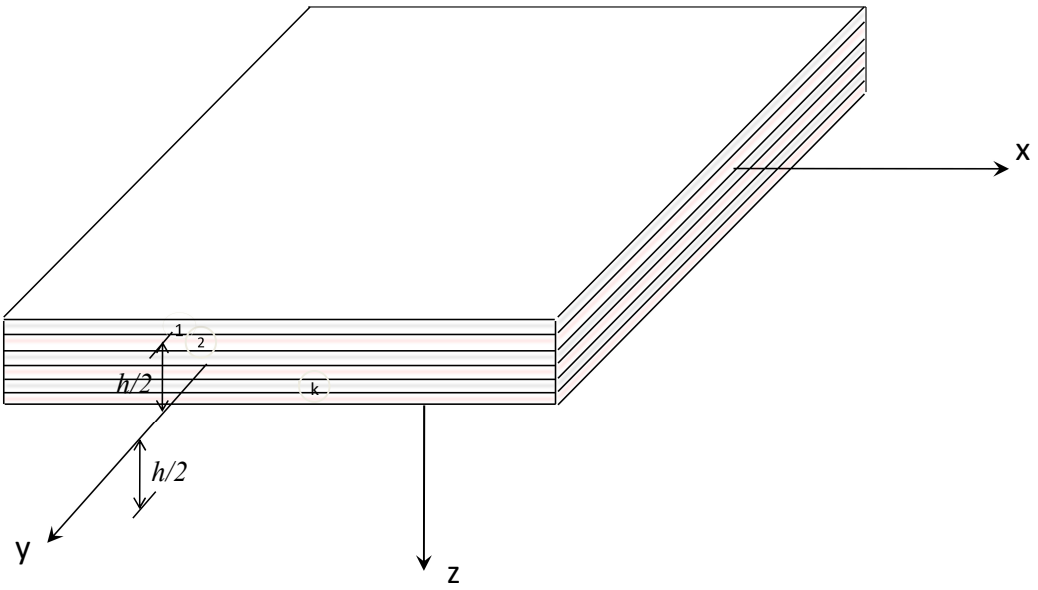

Figure 3.1: Coordinate system and layer numbering used for a laminate plate

The strain vector is obtained in terms of Green-Lagrange strain and accounts for large transverse displacement, small strain and moderate rotation. The strain vector corresponding to

the displacement field is given as,

$$\begin{aligned}
\epsilon_{xx} &= \frac{\partial u}{\partial x} + \frac{1}{2}\left(\frac{\partial w}{\partial x}\right)^2 \\
\epsilon_{yy} &= \frac{\partial v}{\partial y} + \frac{1}{2}\left(\frac{\partial w}{\partial y}\right)^2 \\
\gamma_{yz} &= \frac{\partial w}{\partial y} + \phi_y \\
\gamma_{xz} &= \frac{\partial w}{\partial x} + \phi_x \\
\gamma_{xy} &= \frac{\partial u}{\partial y} + \frac{\partial v}{\partial x} + \frac{\partial w}{\partial x}\frac{\partial w}{\partial y}
\end{aligned} \tag{3.2}$$

Total strain vector ϵ can be decomposed into linear and nonlinear strain vectors.

$$\epsilon = \epsilon^l + \epsilon^{nl} \tag{3.3}$$

ϵ^l, linear strain vector is composed of following terms,

$$\begin{aligned}
\epsilon^l_{xx} &= \frac{\partial u_0}{\partial x} + z\frac{\partial \phi_x}{\partial x} \\
\epsilon^l_{yy} &= \frac{\partial v_0}{\partial y} + z\frac{\partial \phi_y}{\partial y} \\
\gamma^l_{yz} &= \frac{\partial w_0}{\partial x} + \phi_x, \\
\gamma^l_{xz} &= \frac{\partial w_0}{\partial y} + \phi_y, \\
\gamma^l_{xy} &= \frac{\partial u_0}{\partial y} + \frac{\partial v_0}{\partial x} + z\left(\frac{\partial \phi_x}{\partial y} + \frac{\partial \phi_y}{\partial x}\right)
\end{aligned} \tag{3.4}$$

ϵ^{nl}, the nonlinear strain vector contains the following terms,

$$\begin{aligned} \epsilon_{xx}^{nl} &= \frac{1}{2}\left(\frac{\partial w_0}{\partial x}\right)^2 \\ \epsilon_{yy}^{nl} &= \frac{1}{2}\left(\frac{\partial w_0}{\partial y}\right)^2 \\ \gamma_{xy}^{nl} &= \frac{\partial w_0}{\partial x}\frac{\partial w_0}{\partial y} \end{aligned} \tag{3.5}$$

Other higher order terms are considered to be negeligible.

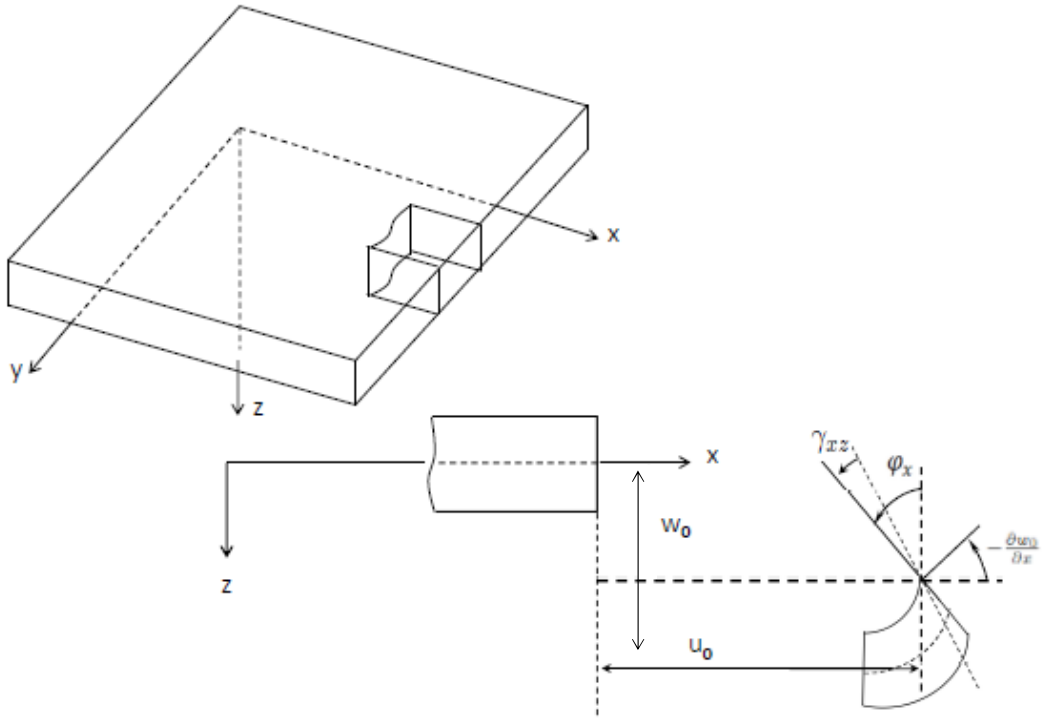

Figure 3.2: Undeformed and deformed configuration of first order shear-deformable plate

Equation of motion

The strong form of the governing equation of motion using first-order shear deformable plate theory are,

$$\begin{aligned}
\left(\frac{\partial N_{xx}}{\partial x}+\frac{\partial N_{xy}}{\partial y}\right)&=0\\
\left(\frac{\partial N_{xy}}{\partial x}+\frac{\partial N_{yy}}{\partial y}\right)&=0\\
\left(\frac{\partial Q_{x}}{\partial x}+\frac{\partial Q_{y}}{\partial y}\right)+q&=0\\
\left(\frac{\partial M_{xx}}{\partial x}+\frac{\partial M_{xy}}{\partial y}\right)-Q_{x}&=0\\
\left(\frac{\partial M_{xy}}{\partial x}+\frac{\partial M_{yy}}{\partial y}\right)-Q_{y}&=0
\end{aligned} \tag{3.6}$$

Where N_{xx}, N_{yy} and N_{xy} are the force resultants, M_{xx}, M_{xy}, M_{yy} are the moment resultants and Q_x and Q_y are the shear force resultants and q corresponds to transverse load.

3.1.2 Variarional Form

Weak form of the governing equations is obtained by pre-multiplying the equation of motion with δu_0, δv_0, δw_0, $\delta \phi_x$ and $\delta \phi_y$ respectively and integrating by parts over the element domain. Substituting force, moment and shear force resultant, the following equations are obtained [116].

$$
\begin{aligned}
0 \;=\; & \int_{\Omega^e} \left[\frac{\partial \delta u_0}{\partial x} \left\{ A_{11} \left(\frac{\partial u_0}{\partial x} + \frac{1}{2} \left(\frac{\partial w_0}{\partial x} \right)^2 \right) + A_{12} \left(\frac{\partial v_0}{\partial y} + \frac{1}{2} \left(\frac{\partial w_0}{\partial y} \right)^2 \right) \right. \right. \\
& \left. + A_{16} \left(\frac{\partial u_0}{\partial y} + \frac{\partial v_0}{\partial x} + \frac{\partial w_0}{\partial x} \frac{\partial w_0}{\partial y} \right) + B_{11} \frac{\partial \phi_x}{\partial x} + B_{12} \frac{\partial \phi_y}{\partial y} + B_{16} \left(\frac{\partial \phi_x}{\partial y} + \frac{\partial \phi_y}{\partial x} \right) \right\} \\
& + \frac{\partial \delta u_0}{\partial y} \left\{ A_{16} \left(\frac{\partial u_0}{\partial x} + \frac{1}{2} \left(\frac{\partial w_0}{\partial x} \right)^2 \right) + A_{26} \left(\frac{\partial v_0}{\partial y} + \frac{1}{2} \left(\frac{\partial w_0}{\partial y} \right)^2 \right) \right. \\
& \left. \left. + A_{66} \left(\frac{\partial u_0}{\partial y} + \frac{\partial v_0}{\partial x} + \frac{\partial w_0}{\partial x} \frac{\partial w_0}{\partial y} \right) + B_{16} \frac{\partial \phi_x}{\partial x} + B_{26} \frac{\partial \phi_y}{\partial y} + B_{66} \left(\frac{\partial \phi_x}{\partial y} + \frac{\partial \phi_y}{\partial x} \right) \right\} \right] dxdy \\
& - \oint_{\Gamma^e} N_n \delta u_{0n} ds
\end{aligned} \tag{3.7}
$$

$$
\begin{aligned}
0 \;=\; & \int_{\Omega^e} \left[\frac{\partial \delta v_0}{\partial x} \left\{ A_{12} \left(\frac{\partial u_0}{\partial x} + \frac{1}{2} \left(\frac{\partial w_0}{\partial x} \right)^2 \right) + A_{22} \left(\frac{\partial v_0}{\partial y} + \frac{1}{2} \left(\frac{\partial w_0}{\partial y} \right)^2 \right) \right. \right. \\
& \left. + A_{26} \left(\frac{\partial u_0}{\partial y} + \frac{\partial v_0}{\partial x} + \frac{\partial w_0}{\partial x} \frac{\partial w_0}{\partial y} \right) + B_{12} \frac{\phi_x}{x} + B_{22} \frac{\phi_y}{\partial y} + B_{26} \left(\frac{\phi_x}{\partial y} + \frac{\phi_y}{\partial x} \right) \right\} \\
& + \frac{\partial \delta v_0}{\partial x} \left\{ A_{16} \left(\frac{\partial u_0}{\partial x} + \frac{1}{2} \left(\frac{\partial w_0}{\partial x} \right)^2 \right) + A_{26} \left(\frac{\partial v_0}{\partial y} + \frac{1}{2} \left(\frac{\partial w_0}{\partial y} \right)^2 \right) \right. \\
& + A_{66} \left(\frac{\partial u_0}{\partial y} + \frac{\partial v_0}{\partial x} + \frac{\partial w_0}{\partial x} \frac{\partial w_0}{\partial y} \right) + B_{16} \frac{\partial \phi_x}{\partial x} + B_{26} \frac{\partial \phi_y}{\partial y} \\
& \left. \left. + B_{66} \left(\frac{\partial \phi_x}{\partial y} + \frac{\partial \phi_y}{\partial x} \right) \right\} \right] dxdy - \oint_{\Gamma^e} N_s \delta v_{0s} ds
\end{aligned} \tag{3.8}
$$

$$
0 \;=\; K_s \int_{\Omega^e} \left[\frac{\partial \delta w_0}{\partial x} \left\{ A_{55} \left(\frac{\partial w_0}{\partial x} + \phi_x \right) + A_{45} \left(\frac{\partial w_0}{\partial y} + \phi_y \right) \right\} \right.
$$

$$
\begin{aligned}
&+\frac{\partial \delta w_0}{\partial y}\left\{A_{45}\left(\frac{\partial w_0}{\partial x}+\phi_x\right)+A_{44}\left(\frac{\partial w_0}{\partial x}+\phi_x\right)\right\}\Bigg]\,dxdy\\
&+\int_{\Omega^e}\Bigg[\frac{\partial \delta w_0}{\partial x}\left\{\frac{\partial w_0}{\partial x}\left\{A_{11}\left(\frac{\partial u_0}{\partial x}+\frac{1}{2}\left(\frac{\partial w_0}{\partial x}\right)^2\right)+A_{12}\left(\frac{\partial v_0}{\partial y}+\frac{1}{2}\left(\frac{\partial w_0}{\partial y}\right)^2\right)\right.\\
&\left.+A_{16}\left(\frac{\partial u_0}{\partial y}+\frac{\partial v_0}{\partial x}+\frac{\partial w_0}{\partial x}\frac{\partial w_0}{\partial y}\right)+B_{11}\frac{\partial \phi_x}{\partial x}+B_{12}\frac{\partial \phi_y}{\partial y}+B_{16}\left(\frac{\partial \phi_x}{\partial y}+\frac{\partial \phi_y}{\partial x}\right)\right\}\right\}\\
&+\frac{\partial w_0}{\partial y}\left\{A_{16}\left(\frac{\partial u_0}{\partial x}+\frac{1}{2}\left(\frac{\partial w_0}{\partial x}\right)^2\right)+A_{26}\left(\frac{\partial v_0}{\partial y}+\frac{1}{2}\left(\frac{\partial w_0}{\partial y}\right)^2\right)\right.\\
&\left.+A_{66}\left(\frac{\partial u_0}{\partial y}+\frac{\partial v_0}{\partial x}+\frac{\partial w_0}{\partial x}\frac{\partial w_0}{\partial y}\right)+B_{16}\frac{\partial \phi_x}{\partial x}+B_{26}\frac{\partial \phi_y}{\partial y}+B_{66}\left(\frac{\partial \phi_x}{\partial y}+\frac{\partial \phi_y}{\partial x}\right)\right\}\\
&+\frac{\partial \delta w_0}{\partial y}\left\{\frac{\partial w_0}{\partial y}\left\{A_{12}\left(\frac{\partial u_0}{\partial x}+\frac{1}{2}\left(\frac{\partial w_0}{\partial x}\right)^2\right)+A_{22}\left(\frac{\partial v_0}{\partial y}+\frac{1}{2}\left(\frac{\partial w_0}{\partial y}\right)^2\right)\right.\right.\\
&\left.+A_{26}\left(\frac{\partial u_0}{\partial y}+\frac{v_0}{\partial x}+\frac{\partial w_0}{\partial x}\frac{\partial w_0}{\partial y}\right)+B_{12}\frac{\phi_x}{\partial x}+B_{22}\frac{\partial \phi_y}{\partial y}+B_{26}\left(\frac{\partial \phi_x}{\partial y}+\frac{\partial \phi_y}{\partial x}\right)\right\}\\
&+\frac{\partial w_0}{\partial x}\left\{A_{16}\left(\frac{\partial u_0}{\partial x}+\frac{1}{2}\left(\frac{\partial w_0}{\partial x}\right)^2\right)+A_{26}\left(\frac{\partial v_0}{\partial y}+\frac{1}{2}\left(\frac{\partial w_0}{\partial y}\right)^2\right)\right.\\
&+A_{66}\left(\frac{\partial u_0}{\partial y}+\frac{\partial v_0}{\partial x}+\frac{\partial w_0}{\partial x}\frac{\partial w_0}{\partial y}\right)+B_{16}\frac{\partial \phi_x}{\partial x}+B_{26}\frac{\partial \phi_y}{\partial y}\\
&\left.\left.+B_{66}\left(\frac{\partial \phi_x}{\partial y}+\frac{\partial \phi_y}{\partial x}\right)\right\}\right\}-\delta w_0 q\Bigg]\,dxdy-\oint_{\Gamma^e}V_n\delta w_0 ds
\end{aligned}
\tag{3.9}
$$

$$
\begin{aligned}
0 \;=\; &\int_{\Omega^e}\Bigg[\frac{\partial \delta\phi_x}{\partial x}\left\{B_{11}\left(\frac{\partial u_0}{\partial x}+\frac{1}{2}\left(\frac{\partial w_0}{\partial x}\right)^2\right)+B_{12}\left(\frac{\partial v_0}{\partial y}+\frac{1}{2}\left(\frac{\partial w_0}{\partial y}\right)^2\right)\right.\\
&+B_{16}\left(\frac{\partial u_0}{\partial y}+\frac{\partial v_0}{\partial x}+\frac{\partial w_0}{\partial x}\frac{\partial w_0}{\partial y}\right)+D_{11}\frac{\partial \phi_x}{\partial x}++D_{12}\frac{\partial \phi_y}{\partial y}\\
&\left.+D_{16}\left(\frac{\partial \phi_x}{\partial y}+\frac{\partial \phi_y}{\partial x}\right)\right\}+\frac{\partial \delta\phi_x}{\partial y}\left\{B_{16}\left(\frac{\partial u_0}{\partial x}+\frac{1}{2}\left(\frac{\partial w_0}{\partial x}\right)^2\right)\right.\\
&\left.+B_{26}\left(\frac{\partial v_0}{\partial y}+\frac{1}{2}\left(\frac{\partial w_0}{\partial y}\right)^2\right)+B_{66}\left(\frac{\partial u_0}{\partial y}+\frac{\partial v_0}{\partial x}+\frac{\partial w_0}{\partial x}\frac{\partial w_0}{\partial y}\right)\right.
\end{aligned}
$$

$$
\begin{aligned}
&+D_{16}\frac{\partial\phi_x}{\partial x}+D_{26}\frac{\partial\phi_y}{\partial y}+D_{66}\left(\frac{\partial\phi_x}{\partial y}+\frac{\partial\phi_y}{\partial x}\right)\Bigg\}\\
&+K_s\delta\phi_x\left(A_{55}\left(\phi_x+\frac{\partial w_0}{\partial x}\right)+A_{45}\left(\phi_y+\frac{\partial w_0}{\partial y}\right)\right)\Bigg]dxdy\\
&-\oint_{\Gamma^e}M_n\delta\phi_n ds
\end{aligned}
\tag{3.10}
$$

$$
\begin{aligned}
0 \;=\; &\int_{\Omega^e}\Bigg[\frac{\partial\delta\phi_y}{\partial y}\left\{B_{12}\left(\frac{\partial v_0}{\partial y}+\frac{1}{2}\left(\frac{\partial w_0}{\partial y}\right)^2\right)+B_{22}\left(\frac{\partial v_0}{\partial y}+\frac{1}{2}\left(\frac{\partial w_0}{\partial y}\right)^2\right)\right.\\
&+B_{26}\left(\frac{\partial u_0}{\partial y}+\frac{\partial v_0}{\partial x}+\frac{\partial w_0}{\partial x}\frac{\partial w_0}{\partial y}\right)+D_{12}\frac{\partial\phi_x}{\partial x}+D_{22}\frac{\partial\phi_y}{\partial y}\\
&\left.+D_{26}\left(\frac{\partial\phi_x}{\partial y}+\frac{\partial\phi_y}{\partial x}\right)\right\}+\frac{\partial\delta\phi_y}{\partial x}\left\{B_{16}\left(\frac{\partial u_0}{\partial x}+\frac{1}{2}\left(\frac{\partial w_0}{\partial x}\right)^2\right)\right.\\
&+B_{26}\left(\frac{\partial v_0}{\partial y}+\frac{1}{2}\left(\frac{\partial w_0}{\partial y}\right)^2\right)+B_{66}\left(\frac{\partial u_0}{\partial y}+\frac{\partial v_0}{\partial x}+\frac{\partial w_0}{\partial x}\frac{\partial w_0}{\partial y}\right)\\
.\quad &\left.+D_{16}\frac{\partial\phi_x}{\partial x}+D_{26}\frac{\partial\phi_y}{\partial y}+D_{66}\left(\frac{\partial\phi_x}{\partial y}+\frac{\partial\phi_y}{\partial x}\right)\right\}\\
&+K_s\delta\phi_y\left\{A_{45}\left(\phi_x+\frac{\partial w_0}{\partial x}\right)+A_{44}\left(\phi_y+\frac{\partial w_0}{\partial y}\right)\right\}\Bigg]dxdy\\
&-\oint_{\Gamma^e}M_s\delta\phi_s ds
\end{aligned}
\tag{3.11}
$$

And, the secondary variables are given as,

$$
\begin{aligned}
N_n = N_{xx}n_x + N_{xy}n_y, \qquad N_s = N_{xy}n_x + N_{yy}n_y\\
M_n = M_{xx}n_x + M_{xy}n_y, \qquad M_s = M_{xy}n_x + M_{yy}n_y
\end{aligned}
\tag{3.12}
$$

$$
V_n = \left(Q_x + N_{xx}\frac{\partial w_0}{\partial x} + N_{xy}\frac{\partial w_0}{\partial y}\right)n_x + \left(Q_y + N_{xy}\frac{\partial w_0}{\partial x} + N_{yy}\frac{\partial w_0}{\partial y}\right)n_y
$$

The laminate constitutive equations relate the force and moment resultant to strains in laminate coordinate system through ABD matrix.

$$\begin{Bmatrix} N_{xx} \\ N_{yy} \\ N_{xy} \end{Bmatrix} = \begin{bmatrix} A_{11} & A_{12} & A_{16} \\ A_{12} & A_{22} & A_{26} \\ A_{16} & A_{26} & A_{66} \end{bmatrix} \begin{Bmatrix} \frac{\partial u_0}{\partial x} + \frac{1}{2}\left(\frac{\partial w_0}{\partial x}\right)^2 \\ \frac{\partial v_0}{\partial y} + \frac{1}{2}\left(\frac{\partial w_0}{\partial y}\right)^2 \\ \frac{\partial u_0}{\partial y} + \frac{\partial v_0}{\partial x} + \left(\frac{\partial w_0}{\partial x}\frac{\partial w_0}{\partial y}\right) \end{Bmatrix} + \begin{bmatrix} B_{11} & B_{12} & B_{16} \\ B_{12} & B_{22} & B_{26} \\ B_{16} & B_{26} & B_{66} \end{bmatrix} \begin{Bmatrix} \frac{\partial \phi_x}{\partial x} \\ \frac{\partial \phi_y}{\partial y} \\ \frac{\partial \phi_x}{\partial y} + \frac{\partial phi_y}{\partial x} \end{Bmatrix} \tag{3.13}$$

$$\begin{Bmatrix} M_{xx} \\ M_{yy} \\ M_{xy} \end{Bmatrix} = \begin{bmatrix} B_{11} & B_{12} & B_{16} \\ B_{12} & B_{22} & B_{26} \\ B_{16} & B_{26} & B_{66} \end{bmatrix} \begin{Bmatrix} \frac{\partial u_0}{\partial x} + \frac{1}{2}\left(\frac{\partial w_0}{\partial x}\right)^2 \\ \frac{\partial v_0}{\partial y} + \frac{1}{2}\left(\frac{\partial w_0}{\partial y}\right)^2 \\ \frac{\partial u_0}{\partial y} + \frac{\partial v_0}{\partial x} + \left(\frac{\partial w_0}{\partial x}\frac{\partial w_0}{\partial y}\right) \end{Bmatrix} + \begin{bmatrix} D_{11} & D_{12} & D_{16} \\ D_{12} & D_{22} & D_{26} \\ D_{16} & D_{26} & D_{66} \end{bmatrix} \begin{Bmatrix} \frac{\partial \phi_x}{\partial x} \\ \frac{\partial \phi_y}{\partial y} \\ \frac{\partial \phi_x}{\partial y} + \frac{\partial \phi_y}{\partial x} \end{Bmatrix} \tag{3.14}$$

$$\begin{Bmatrix} Q_y \\ Q_x \end{Bmatrix} = K \begin{bmatrix} A_{44} & A_{45} \\ A_{45} & A_{55} \end{bmatrix} \begin{Bmatrix} \frac{\partial w_0}{\partial y} + \phi_y \\ \frac{\partial w_0}{\partial y} + \phi_y \end{Bmatrix} \tag{3.15}$$

$$(A_{ij}, B_{ij}, D_{ij}) = \sum_{k=1}^{N} \left(\overline{Q}_{ij}^{k} \left(z_{k+1} - z_k \right), \frac{1}{2} \overline{Q}_{ij}^{k} \left(z_{k+1}^2 - z_k^2 \right), \frac{1}{3} \overline{Q}_{ij}^{k} \left(z_{k+1}^3 - z_k^3 \right) \right)$$

$$(A_{44}, A_{45}, A_{55}) = \sum_{k=1}^{N} \left(\overline{Q}_{44}^{k}, \overline{Q}_{45}^{k}, \overline{Q}_{55}^{k} \right) \left(z_{k+1} - z_k \right) \tag{3.16}$$

In ABD matrix, A_{ij}, B_{ij} and D_{ij} represent extensional and shear, extensional-bending coupling and bending stiffness terms and Q_{ij}^{k}s are plane-stress reduced stiffness terms.

3.2 Geometrically Nonlinear Nurbs Isogeometric Finite Element Formulation

3.2.1 Displacement field approximation

The dependent displacement field variables are approximated by Nurbs basis as follows,

$$u_0(x, y) = \sum_{j=1}^{nCP} u_j R_j(x(\xi, \eta), y(\xi, \eta)), v_0(x, y) = \sum_{j=1}^{nCP} v_j R_j(x(\xi, \eta), y(\xi, \eta))$$

$$w_0(x, y) = \sum_{j=1}^{nCP} w_j R_j(x(\xi, \eta), y(\xi, \eta)) \tag{3.17}$$

$$\phi_x(x,y) = \sum_{j=1}^{nCP} \phi_{xj} R_j(x(\xi,\eta), y(\xi,\eta)), \phi_y(x,y) = \sum_{j=1}^{nCP} \phi_{yj} R_j(x(\xi,\eta), y(\xi,\eta))$$

where nCP are the number of control points per element and R_j are $2D$ Nurbs basis.

3.2.2 Nurbs Basis

In this section, h, p and k-refined Nurbs elements are derived. This subsection details the step by step B-spline and rational basis generation and describes the transformation from physical to parametric to parent domain using schematic iustration. h, p and k-refinement elements are constructed by different ways of modifying the knot vector by knot-insertion. Last part of this subsection describes the construction of various elements.

B-spline Basis

A knot vector in one dimension is a set of co-ordinates in the parametric space,
$\Xi = \{\xi_1, \xi_2, ..., \xi_{n+p+1}\}$, where ξ_i is the i^{th} knot, i is the knot index where $i = 1, 2, ..., n + p + 1$, p is the order of the polynomial and n is the number of basis functions. The order of the polynomial, $p = 0, 1, 2, 3....$, refer to the constant, linear, quadratic, cubic piecewise polynomials, respectively. If more than one knot is located at the same parametric co-ordinate, these are termed as repeated knots. In case of open knot vector, first and last knots are repeated $p+1$ times. Basis functions formed using open knot vector are interpolatory at the beginning and end of the parametric space interval, *i.e.* $[\xi_1, \xi_{n+p+1}]$. This distinguishes

the knots from the nodes in the finite element analysis as all the nodes are interpolatory. As a starting point, B-spline basis functions are defined recursively using Cox-Deboor algorithm, starting with piecewise constants ($p = 0$).

$$N_i^p(\xi) = \begin{cases} 1 & if\ \xi_i \leq \xi < \xi_{i+1}, \\ 0 & otherwise \end{cases} \tag{3.18}$$

And, subsequently, basis functions for orders $p = 1, 2, 3, ...$, are defined as follows,

$$N_i^p(\xi) = \frac{\xi - \xi_i}{\xi_{i+p} - \xi_i} N_i^{p-1}(\xi) + \frac{\xi_{i+p+1} - \xi}{\xi_{i+p+1} - \xi_{i+1}} N_{i+1}^{p-1}(\xi) \tag{3.19}$$

Rational B-spline (Nurbs) Basis

Nurbs basis are formed by a tensor product of B-spline basis in ξ and η direction and using projective weights associated with the control points. Rational basis are very similar to B-spline basis and derive the continuity and support for the functional from the knot vector. Also, Nurbs basis form a partition of unity and are pointwise non-negetive. These properties result in a strong convex hull property. Rational basis are formed as follows,

$$R_{i,j}^{p,q}(\xi, \eta) = \frac{N_i^p(\xi) M_j^q(\eta) W_{i,j}}{\sum_{i=1}^{CPw} \sum_{i=1}^{CPu} N_i^p(\xi) M_j^q(\eta) W_{i,j}} \approx R_k^p \{k = 1 : nCP\} \tag{3.20}$$

Nurbs surface is defined as,

$$S(x,y) = \sum_{j=1}^{CPw} \sum_{i=1}^{CPu} R_{i,j}^{p,q}(\xi,\eta) B_{i,j} \tag{3.21}$$

where $N_i^p(\xi)$ and $M_j^q(\eta)$ are the B-spline basis in ξ and η direction and $R_{i,j}^{p,q}$ denotes a 2D Nurbs basis function. CPw and CPu are the number of control points in ξ and η directions and $nCP = CPu \times CPw$ is the total number of control points per element. $W_{i,j}$s are the weights associated with the control points, $B_{i,j}$ and weights are the vertical coordinates of the corresponding control points. Here, weights are equal to one resulting in specialized form.

3.2.3 Numerical Integration

A multi-element patch, a tensor product of knot vectors in ξ and η directions, i.e. $\{0 \;\; 0 \;\; 0.5 \;\; 1 \;\; 1\}\times$ $\{0 \;\; 0 \;\; 0.5 \;\; 1 \;\; 1\}$, creates a 2×2 plate mesh in physical domain. Nurbs basis multiplied with respective control points constructs a geometric model of plate.

In order to perform numerical integration, Guass quadrature is employed. The integration on physical domain is performed by transformation from physical to parametric to parent domain and is performed over the index space. Index space is the space of a tensor product of knot vectors in $\hat{\xi}$ and $\hat{\eta}$ directions. The mapping between physical and parametric domain

is performed as follows,

$$\begin{Bmatrix} x \\ y \end{Bmatrix} = \sum_{k=1}^{nCP} R_k^1(\xi,\eta) \begin{Bmatrix} Bx_k \\ By_k \end{Bmatrix}$$

$$\begin{Bmatrix} \frac{\partial R_k^p}{\partial x} \\ \frac{\partial R_k^p}{\partial y} \end{Bmatrix} = [J^{-1}] \begin{Bmatrix} \frac{\partial R_k^p(\xi,\eta)}{\partial \xi} \\ \frac{\partial R_k^p(\xi,\eta)}{\partial \eta} \end{Bmatrix} \tag{3.22}$$

$$[J] = \begin{bmatrix} \frac{\partial x}{\partial \xi} & \frac{\partial y}{\partial \xi} \\ \frac{\partial x}{\partial \eta} & \frac{\partial y}{\partial \eta} \end{bmatrix}$$

Bx_k and By_k are control point coordinates and $J_{x\xi y\eta}$ is the mapping from physical to parametric domain. Mapping from parametric to parent domain is the standard mapping as is done in finite element. Figure 6.3 shows schematic of Isogeometric framework.

3.2.4 Nurbs Elements

Various lower and higher order Nurbs elements can be constructed by utilizing various element k-refinement techniques. 9LinNurbsKR^{1,2}/F (k-refined, 9 control point/element, linear Nurbs element with knot insertion at location 0.25 and 0 in knot vector respectively), 9QuadNurbs/(F/R) element with 9 control point/element, 16CubicNurbs/(F/R) and (k-refined) 16QuadNurbsKR/F with 16 control point/element and 25QuarticNurbs, 25Cubic-

NurbsKR/F and (k-refined) 25QuadNurbsKR/F with 25 control point/element are contructed. Element notation is as follows: number in the front denotes the number of control points/element, KR denotes the k-refined element and R or F denote reduced or full integration. For full integration, the number of quadrature points required is the smallest integer greater than or equal to $N = (1/2)(p+1)$, where p is the polynomial order. For k-refined element with full integration, the number of Gauss point required is equivalent to that of p-refined element with same number of control points. Here, some of the element constructed are described in detail.

Quadratic Nurbs Element (9QuadNurbs/(F/R))

A tensor product of knot vector $\{-1\ -1\ -1\ 1\ 1\ 1\}$ in $\hat{\xi}$ and $\hat{\eta}$ direction results in a bi-quadratic Nurbs element in the parent domain. $\hat{\xi}_i$ denote the i^{th} knot value in the knot vector. The element consists of 9 control points and require 3×3 (full integration) and 2×2 (reduced integration). For shear locking test, k-refined linear Nurbs elements with knot vector as $\{-1\ -1\ 0.25\ 1\ 1\}$ $(9LinNurbsKR^1) and \{-1\ -1\ 0\ 1\ 1\}$ $(9LinNurbsKR^2) with 2\times2$ Gauss integration are constructed in parent domain.

$$
\begin{aligned}
M_1^2(\hat{\xi}) &= \left(\frac{\hat{\xi}_4-\hat{\xi}}{\hat{\xi}_4-\hat{\xi}_2}\right)\left(\frac{\hat{\xi}_4-\hat{\xi}}{\hat{\xi}_4-\hat{\xi}_3}\right) \\
M_2^2(\hat{\xi}) &= \left(\frac{\hat{\xi}-\hat{\xi}_2}{\hat{\xi}_4-\hat{\xi}_2}\right)\left(\frac{\hat{\xi}_4-\hat{\xi}}{\hat{\xi}_4-\hat{\xi}_3}\right)+\left(\frac{\hat{\xi}_5-\hat{\xi}}{\hat{\xi}_5-\hat{\xi}_3}\right)\left(\frac{\hat{\xi}-\hat{\xi}_3}{\hat{\xi}_4-\hat{\xi}3}\right) \qquad \hat{\xi}_3 \le \hat{\xi} < \hat{\xi}_4 \\
M_3^2(\hat{\xi}) &= \left(\frac{\hat{\xi}-\hat{\xi}_3}{\hat{\xi}_5-\hat{\xi}_3}\right)\left(\frac{\hat{\xi}-\hat{\xi}}{\hat{\xi}_4-\hat{\xi}3}\right)
\end{aligned}
\tag{3.23}
$$

Similarly, the shape functions in $\hat{\eta}$ direction are obtained. The product rule yields the following bi-quadratic shape functions,

$$\begin{aligned}
&R_1^2(\hat{\xi},\hat{\eta}) = M_1^2(\hat{\xi})N_1^2(\hat{\eta}) \quad R_2^2(\hat{\xi},\hat{\eta}) = M_1^2(\hat{\xi})N_2^2(\hat{\eta}) \quad R_3^2(\hat{\xi},\hat{\eta}) = M_1^2(\hat{\xi})N_3^2(\hat{\eta}) \\
&R_4^2(\hat{\xi},\hat{\eta}) = M_2^2(\hat{\xi})N_1^2(\hat{\eta}) \quad R_5^2(\hat{\xi},\hat{\eta}) = M_2^2(\hat{\xi})N_2^2(\hat{\eta}) \quad R_6^2(\hat{\xi},\hat{\eta}) = M_2^2(\hat{\xi})N_3^2(\hat{\eta}) \\
&R_7^2(\hat{\xi},\hat{\eta}) = M_3^2(\hat{\xi})N_1^2(\hat{\eta}) \quad R_8^2(\hat{\xi},\hat{\eta}) = M_3^2(\hat{\xi})N_2^2(\hat{\eta}) \quad R_9^2(\hat{\xi},\hat{\eta}) = M_3^2(\hat{\xi})N_3^2(\hat{\eta})
\end{aligned} \tag{3.24}$$

Figure 3.3 shows Nurbs basis in $\hat{\xi}$ and $\hat{\eta}$ directions along with the parent element.

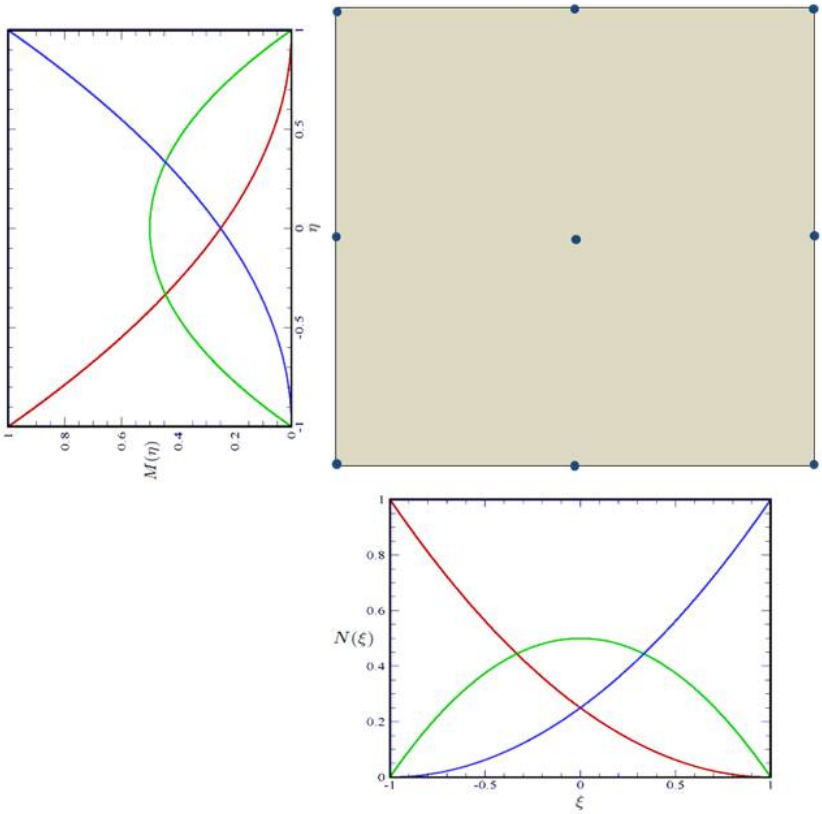

Figure 3.3: Quadratic Nurbs element with basis functions in each direction

k-refined Quadratic Nurbs element I(16QuadNurbsKR/F)

A tensor product of knot vector $\{-1\ -1\ -1\ 0\ 1\ 1\ 1\}$ in $\hat{\xi}$ and $\hat{\eta}$ direction results in a bi-quadratic Nurbs element in the parent domain. The knot vector is divided into two intervals and shape functions have unique value over each interval. $\hat{\xi}_i$ denote the i^{th} knot value in the knot vector. The shape functions in $\hat{\xi}$ direction over each interval are derived as follows,

$$\begin{aligned}
M_1^2(\hat{\xi}) &= \left(\frac{\hat{\xi}_4-\hat{\xi}}{\hat{\xi}_4-\hat{\xi}_2}\right)\left(\frac{\hat{\xi}_4-\hat{\xi}}{\hat{\xi}_4-\hat{\xi}_3}\right) \\
M_2^2(\hat{\xi}) &= \left(\frac{\hat{\xi}-\hat{\xi}_2}{\hat{\xi}_4-\hat{\xi}_2}\right)\left(\frac{\hat{\xi}4-\hat{\xi}}{\hat{\xi}_4-\hat{\xi}_3}\right)+\left(\frac{\hat{\xi}_5-\hat{\xi}}{\hat{\xi}_5-\hat{\xi}_3}\right)\left(\frac{\hat{\xi}-\hat{\xi}_3}{\hat{\xi}_4-\hat{\xi}3}\right) \qquad \hat{\xi}_3 \le \hat{\xi} < \hat{\xi}_4 \\
M_3^2(\hat{\xi}) &= \left(\frac{\hat{\xi}-\hat{\xi}_3}{\hat{\xi}_5-\hat{\xi}_3}\right)\left(\frac{\hat{\xi}-\hat{\xi}}{\hat{\xi}_4-\hat{\xi}3}\right) \\
M_4^2(\hat{\xi}) &= 0
\end{aligned} \tag{3.25}$$

$$\begin{aligned}
M_1^2(\hat{\xi}) &= 0 \\
M_2^2(\hat{\xi}) &= \left(\frac{\hat{\xi}_5-\hat{\xi}}{\hat{\xi}_5-\hat{\xi}_3}\right)\left(\frac{\hat{\xi}_5-\hat{\xi}}{\hat{\xi}_5-\hat{\xi}_4}\right) \\
M_3^2(\hat{\xi}) &= \left(\frac{\hat{\xi}-\hat{\xi}_3}{\hat{\xi}_5-\hat{\xi}_3}\right)\left(\frac{\hat{\xi}-\hat{\xi}}{\hat{\xi}_4-\hat{\xi}3}\right)+\left(\frac{\hat{\xi}-\hat{\xi}_3}{\hat{\xi}_5-\hat{\xi}_3}\right)\left(\frac{\hat{\xi}_5-\hat{\xi}}{\hat{\xi}_5-\hat{\xi}_3}\right) \qquad \hat{\xi}_4 \le \hat{\xi} < \hat{\xi}_5 \\
M_4^2(\hat{\xi}) &= \left(\frac{\hat{\xi}-\hat{\xi}_4}{\hat{\xi}_6-\hat{\xi}_4}\right)\left(\frac{\hat{\xi}_4-\hat{\xi}}{\hat{\xi}_5-\hat{\xi}_4}\right)
\end{aligned} \tag{3.26}$$

Similarly, the shape functions in the $\hat{\eta}$ direction are obtained. The product rule yields the 16 bi-quadratic shape functions, R_k^2, requiring 4×4 Gauss points. In k-refinement process, the order of the existing knot vector is elevated first and then, a knot is inserted instead of

elevating the order after knot insertion. This results in $q-1$ continuous derivatives instead of $p-1$ continuous derivatives, where p and q are the order of the knot vector before and after the order elevation, respectively. Figure 3.4 shows k-refined, quadratic Nurbs element in the parent domain and Nurbs basis in each direction.

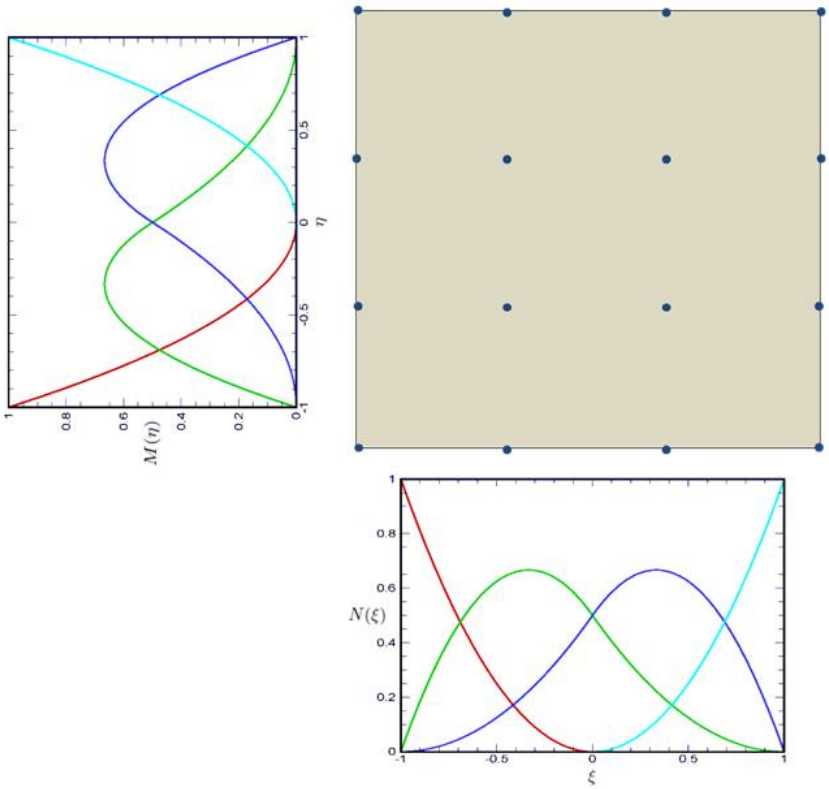

Figure 3.4: k-refined Quadratic Nurbs element with basis functions in each direction

k-refined Quadratic Nurbs element II(25QuadNurbsKR/F)

A tensor product of knot vector $\{-1\ -1\ -1\ -0.5\ 0.5\ 1\ 1\ 1\}$ in $\hat{\xi}$ and $\hat{\eta}$ direction results in a k-refined, bi-quadratic Nurbs element in parent domain. The knot vector is divided into

three knot intervals and shape functions have unique value over each interval. $\hat{\xi}_i$ denote the i^{th} knot value in the knot vector. The shape functions in $\hat{\xi}$ direction, over each interval, are derived as follows,

$$\begin{aligned}
M_1^2(\hat{\xi}) &= \left(\frac{\hat{\xi}_4 - \hat{\xi}}{\hat{\xi}_4 - \hat{\xi}_2}\right)\left(\frac{\hat{\xi}_4 - \hat{\xi}}{\hat{\xi}_4 - \hat{\xi}_3}\right) \\
M_2^2(\hat{\xi}) &= \left(\frac{\hat{\xi} - \hat{\xi}_2}{\hat{\xi}_4 - \hat{\xi}_2}\right)\left(\frac{\hat{\xi}_4 - \hat{\xi}}{\hat{\xi}_4 - \hat{\xi}_3}\right) + \left(\frac{\hat{\xi}_5 - \hat{\xi}}{\hat{\xi}_5 - \hat{\xi}_3}\right)\left(\frac{\hat{\xi} - \hat{\xi}_3}{\hat{\xi}_4 - \hat{\xi}_3}\right) \qquad \hat{\xi}_3 \le \hat{\xi} < \hat{\xi}_4 \\
M_3^2(\hat{\xi}) &= \left(\frac{\hat{\xi} - \hat{\xi}_3}{\hat{\xi}_5 - \hat{\xi}_3}\right)\left(\frac{\hat{\xi} - \hat{\xi}_3}{\hat{\xi}_4 - \hat{\xi}3}\right) \\
M_4^2(\hat{\xi}) &= 0 \\
M_5^2(\hat{\xi}) &= 0
\end{aligned} \tag{3.27}$$

$$\begin{aligned}
M_1^2(\hat{\xi}) &= 0 \\
M_2^2(\hat{\xi}) &= \left(\frac{\hat{\xi}_5 - \hat{\xi}}{\hat{\xi}_5 - \hat{\xi}_3}\right)\left(\frac{\hat{\xi}_5 - \hat{\xi}}{\hat{\xi}_5 - \hat{\xi}_4}\right) \\
M_3^2(\hat{\xi}) &= \left(\frac{\hat{\xi} - \hat{\xi}_3}{\hat{\xi}_5 - \hat{\xi}_3}\right)\left(\frac{\hat{\xi}_5 - \hat{\xi}}{\hat{\xi}_5 - \hat{\xi}_4}\right) + \left(\frac{\hat{\xi}_6 - \hat{\xi}}{\hat{\xi}_6 - \hat{\xi}_4}\right)\left(\frac{\hat{\xi} - \hat{\xi}_4}{\hat{\xi}_5 - \hat{\xi}_4}\right) \qquad \hat{\xi}_4 \le \hat{\xi} < \hat{\xi}_5 \\
M_4^2(\hat{\xi}) &= \left(\frac{\hat{\xi} - \hat{\xi}_4}{\hat{\xi}_6 - \hat{\xi}_4}\right)\left(\frac{\hat{\xi} - \hat{\xi}_4}{\hat{\xi}_5 - \hat{\xi}_4}\right) \\
M_5^2(\hat{\xi}) &= 0
\end{aligned} \tag{3.28}$$

$$
\begin{aligned}
M_1^2(\hat{\xi}) &= 0 \\
M_2^2(\hat{\xi}) &= 0 \\
M_3^2(\hat{\xi}) &= \left(\frac{\hat{\xi}_6 - \hat{\xi}}{\hat{\xi}_6 - \hat{\xi}_4}\right)\left(\frac{\hat{\xi}_6 - \hat{\xi}}{\hat{\xi}_6 - \hat{\xi}_5}\right) \\
M_4^2(\hat{\xi}) &= \left(\frac{\hat{\xi}_7 - \hat{\xi}}{\hat{\xi}_7 - \hat{\xi}_5}\right)\left(\frac{\hat{\xi} - \hat{\xi}_5}{\hat{\xi}_6 - \hat{\xi}_5}\right) \qquad \hat{\xi}_5 \leq \hat{\xi} < \hat{\xi}_6 \\
M_5^2(\hat{\xi}) &= \left(\frac{\hat{\xi} - \hat{\xi}_5}{\hat{\xi}_7 - \hat{\xi}_5}\right)\left(\frac{\hat{\xi} - \hat{\xi}_5}{\hat{\xi}_6 - \hat{\xi}_5}\right)
\end{aligned} \tag{3.29}
$$

The element consists of 25 control functions and require 5×5 Gauss integration points. The derivatives are $q-1$ continuous instead of $p-1$ continuous. Figure 3.5 shows the Nurbs element and the basis in $\hat{\xi}$ and $\hat{\eta}$ directions.

Quartic Nurbs element (25QuarticNurbs/F)

A tensor product of knot vector, $\{-1\ -1\ -1\ -1\ -1\ 1\ 1\ 1\ 1\ 1\}$ in $\hat{\xi}$ and $\hat{\eta}$ directions result in a bi-quartic Nurbs element in the parent domain. Quartic Nurbs element consists of 25 control points and requires 5×5 Gauss points. It is equivalent to 25QuadNurbsKR/F element in terms of number of control points/element and Gauss integration points. The shape functions in explicit form are not provided here. Figure 3.6 shows the Nurbs element and basis in $\hat{\xi}$ and $\hat{\eta}$ directions.

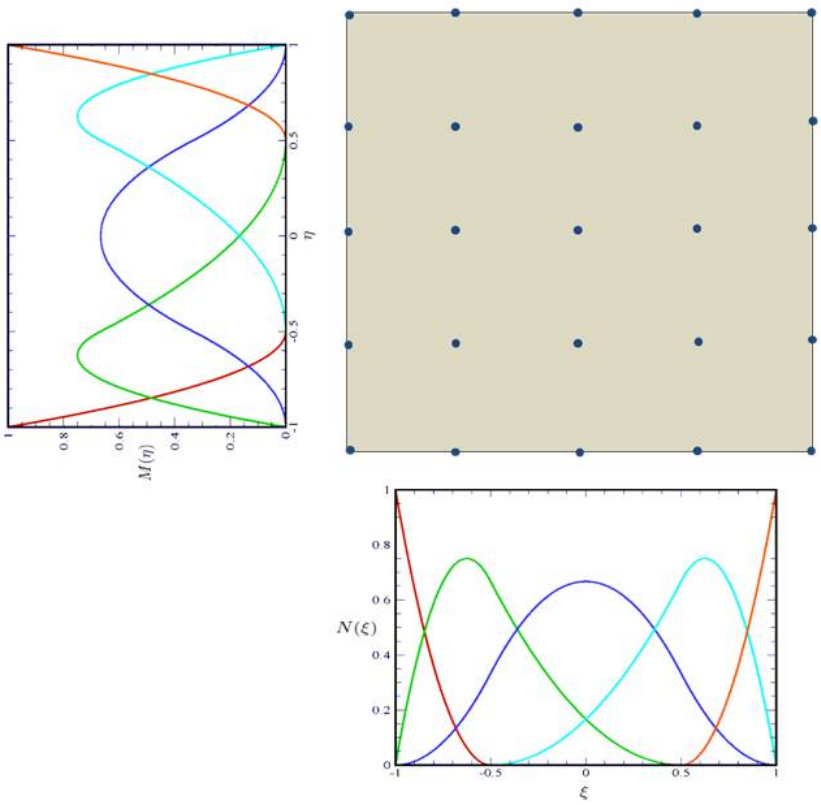

Figure 3.5: k-refined Quadratic Nurbs element with basis functions in each direction

3.2.5 Geometric nonlinear stiffness matrix

Substituting the displacement field approximation into the weak form, we obtain element stiffness matrix and load vector. The size of a sub-matrix, K^{11}, in element stiffness matrix, is $(nCP) \times (nCP)$ and the size of element load vector, F, is $(nCP \times dof, 1)$. nCP stands for control points per element and dof are the number of degrees of freedom /control point. Parameters, α and β are the degrees of freedom per control point.

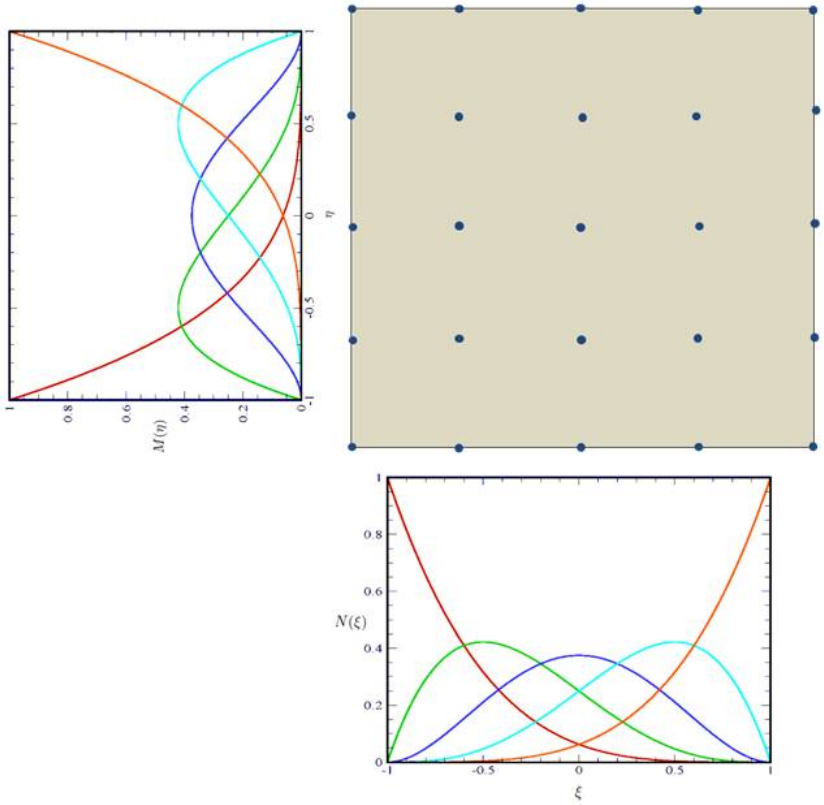

Figure 3.6: Quartic Nurbs element with basis functions in each direction

$$\left[K^{\alpha\beta}\right] = \begin{bmatrix} [K^{11}] & [K^{12}] & [K^{13}] & [K^{14}] & [K^{15}] \\ [K^{21}] & [K^{22}] & [K^{23}] & [K^{24}] & [K^{25}] \\ [K^{31}] & [K^{32}] & [K^{33}] & [K^{34}] & [K^{35}] \\ [K^{41}] & [K^{43}] & [K^{43}] & [K^{44}] & [K^{45}] \\ [K^{51}] & [K^{52}] & [K^{53}] & [K^{54}] & [K^{55}] \end{bmatrix} \tag{3.30}$$

$$F_i^{\alpha=3} = \int_{\Omega^e} qR_i^p dxdy \tag{3.31}$$

From the element stiffness matrix, the expression for K^{11}, a sub-matrix of element stiffness matrix, K, is as follows,

$$K_{ij}^{11}(x,y) = \int_{\Omega^e} \left[A_{11} \frac{\partial R_i^p}{\partial x} \frac{\partial R_j^p}{\partial x} + A_{66} \frac{\partial R_i^p}{\partial y} \frac{\partial R_j^p}{\partial y} + A_{16} \left(\frac{\partial R_i^p}{\partial x} \frac{\partial R_j^p}{\partial y} + \frac{\partial R_i^p}{\partial y} \frac{\partial R_j^p}{\partial x} \right) \right] dxdy \quad (3.32)$$

The equation of motion can be written in the matrix form as,

$$[K]\{\Delta\} = \{F\} \quad (3.33)$$

The solution of nonlinear equations is obtained by Newton-Raphson iterative process as follows,

$$\{R\}(\{\Delta\}) = \left[K^T(\{\Delta\})\right]\{\Delta\} - \{F\} = 0 \quad (3.34)$$

Tangent stiffness matrix is obtained as,

$$K_{ij}^{T,\alpha\beta} = \frac{\partial R_i^\alpha}{\partial \Delta_j^\beta}$$

$$K_{ij}^{T,\alpha\beta} = \frac{\partial}{\partial \Delta_j^\beta} \left(\sum_{\gamma=1}^{5} \sum_{k=1}^{nCP} K_{ik}^{\alpha\gamma} \Delta_k^\gamma - F_i^\alpha \right) \quad (3.35)$$

For example, a sub-matrix in element tangent stiffness matrix is,

$$K_{ij}^{T,33} = \sum_{\gamma=1}^{5} \sum_{k=1}^{nCP} \frac{\partial K_{ik}^{3\gamma}}{\partial w_j} \Delta_k^\gamma + K_{ij}^{33} \quad (3.36)$$

The incremental displacement vector is given as,

$$\{\delta\Delta\} = -[K^T(\{\Delta\}^r)]^{-1}\{R\}^r \tag{3.37}$$

And, total displacement vector is obtained as,

$$\{\Delta\}^{r+1} = \{\Delta\}^r + \{\delta\Delta\} \tag{3.38}$$

K^T and R are the tangent stiffness and residual load vector. At the beginning of iteration, $r = 0$ and nonlinear stiffness terms reduces to zero. The iterative process is continued till the convergence is obtained within the error tolerance of 10^{-3}. The error norm used for convergence is as follows,

$$\sqrt{\frac{\sum_{I=1}^{N}\left|\Delta_I^{r+1} - \Delta_I^r\right|^2}{\sum_{I=1}^{N}\left|\Delta_I^{r+1}\right|^2}} < 10^{-3} \tag{3.39}$$

3.3 Numerical Testing

Isotropic, orthotropic and laminated composite plates are studied here. Geometric nonlinearity is accounted for in von-Karman sense, including membrane-bending coupling effects. Several, thin and moderately thick, isotropic, orthotropic and laminated composite plate examples are studied for the validation purposes. Different boundary conditions, plate to thickness ratios and ply angles are considered. Due to bi-axial symmetry, only a quadrant of the plate is modeled and the center deflections are computed and validated with the liter-

ature. The computed center deflection is normalised as $\overline{w} = w/h$. Three different boundary conditions are considered for the analysis.

$$SS1 : v_0 = w_0 = \phi_y = 0, at \quad x = a/2;$$

$$u_0 = w_0 = \phi_x = 0, at \quad y = b/2$$

$$SS3 : u_0 = v_0 = w_0 = 0 \quad at \quad x = a/2, y = b/2$$

$$Clamped : u_0 = v_0 = w_0 = \phi_x = \phi_y = 0; \quad at \quad x = a/2 \quad and \quad y = b/2$$

$$symmetry \quad B.C., \quad x = 0, \quad u_0 = \phi_x = 0$$

$$y = 0, \quad v_0 = \phi_y = 0$$

3.3.1 Clamped Isotropic plate under uniform loading

In this example, a thin $a/h = 100$, clamped, isotropic square plate under uniform loading is analyzed. The plate length and thickness are $a = 300\ in$ and $h = 3\ in$ respectively and the material properties are $E_1 = 30E6\ psi$ and $\nu = 0.316$. The center deflection of a quarter plate is computed and is validated with Levy's analytical([110]) and Urthaler and Reddy([39])'s mixed finite element solution. Levy's solution is considered as a benchmark solution for validating geometrically nonlinear analysis of thin plates. For most of the elements tested, solution converged well with the analytical and Reddy's mixed finite element solution. Urthaler and Reddy[39] required 4×4 mesh of 9 node quadratic element with 7 dof/node to compute the center deflection while 9QuadNurbs/R required 2×2 mesh with 5 dof/control point. From the integration point of view, quadratic and cubic Nurbs, with reduced integration produced equivalent center deflection and higher-order p and k-refined

Nurbs element performed equally well using full integration. Similarly, k-refined quadratic Nurbs elements (25QuadNurbsKR and 16QuadNurbsKR) with full integration produced the equivalent center deflection as its counterpart 9QuadNurbs/R element did with reduced integration. Table 3.1 and Fig. 3.7 give the load vs deflection data and the curve, respectively.

Next, the % error in center displacement w.r.t Levy's solution in nonlinear analysis is plotted for 9LinNurbsKR^2 and quadratic Nurbs elements. % error is greater in the case of 9QuadNurbs/F as compared with 9QuadNurbs/R due to slenderness of the plate. Linear Nurbs element, 9LinNurbsKR^2, seems to perform well due to increased smoothness of basis function in solution space. Figure 3.8 shows the % error in nonlinear deflection for increasing loads.

Load, $\bar{p}$	Levy's Analytical	MXFEM/Reddy	9QuadNurbs/R	16QuadNurbsKR	25QuadNurbsKR
0	0	0	0	0	0
17.8	0.237	0.2392	0.2393	0.2354	0.2328
38.3	0.471	0.4738	0.4741	0.4678	0.4635
63.4	0.695	0.6965	0.6975	0.6951	0.6854
95	0.912	0.9087	0.9103	0.9036	0.8985
134.9	1.1210	1.1130	1.1148	1.1092	1.1045
184	1.323	1.308	1.3101	1.3059	1.302
245	1.521	1.501	1.5024	1.4942	1.4969
318	1.714	1.688	1.6885	1.6758	1.6856
402	1.902	1.866	1.8657	1.8662	1.8652

Table 3.1: Comparison of various Nurbs elements, including k-refined with analytical solution for clamped, isotropic plate under uniform loading

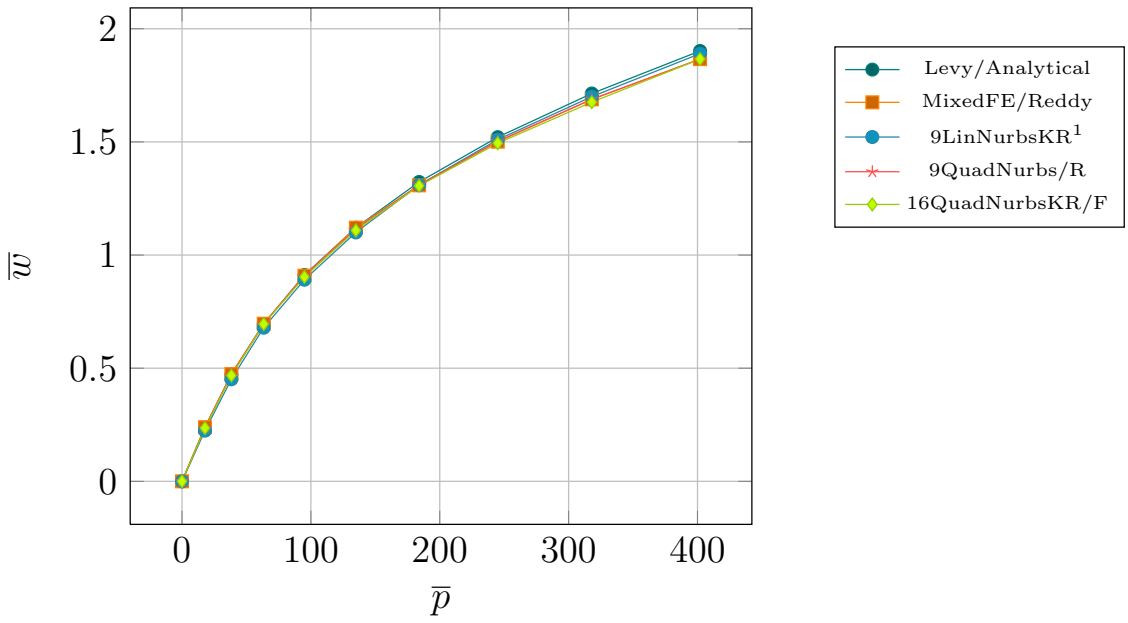

Figure 3.7: Load vs deflection curve for a clamped, isotropic plate under increasing uniform load

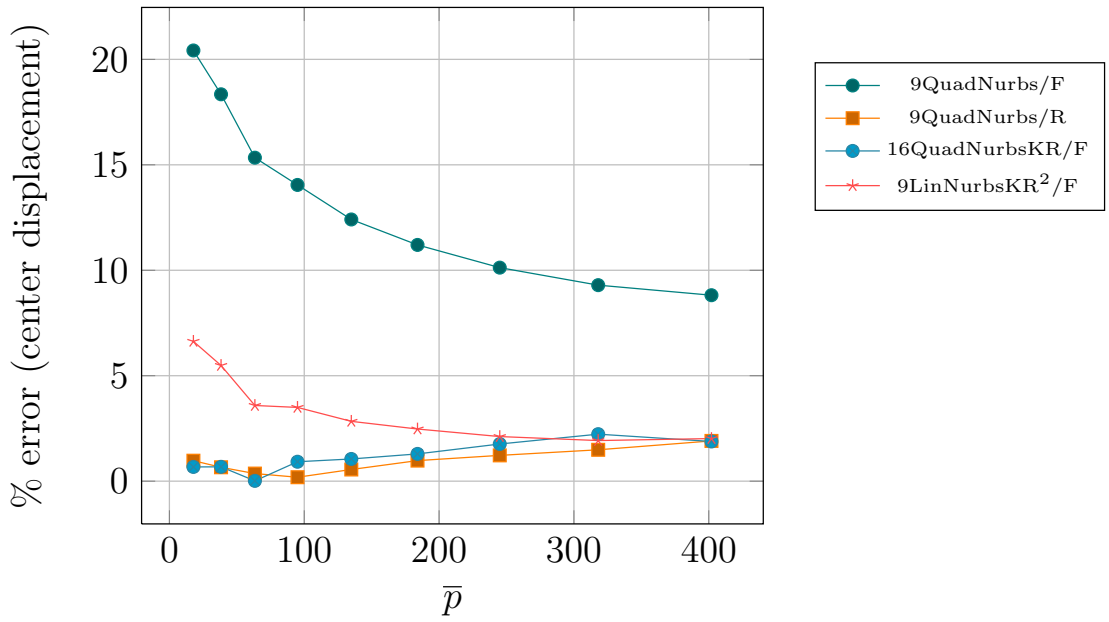

Figure 3.8: % error in displacement w.r.t Levy's analytical solution for various Nurbs elements for 2×2 mesh in nonlinear analysis

3.3.2 Shear Locking Test for Thin Plates

Shear locking is the over constraining of element stiffness matrix as the side to thickness ratio become large, resulting in underestimation of displacement. Shear locking test for linear analysis is performed with h-refined linear and quadratic Nurbs element for various a/h ratios and % error in nonlinear displacement w.r.t to Levy's solution for slender plates is analyzed.

A square plate with length, $L = 10$ and material properties as $E = 10.92$ and $\nu = 0.3$ with simply-supported boundary condition $SS1$ under uniform loading for various a/h ratios is analyzed. % error in center displacement w.r.t reference solution is computed to study the shear locking effects. Figures 3.9 and 3.10 shows shear locking effect for increasing a/h ratios for 2×2 and 3×3 meshes. Most of the elements perform well for increasing a/h ratios. In case of k-refined linear Nurbs element, addition of a knot in the knot vector provide increased smoothness and seems to remove numerical ill-conditioning effects. Quadratic Nurbs element also performs excellently with full and reduced integration for linear problem.

3.3.3 Simply Supported Isotropic plate under uniform loading

A square plate with length, $L = 10$ in, thickness, $h = 1$ in and material properties $E_1 = 7.8E6$ *psi* and $\nu = 0.3$ with simply-supported boundary conditions, $SS1$ and $SS3$, under uniform

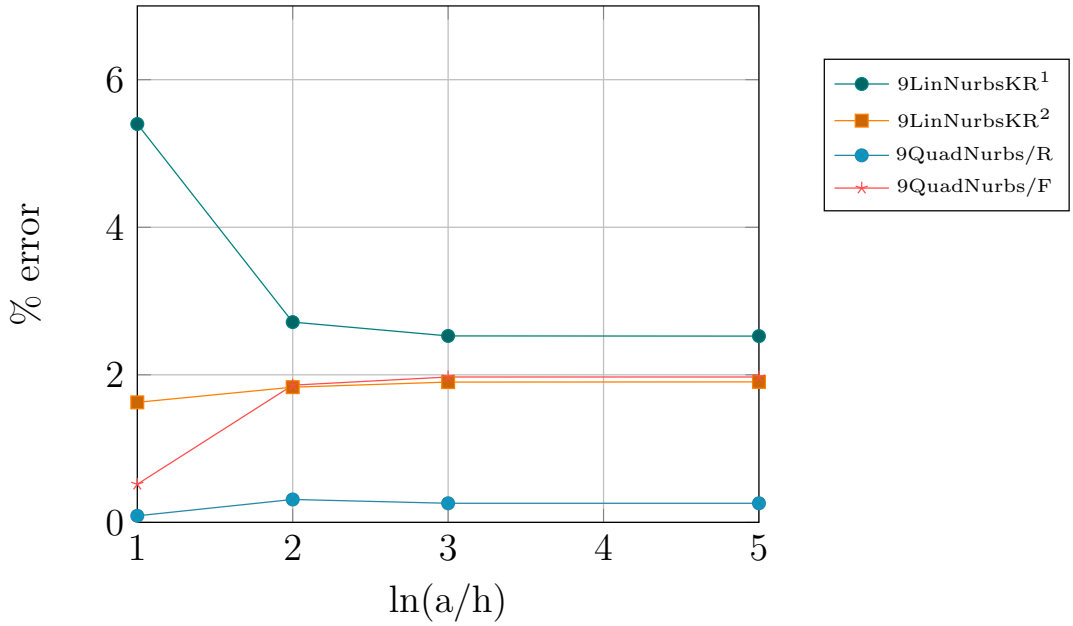

Figure 3.9: Shear locking test for various Nurbs elements for 2×2 mesh

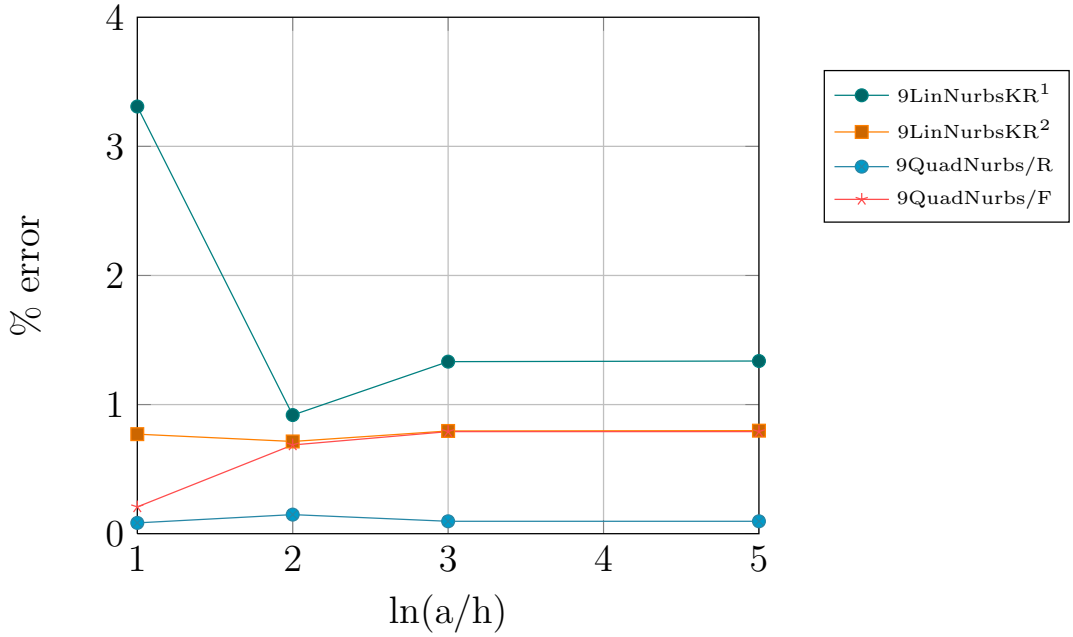

Figure 3.10: Shear locking test for various Nurbs elements for 3×3 mesh

loading is considered here. The computed center deflection is compared with Reddy and Putcha([40])'s solution. Tables 3.2, 3.3 and 3.4 show the center deflection data for various Nurbs elements under increasing load. 9QuadraticNurbs/R element (4 elements, 25 control

point, 125 degrees of freedom) is in an excellent agreement with 4×4 mesh (16 elements, 81 nodes and 405 dof) 9QuadraticReddy/(F/R) finite element analysis. Also, the center deflection values computed using h, p and k-refined Nurbs element converge to the required solution. The load vs deflection curve for $SS3$ boundary condition with full and reduced integration and for $SS1$ boundary condition with full integration are shown in Figs. 3.11, 3.12 and 3.13 respectively. It is observed that $SS3$ boundary constraint results in a lower deflection than $SS1$ boundary condition.

Load, $\bar{P}$	FE/Reddy	9QuadNurbs	9QuadNurbsHR	25QuarticNurbs	25QuadNurbsKR
0	0	0	0	0	0
6.25	0.278	0.2735	0.2752	0.2778	0.2802
12.5	0.4619	0.4575	0.459	0.4617	0.4645
25	0.6902	0.6874	0.6879	0.6899	0.6925
50	0.957	0.9563	0.9563	0.9566	0.9586
75	1.133	1.1337	1.132	1.1326	1.1342
100	1.2686	1.2702	1.2679	1.2682	1.2694
125	1.3809	1.382	1.3803	1.3803	1.3813
150	1.4774	1.4802	1.4771	1.4769	1.4776
175	1.5629	1.5661	1.5627	1.5624	1.5629
200	1.6399	1.6437	1.6399	1.6395	1.6398

Table 3.2: Center deflection (F) vs load values of a simply supported (SS3) isotropic square plate under uniform loading

Load, $\bar{P}$	FE/Reddy	9QuadNurbs	9QuadNurbsHR	25QuarticNurbs	16QuadNurbsKR
0	0	0	0	0	0
6.25	0.279	0.2784	0.278	0.278	0.2811
12.5	0.463	0.4626	0.4618	0.4619	0.4681
25	0.6911	0.691	0.6897	0.6901	0.7007
50	0.9575	0.9579	0.9561	0.9567	0.9728
75	1.1333	1.1339	1.1319	1.1327	1.1524
100	1.2688	1.2696	1.2674	1.2683	1.2907
125	1.3809	1.3817	1.3794	1.3804	1.4051
150	1.4774	1.4783	1.476	1.477	1.5036
175	1.5628	1.5638	1.5614	1.5625	1.5909
200	1.6398	1.6408	1.6385	1.6396	1.6695

Table 3.3: Center deflection (R) of a simply supported (SS3) isotropic square plate under uniform loading

Load, $\bar{P}$	FE/Reddy	9QuadNurbs	9QuadNurbsHR	25QuarticNurbs	16QuadNurbsKR
0	0	0	0	0	0
6.25	0.2812	0.284	0.2836	0.2842	0.2854
12.5	0.5185	0.5244	0.5229	0.524	0.5256
25	0.8672	0.879	0.8725	0.8765	0.8778
50	1.3147	1.3341	1.3267	1.3296	1.3294
75	1.6237	1.6467	1.6385	1.6433	1.6411
100	1.8679	1.8918	1.8849	1.8921	1.8876
125	2.0746	2.0967	2.0925	2.1028	2.0957
150	2.2549	2.2744	2.274	2.2881	2.2779
175	2.4168	2.4322	2.4364	2.455	2.4414
200	2.5645	2.5747	2.5841	2.608	2.5903

Table 3.4: Center deflection of a simply supported (SS1/F) isotropic square plate under uniform loading

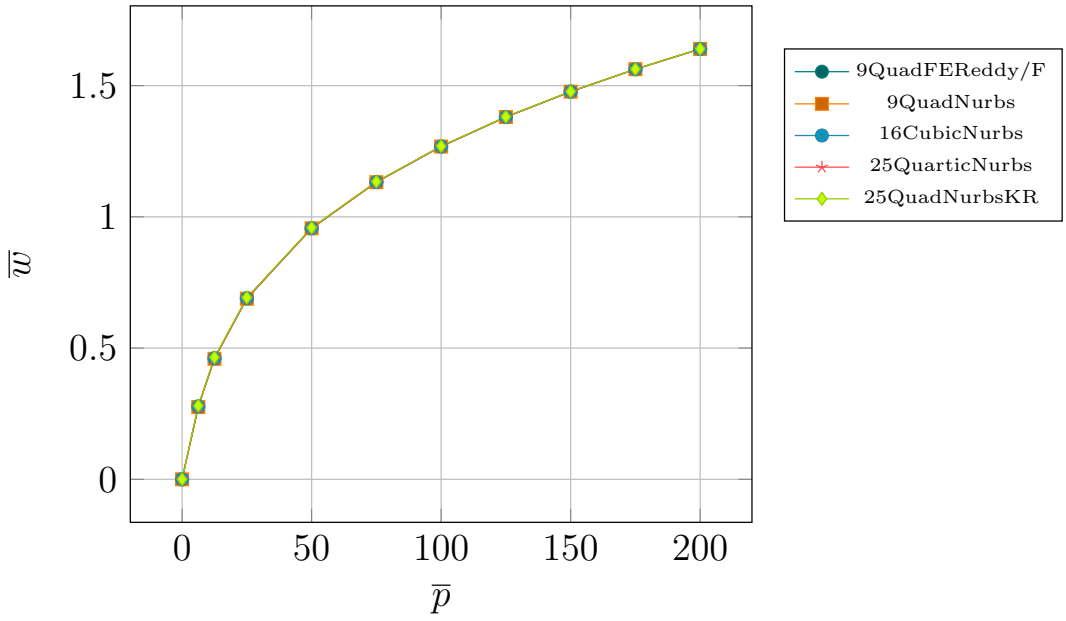

Figure 3.11: Load vs deflection curve for a simply supported (SS3/F), isotropic plate under increasing uniform load

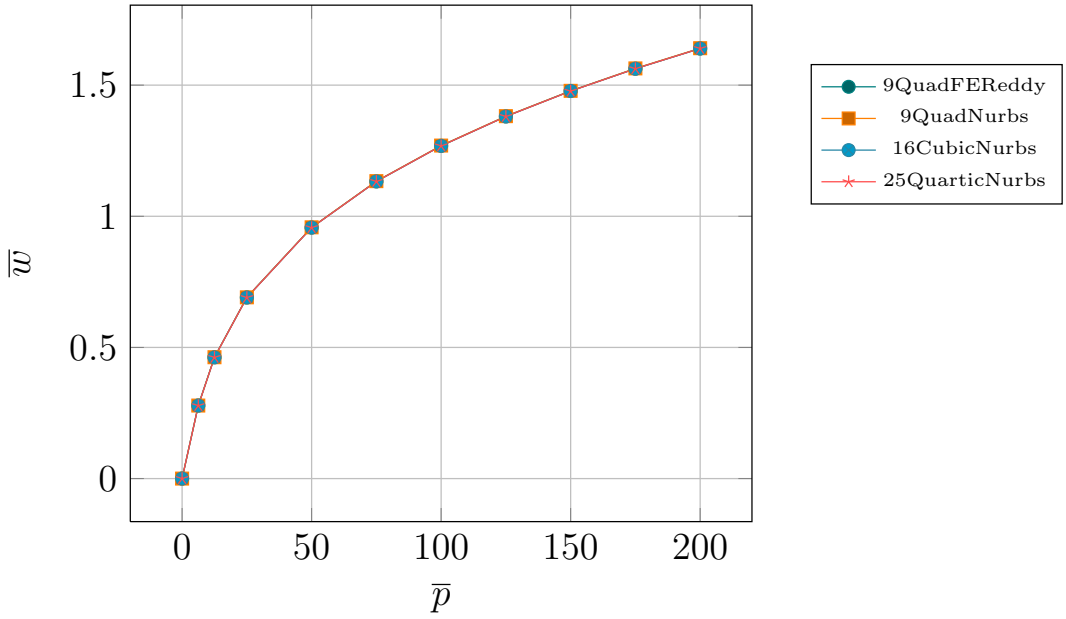

Figure 3.12: Load vs deflection curve for a simply supported (SS3/R), isotropic plate under increasing uniform load

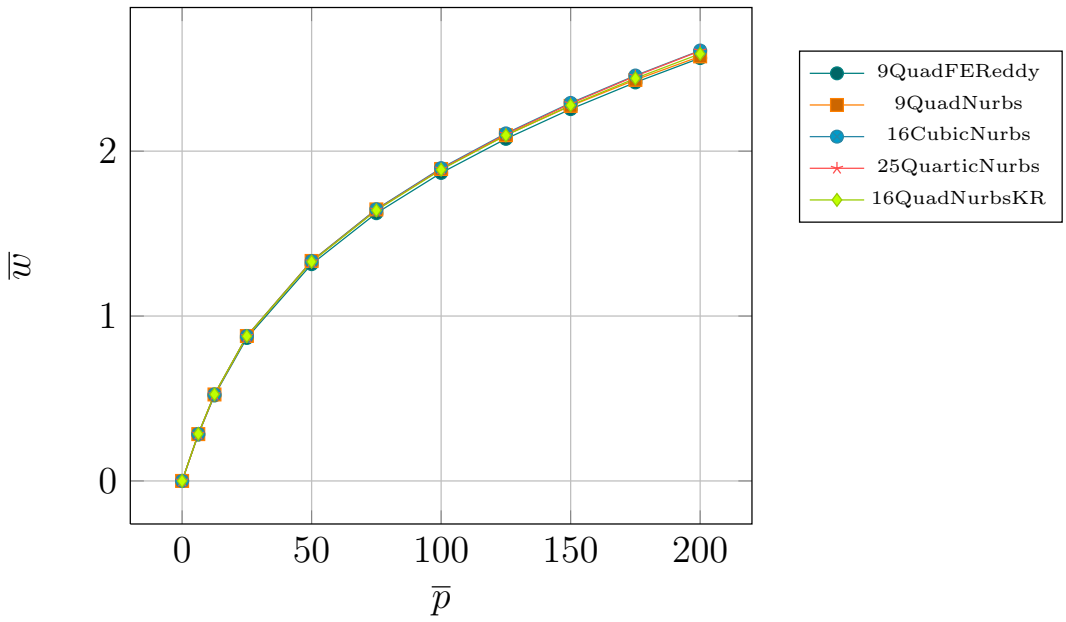

Figure 3.13: Load vs deflection curve for a simply supported (SS1/F), isotropic plate under increasing uniform load

3.3.4 Square, symmetric cross-ply (0/90/90/0) laminated composite plate under uniform loading

A square, symmetric cross-ply (0/90/90/0) laminated composite plate subjected to uniform loading is considered. The dimensions of the plate are $a = 12$ in, thickness, $t = 0.096$ in and the material properties are $E_1 = 1.8282e6$ psi, $E_2 = 1.8315e6$ psi, $G_{12} = G_{13} = G_{23} = 0.3125e6$ psi and $\nu = 0.2395$. The center deflection computed using h, p and k-refined Nurbs elements compare well with those in the literature. The center deflection computed using Nurbs quadratic element is in excellent agreement with Reddy's finite element solution ([116]) and requires a lesser number of degrees of freedom. Also, the center deflection is found to be closer to the experimental curve than Reddy and Putcha([40]) and Zhang([54])'s deflection response. Table 3.5 and fig. 3.14 shows load vs deflection data and curve.

Load, $\bar{P}$	FE/Reddy	9QuadNurbs/R	9QuadNurbsHR/R	16CubicNurbs/F	25QuarticNurbs/F
0	0	0	0	0	0
0.2	0.3773	0.3815	0.3781	0.3773	0.3773
0.4	0.6504	0.6573	0.6517	0.6503	0.6504
0.6	0.8489	0.8574	0.8504	0.8486	0.8488
0.8	1.0039	1.0134	1.0054	1.0035	1.00376
1	1.1316	1.142	1.1331	1.131	1.1314
1.2	1.2406	1.2512	1.242	1.24	1.2405
1.4	1.3362	1.3471	1.3378	1.3356	1.3361
1.6	1.4216	1.4328	1.423	1.4211	1.4216
1.8	1.4991	1.5105	1.5007	1.4985	1.4991
2	1.5701	1.58175	1.5717	1.5696	1.5702
2.2	1.6359	1.6477	1.6375	1.6354	1.636
2.4	1.6972	1.7092	1.6988	1.69667	1.6974

Table 3.5: Center deflection(F) of a clamped, square, cross-ply (0/90/90/0), laminated composite plate under uniform loading

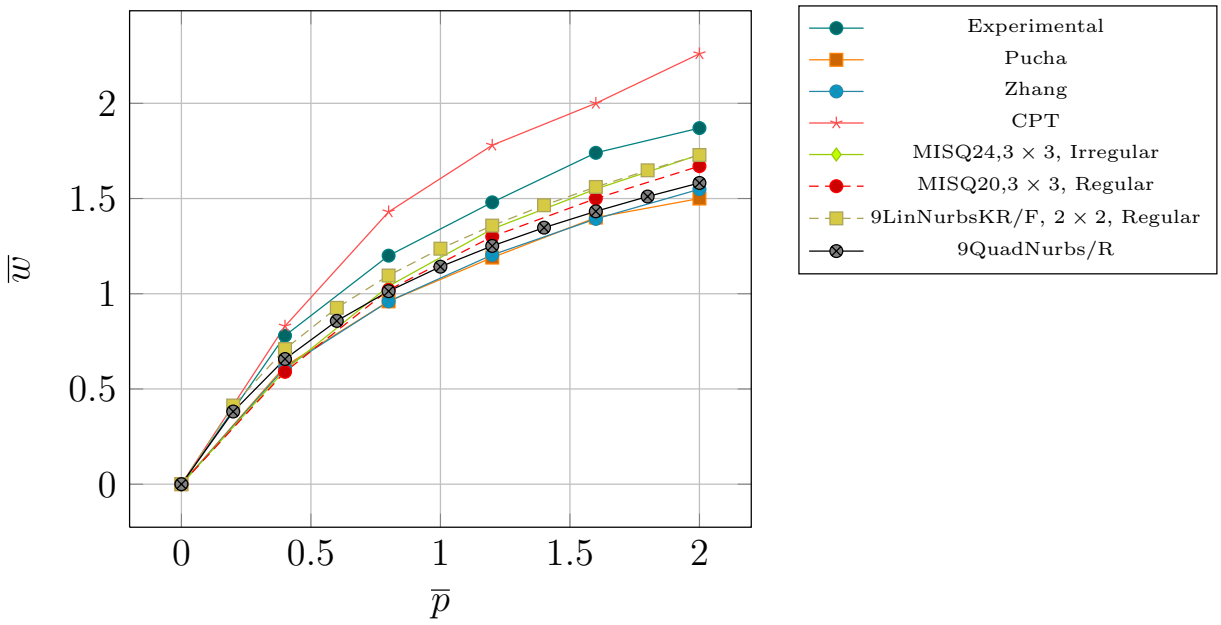

Figure 3.14: Load vs deflection curve for clamped, cross ply (0/90/90/0) laminated composite plate under uniform loading

3.3.5 Effect of number of layers and thickness on Laminated Composite Plate

This example studies the effect of no. of layers on the center deflection in a 2 layer cross-ply, (0/90) and 6 layer cross-ply, (0/90/0/90/0/90), cross-ply laminates and the effect of thickness on 2 layer $(45/-45)$ angle ply laminate. The dimension of the plate considered are $a = 12$ in, $a/h = 10, 40$ and the material properties are $E_1 = 40e6$ psi, $E_2 = 1e6$ psi, $G_{12} = G_{13} = 0.6e6, G_{23} = 0.5e6$ psi and $\nu = 0.25$. Increasing number of layers reduces the bending deflection in a cross-ply laminate. Figures 3.15 and 3.16 shows the deflection curve for 6 and 2 layer (0/90) cross-ply composite plates. Figures 3.17 and 3.18 show the effect of thickness on nonlinear deflection on a 2-layer, (45/-45) angle ply, laminated composite plate. In the case of $a/h = 10$, the nonlinear effects are reduced, resulting in straightening

of the deflection curve towards the linear solution.

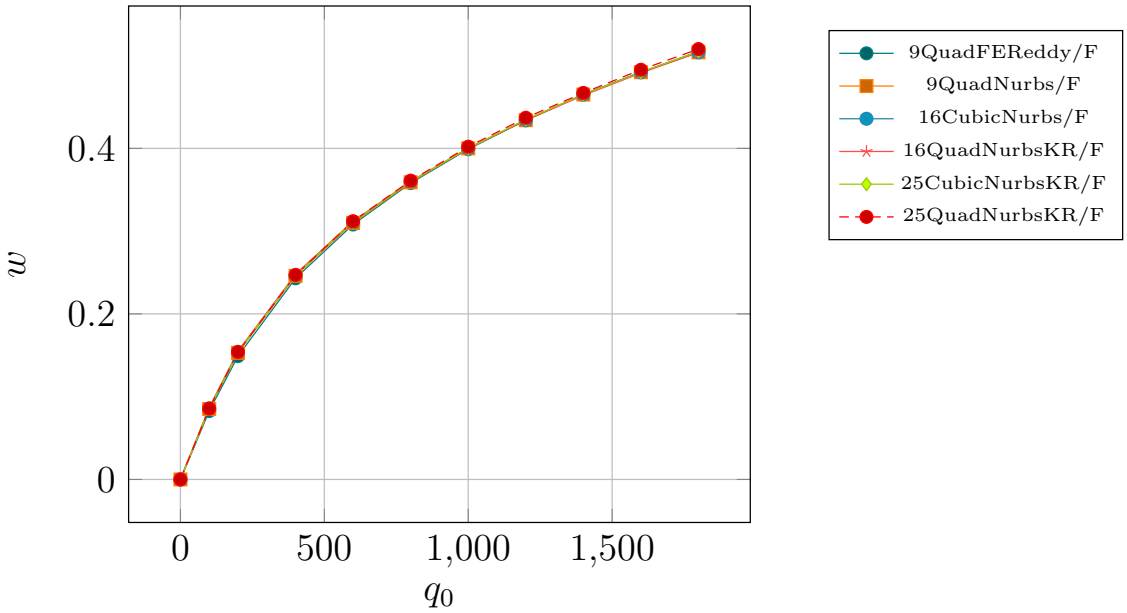

Figure 3.15: Load vs deflection curve for 6 layer cross ply (0/90) laminated composite plate under uniform loading

3.3.6 Orthotropic Square Plate under uniform loading

An orthotropic plate with dimension of $a = 12in$, thickness of $h = 0.138in$ and material properties, $E_1 = 3e6$ psi, $E_2 = 1.28e6$ psi, $G_{12} = G_{13} = G_{23} = 0.37e6$ psi and $\nu = 0.32$ is considered here. $SS1$ and $SS3$ boundary conditions are considered for the analysis. The results are compared with the Agyris([111]) and Zhang([54]) results. Zhang's element requires $10 * 10$ mesh to compute nonlinear center deflection as compared to 2×2 mesh using Nurbs elements. Figures 3.19 and 3.20 show the deflection vs load curve for $SS1$ and $SS3$ boundary conditions respectively. Center deflection is in excellent agreement with the experimental data given by Agyris([111]). k-refined quadratic Nurbs element produce

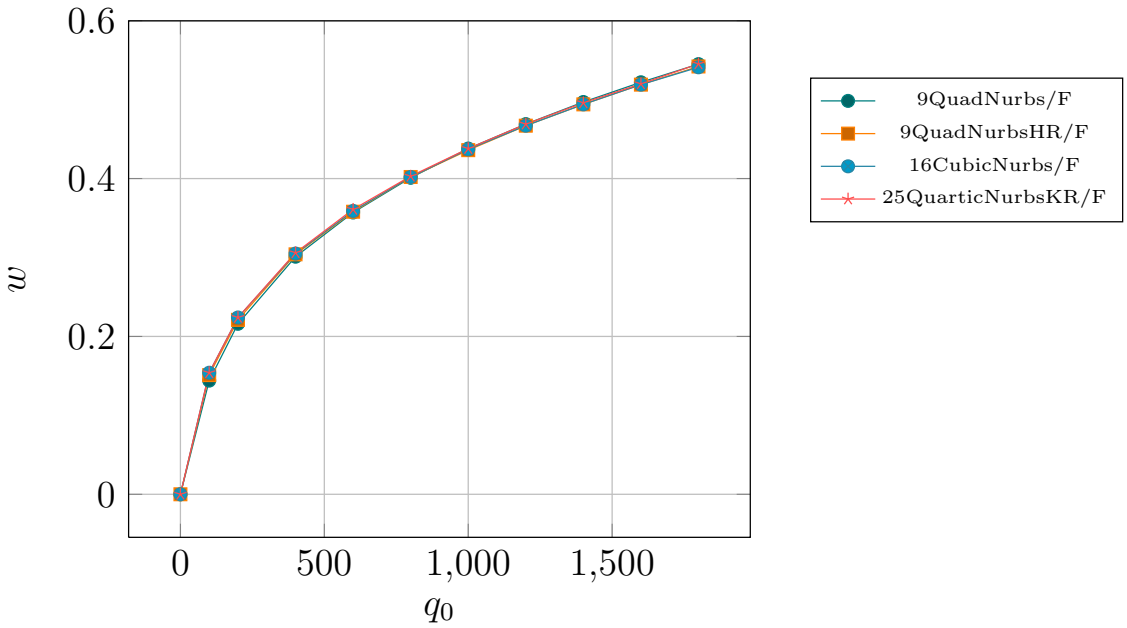

Figure 3.16: Load vs deflection curve for 2 layer cross ply (0/90) laminated composite plate under uniform loading

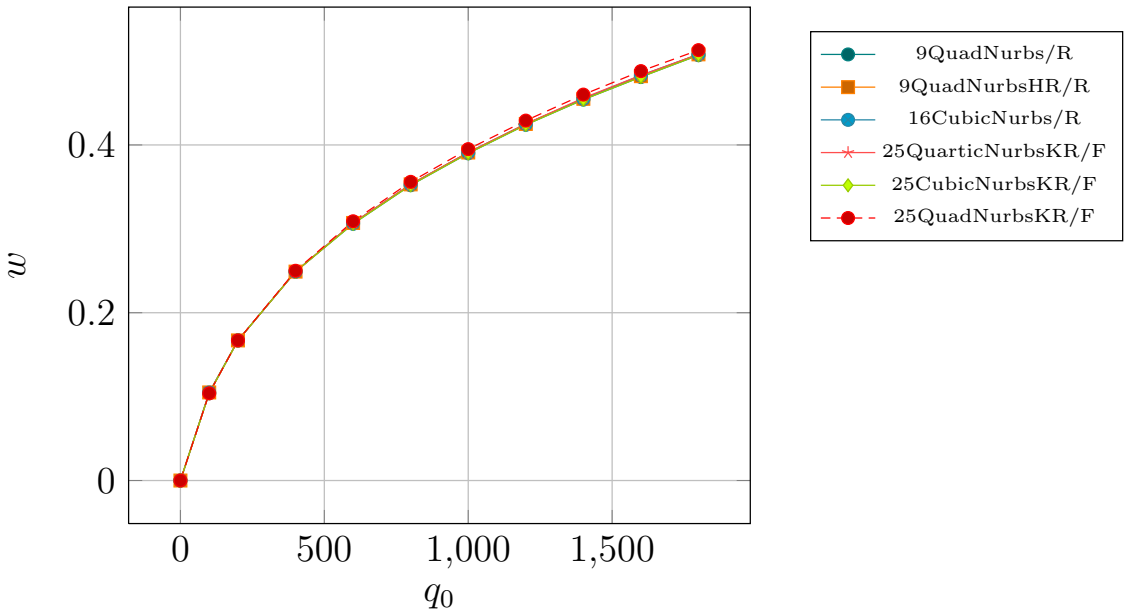

Figure 3.17: Load vs deflection curve for angle ply (45/-45) laminated composite plate under uniform loading for a/h = 40

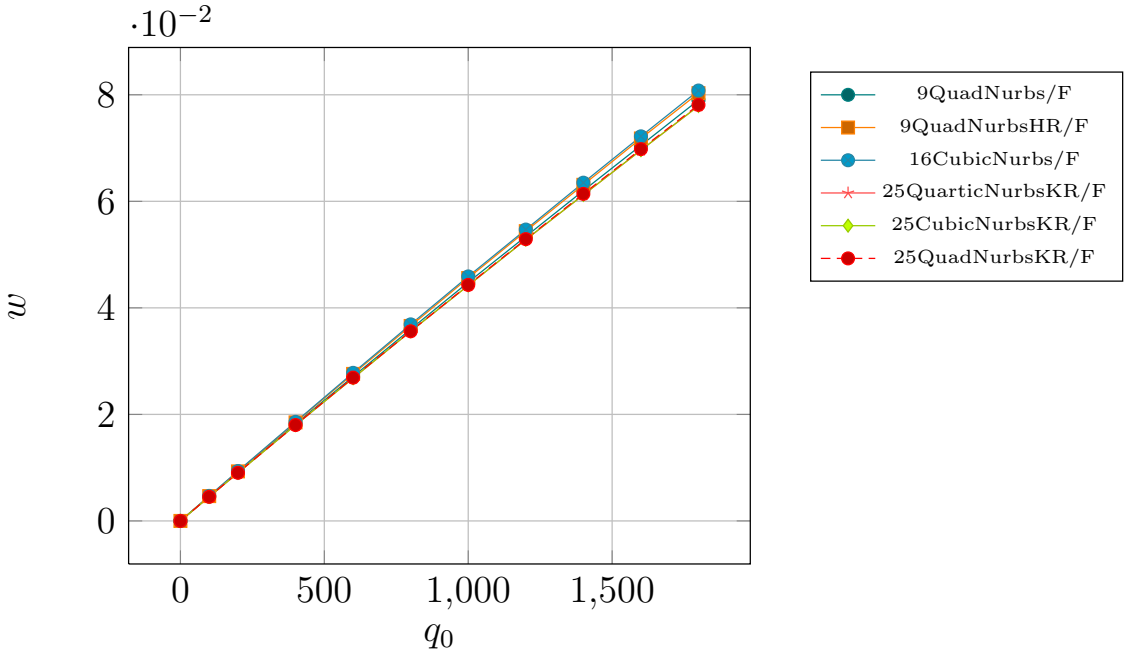

Figure 3.18: Load vs deflection curve for angle ply (45/-45) laminated composite plate under uniform loading, a/h = 10

excellent results as compared to the quadratic Nurbs element with full integration. $SS1$ boundary condition provide lesser contraint on deflection than $SS3$ boundary condition.

3.3.7 Clamped, Isotropic square plate with diffferent level of mesh distortion

A thin $a/h = 100$, clampled, isotropic square plate under uniform loading is analyzed here. The plate length, thickness and material properties are $a = 300in$, $h = 3\ in$ and $E_1 = 30E6\ psi$, $\nu = 0.316$ respectively. Analysis is performed with a 2×2 unstructured physical mesh for different levels of distortion. Figure 3.21 shows the unstructured meshes with different level of distortion in the physical domain. 9QuadraticNurbs/R, 25Quadratic-

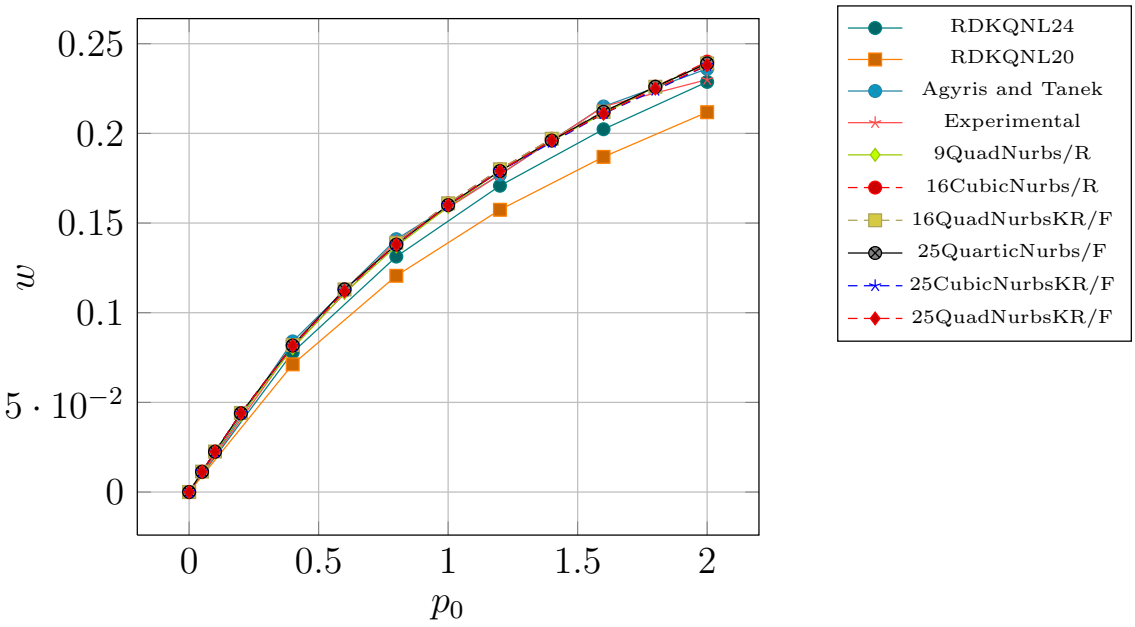

Figure 3.19: Load vs deflection curve for Orthotropic plate under uniform loading and SS1 boundary condition

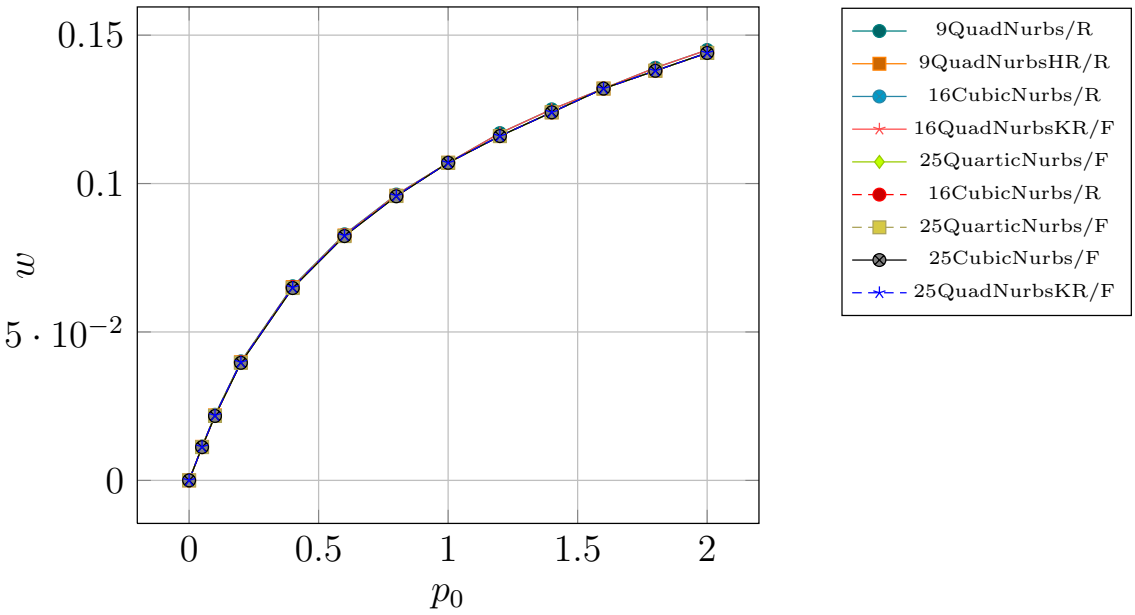

Figure 3.20: Load vs deflection curve for Orthotropic plate under uniform loading and SS3 boundary condition

NurbsKR/F and 25QuarticNurbs/F elements are considered for the analysis. Figures 3.22, 3.23 and 3.24 show the comparison of load vs nonlinear deflection response for the various

Nurbs elements. 9QuadraticNurbs/R element exhibit hourglass instability as the deflection response increases with each level of mesh distortion due to under-integrated stiffness matrix. However, k-refined quadratic and higher order Nurbs element with full integration produce a stabilized nonlinear deflection vs load response i.e. element does not exhibit hourglass instability without increasing the order of the polynomial.

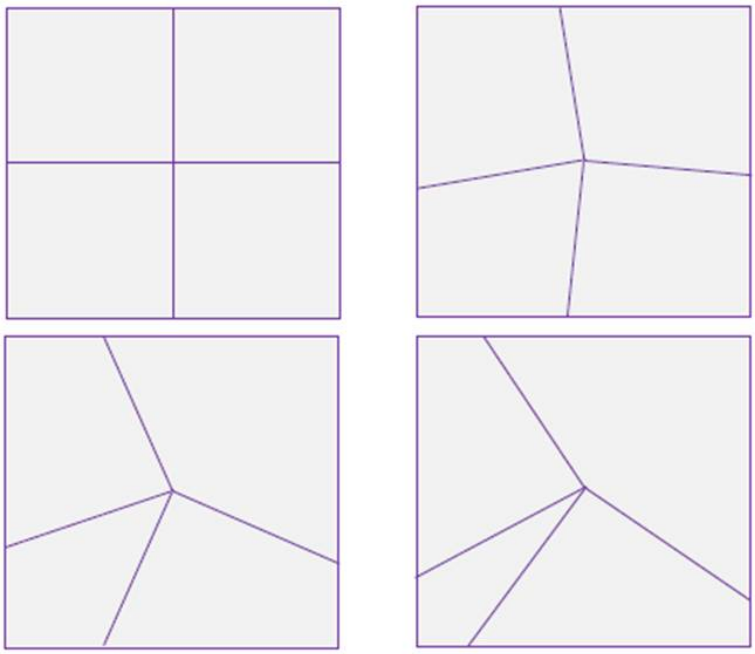

Figure 3.21: Physical meshes with different level of mesh distortion for a clamped, Isotropic, square plate

3.4 Conclusions

Geometrically nonlinear Nurbs Isogeometric finite element analysis of laminated composite plate is presented here. h, p and k-refinement techniques are utilized and various lower and

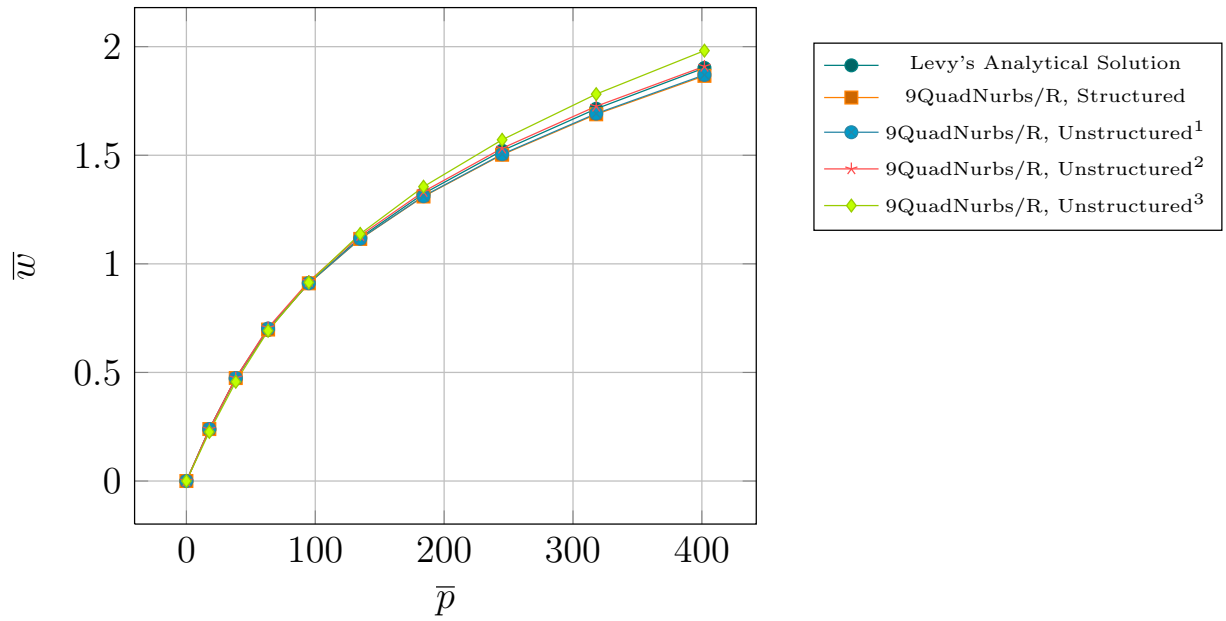

Figure 3.22: Mesh distortion sensitivity test using 9QuadNurbs/R element for 2×2 mesh

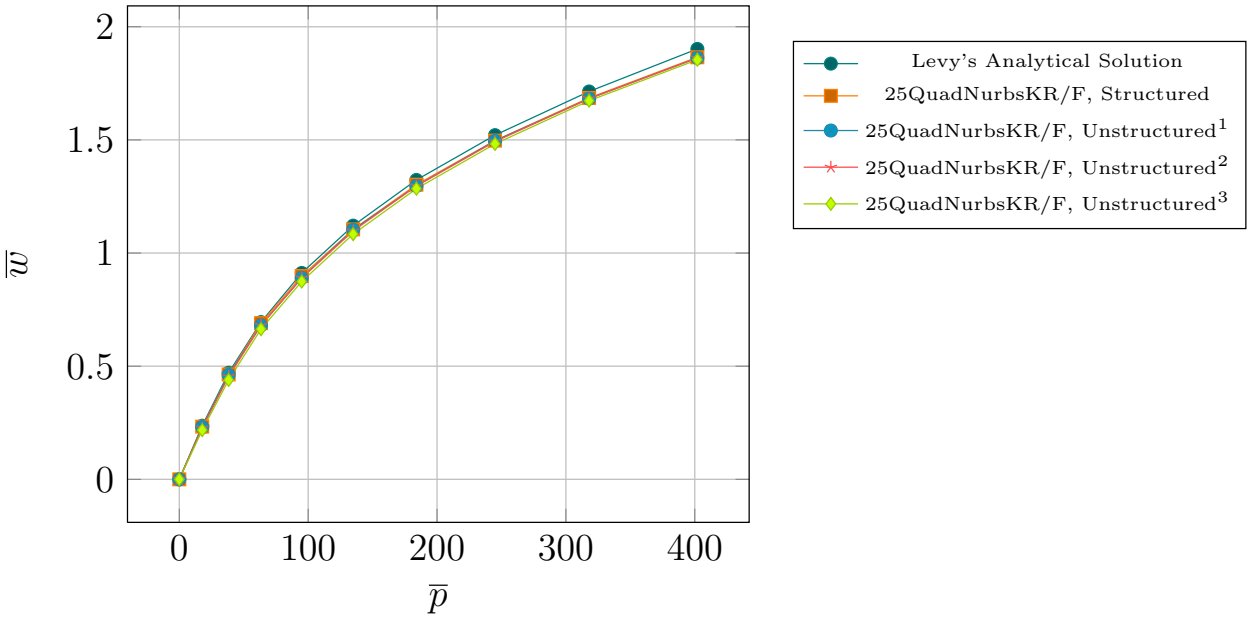

Figure 3.23: Mesh distortion sensitivity test using 25QuadNurbsKR/F element for 2×2 mesh

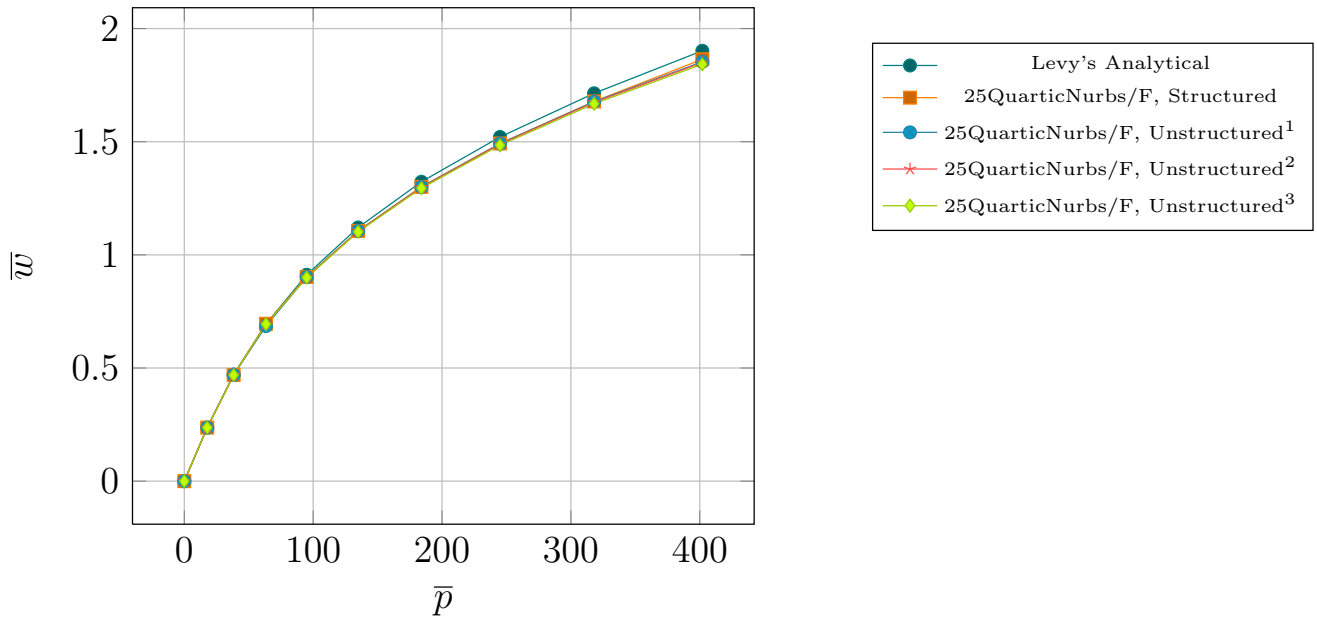

Figure 3.24: Mesh distortion sensitivity test using 25QuarticNurbs/F element for 2×2 mesh

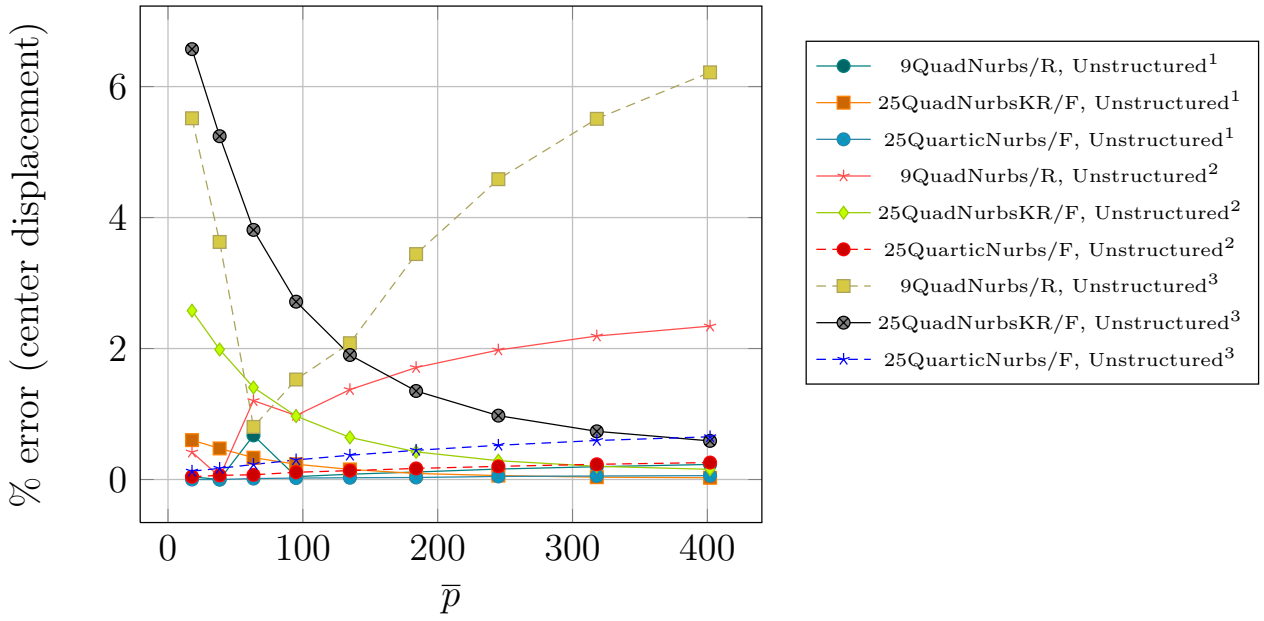

Figure 3.25: % error (center displacement) w.r.t structured mesh in Mesh distortion sensitivity test

higher-order elements are contructed. Numerical results are presented for thin to moderately thick plates for various length to thickness ratios, ply-angles and boundary conditions. The computed center deflection is found to be in excellent agreement with the literature and requires fewer degrees of freedom/control points when compared with regular finite element analysis. For thin plates analysis, k-refined, quadratic Nurbs element remedies the shear locking problem and removes hourglass instability experienced in reduced integrated Nurbs and regular finite element analysis, though at the expense of computational time.

Chapter 4

Interlaminar Stress Recovery by Direct Post-Processing in Nurbs Isogeometric Finite Element Framework

This chapter describes the development of Nurbs post-processor for in-plane and interlaminar stress calculation in laminated composite and sandwich plates. First-order, shear-deformable laminate composite plate theory is utilized in deriving the governing equations using a variational formulation. Linear, quadratic, higher order and k-refined Nurbs elements are constructed and numerical validation is performed for orthotropic, laminated composite and

sandwich plates. Lagrange finite element suffers from higher order stress gradient oscillations due to Gibbs phenomenon and require alternative stress recovery procedures for accurate interlaminar stress calculations, especially interlaminar normal stress. In this chapter, direct Nurbs based post-processing is performed which computes the interlaminar shear and normal stresses from higher order gradients of Nurbs basis in a single step procedure. The stresses are found to be in an excellent agreement with 3D elasticity solution. FSDT along with k-refinement procedure of Nurbs basis computes equivalent or better stresses than higher-order shear deformation theory.

4.1 First-order shear deformation plate theory for Laminated Composite Plates

4.1.1 Governing Equations

The origin of material coordinate system is considered to be the mid-plane of the laminate and Kirchhoff assumption that the transverse normal remain perpendicular to the mid-surface after deformation is relaxed. However, transverse strain, ϵ_z, and out-of plane normal stress, σ_z are considered negeligible. Layers are assumed to be perfectly bonded. Figure 6.1 shows the coordinate system and layer numbering of a laminated composite plate. Figure 6.2 shows the undeformed and deformed configuration of first order shear-deformable laminated composite plate. The displacement field is defined as,

$$u(x, y, z) = u_0(x, y) + z\phi_x(x, y)$$

$$v(x, y, z) = v_0(x, y) + z\phi_y(x, y) \tag{4.1}$$

$$w(x, y, z) = w_0(x, y)$$

where u_0, v_0, w_0, are the displacement along the x, y and z-axis and ϕ_x, ϕ_y are the rotation of transverse normal of the mid-plane about the y and x-axis respectively.

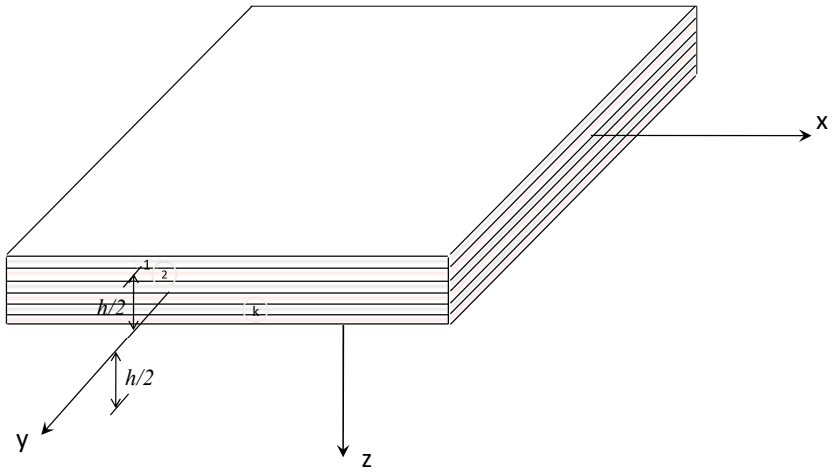

Figure 4.1: Coordinate system and layer numbering used for a laminate plate

Total in-plane strain ϵ is decomposed into membrane and bending strains.

$$\epsilon = \epsilon^m + z\epsilon^b \tag{4.2}$$

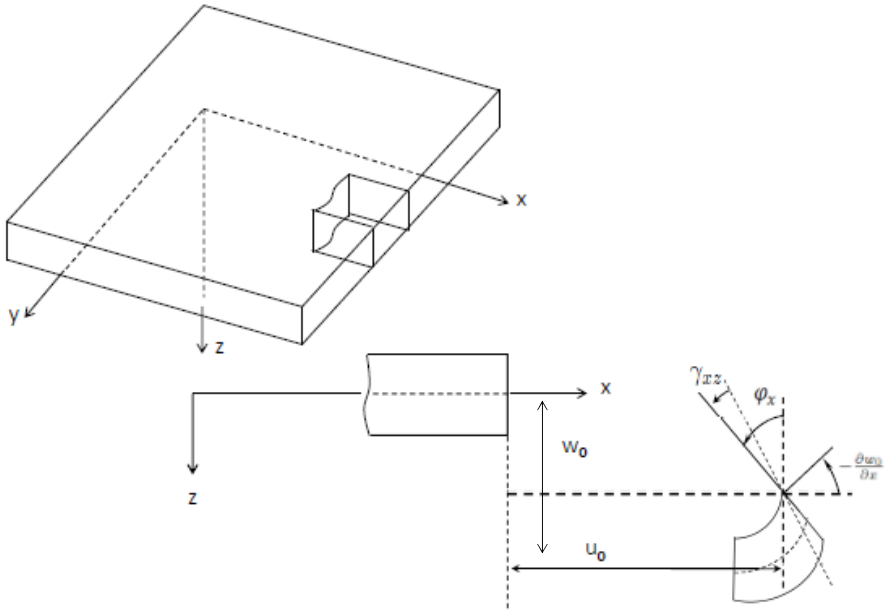

Figure 4.2: Undeformed and deformed configuration of first order shear-deformable plate

ϵ^m, the membrane strain can be written as follows,

$$\epsilon^m = \left\{ \begin{array}{c} \epsilon_x^m \\ \epsilon_y^m \\ \gamma_{xy}^m \end{array} \right\} = \left\{ \begin{array}{c} \frac{\partial u_0}{\partial x} \\ \frac{\partial v_0}{\partial y} \\ \frac{\partial u_0}{\partial y} + \frac{\partial v_0}{\partial x} \end{array} \right\} \tag{4.3}$$

ϵ^b, the bending strain can be written as follows,

$$\epsilon^b = \left\{ \begin{array}{c} \epsilon_x^b \\ \epsilon_y^b \\ \gamma_{xy}^b \end{array} \right\} = \left\{ \begin{array}{c} \frac{\partial \phi_y}{\partial y} \\ \frac{\partial \phi_y}{\partial y} \\ \frac{\partial \phi_x}{\partial y} + \frac{\partial \phi_y}{\partial x} \end{array} \right\} \tag{4.4}$$

The transverse shear strain can be written as follows,

$$\begin{Bmatrix} \gamma_{yz} \\ \gamma_{xz} \end{Bmatrix} = \begin{Bmatrix} \frac{\partial w_0}{\partial x} + \phi_x \\ \frac{\partial w_0}{\partial y} + \phi_y \end{Bmatrix} \tag{4.5}$$

The stress strain relation of a lamina can be written as,

$$\begin{Bmatrix} \sigma_{xx} \\ \sigma_{yy} \\ \sigma_{xy} \end{Bmatrix}^{(k)} = \begin{bmatrix} \overline{Q}_{11} & \overline{Q}_{12} & \overline{Q}_{16} \\ \overline{Q}_{12} & \overline{Q}_{22} & \overline{Q}_{26} \\ \overline{Q}_{16} & \overline{Q}_{26} & \overline{Q}_{66} \end{bmatrix}^{(k)} \begin{Bmatrix} \epsilon_{xx} \\ \epsilon_{yy} \\ \gamma_{xy} \end{Bmatrix} \tag{4.6}$$

$$\begin{Bmatrix} \tau_{yz} \\ \tau_{xz} \end{Bmatrix}^{(k)} = \begin{bmatrix} \overline{Q}_{44} & \overline{Q}_{45} \\ \overline{Q}_{45} & \overline{Q}_{55} \end{bmatrix}^{(k)} \begin{Bmatrix} \gamma_{yz} \\ \gamma_{xz} \end{Bmatrix} \tag{4.7}$$

The equilibrium equations are developed from stress resultants by considering balance of force and moment on an infinitesimal area of the laminate. The strong form of the governing equation of motion can, then, be written as,

$$\begin{aligned} \frac{\partial N_{xx}}{\partial x} + \frac{\partial N_{xy}}{\partial y} &= 0 \\ \frac{\partial N_{xy}}{\partial x} + \frac{\partial N_{yy}}{\partial y} &= 0 \\ \frac{\partial Q_x}{\partial x} + \frac{\partial Q_y}{\partial y} + q &= 0 \\ \frac{\partial M_{xx}}{\partial x} + \frac{\partial M_{xy}}{\partial y} - Q_x &= 0 \end{aligned} \tag{4.8}$$

$$\frac{\partial M_{xy}}{\partial x} + \frac{\partial M_{yy}}{\partial y} - Q_y = 0$$

Where $N = \{N_{xx}, N_{yy}, N_{xy}\}$ are the force resultants, $M = \{M_{xx}, M_{xy}, M_{yy}\}$ are the moment resultants and $Q = \{Q_x, Q_y\}$ are the shear force resultants. These resultants acting per unit length can be written as,

$$\begin{aligned}
\left\{ \begin{array}{c} N_{xx} \\ N_{yy} \\ N_{xy} \end{array} \right\} &= \int_{-h/2}^{h/2} \left\{ \begin{array}{c} \sigma_x \\ \sigma_y \\ \sigma_{xy} \end{array} \right\} dz \\
\left\{ \begin{array}{c} M_{xx} \\ M_{yy} \\ M_{xy} \end{array} \right\} &= \int_{-h/2}^{h/2} \left\{ \begin{array}{c} \sigma_x \\ \sigma_y \\ \sigma_{xy} \end{array} \right\} z dz \\
\left\{ \begin{array}{c} Q_x \\ Q_y \end{array} \right\} &= \int_{-h/2}^{h/2} \left\{ \begin{array}{c} \tau_x \\ \tau_y \end{array} \right\} dz
\end{aligned} \tag{4.9}$$

The laminate constitutive equations relate the force and moment resultant to strains in laminate coordinate system through ABD matrix.

$$\left\{ \begin{array}{c} N_{xx} \\ N_{yy} \\ N_{xy} \end{array} \right\} = \left[\begin{array}{ccc} A_{11} & A_{12} & A_{16} \\ A_{12} & A_{22} & A_{26} \\ A_{16} & A_{26} & A_{66} \end{array} \right] \left\{ \begin{array}{c} \epsilon_x^m \\ \epsilon_y^m \\ \epsilon_{xy}^m \end{array} \right\} \quad +$$

$$\begin{bmatrix} B_{11} & B_{12} & B_{16} \\ B_{12} & B_{22} & B_{26} \\ B_{16} & B_{26} & B_{66} \end{bmatrix} \begin{Bmatrix} \epsilon_x^b \\ \epsilon_y^b \\ \epsilon_{xy}^b \end{Bmatrix} \tag{4.10}$$

$$\begin{Bmatrix} M_{xx} \\ M_{yy} \\ M_{xy} \end{Bmatrix} = \begin{bmatrix} B_{11} & B_{12} & B_{16} \\ B_{12} & B_{22} & B_{26} \\ B_{16} & B_{26} & B_{66} \end{bmatrix} \begin{Bmatrix} \epsilon_x^m \\ \epsilon_y^m \\ \epsilon_{xy}^m \end{Bmatrix} + \begin{bmatrix} D_{11} & D_{12} & D_{16} \\ D_{12} & D_{22} & D_{26} \\ D_{16} & D_{26} & D_{66} \end{bmatrix} \begin{Bmatrix} \epsilon_x^b \\ \epsilon_y^b \\ \epsilon_{xy}^b \end{Bmatrix} \tag{4.11}$$

$$\begin{Bmatrix} Q_y \\ Q_x \end{Bmatrix} = kk \begin{bmatrix} A_{44} & A_{45} \\ A_{45} & A_{55} \end{bmatrix} \begin{Bmatrix} \gamma_{yz} \\ \gamma_{xz} \end{Bmatrix} \tag{4.12}$$

$$(A_{ij}, B_{ij}, D_{ij}) = \sum_{k=1}^{N} \left(\overline{Q}_{ij}^k \left(z_{k+1} - z_k \right), \frac{1}{2} \overline{Q}_{ij}^k \left(z_{k+1}^2 - z_k^2 \right), \frac{1}{3} \overline{Q}_{ij}^k \left(z_{k+1}^3 - z_k^3 \right) \right)$$

$$(A_{44}, A_{45}, A_{55}) = \sum_{k=1}^{N} \left(\overline{Q}_{44}^k, \overline{Q}_{45}^k, \overline{Q}_{55}^k \right) \left(z_{k+1} - z_k \right) \tag{4.13}$$

In ABD matrix, A_{ij}, B_{ij} and D_{ij} terms represent extensional and shear, extensional-bending coupling and bending stiffness terms and $\overline{Q}_{ij}^{k}$s are plane-stress reduced stiffness terms. kk is the shear correction factor.

Weak form of the governing equations is obtained by pre-multipying the equation of motion with δu_0, δv_0, δw_0, $\delta\phi_x$ and $\delta\phi_y$ respectively and integrating by parts over the element domain. Substituting force, moment and shear force resultant,

$$
\begin{aligned}
0 &= \int_{\Omega^e}\left(\frac{\partial\delta u_0}{\partial x}N_{xx}+\frac{\partial\delta u_0}{\partial y}N_{yy}\right)dxdy-\oint_{\Gamma^e}P_x\delta u_0 ds\\
0 &= \int_{\Omega^e}\left(\frac{\partial\delta v_0}{\partial x}N_{xy}+\frac{\partial\delta v_0}{\partial y}N_{yy}\right)dxdy-\oint_{\Gamma^e}P_y\delta u_0 ds\\
0 &= \int_{\Omega^e}\left[\frac{\partial\delta w_0}{\partial x}Q_x+\frac{\partial\delta W_0}{\partial y}Q_y-\delta w_0 q+\frac{\partial\delta w_0}{\partial x}\left(\hat{N}_{xx}\frac{\partial\delta w_0}{\partial x}+\hat{N}_{xy}\frac{\partial\delta w_0}{\partial y}\right)\right.\\
&\quad\left.+\frac{\partial\delta w_0}{\partial y}\left(\hat{N}_{xy}\frac{\partial\delta w_0}{\partial x}+\hat{N}_{yy}\frac{\partial\delta w_0}{\partial y}\right)\right]dxdy\\
0 &\quad -\oint_{\Gamma^e}\left[\left(Q_x+\hat{N}_{xx}\frac{\partial\delta w_0}{\partial x}+\hat{N}_{xy}\frac{\partial\delta w_0}{\partial y}\right)n_x+\left(Q_y+\hat{N}_{xy}\frac{\partial\delta w_0}{\partial x}+\hat{N}_{yy}\frac{\partial\delta w_0}{\partial y}\right)n_y\right]\delta w_0 ds\\
0 &= \int_{\Omega^e}\left(\frac{\partial\delta\phi_x}{\partial x}M_{xx}+\frac{\partial\delta\phi_x}{\partial y}M_{xy}+\delta\phi_x Q_x\right)dxdy-\oint_{\Gamma^e}T_x\delta\phi_x ds \qquad (4.14)\\
0 &= \int_{\Omega^e}\left(\frac{\partial\delta\phi_y}{\partial x}M_{xy}+\frac{\partial\delta\phi_y}{\partial y}M_{yy}+\delta\phi_y Q_y\right)dxdy-\oint_{\Gamma^e}T_y\delta\phi_y ds0
\end{aligned}
$$

And, the secondary variables are given as,

$$
\begin{aligned}
P_x &= N_{xx}n_x+N_{xy}n_y, \quad P_y = N_{xy}n_x+N_{yy}n_y\\
T_x &= M_{xx}n_x+M_{xy}n_y, \quad T_y = M_{xy}n_x+M_{yy}n_y \qquad (4.15)\\
Q_n &= \left(Q_x+\hat{N}_{xx}\frac{\partial w_0}{\partial x}+\hat{N}_{xy}\frac{\partial w_0}{\partial y}\right)n_x+\left(Q_y+\hat{N}_{xy}\frac{\partial w_0}{\partial x}+\hat{N}_{yy}\frac{\partial w_0}{\partial y}\right)n_y
\end{aligned}
$$

where n_x and n_y are the directional cosines of the outward normal vector.

4.2 Linear Nurbs Isogeometric Finite Element Formulation

4.2.1 Finite Element Model

The dependent displacement field variables are approximated by Nurbs basis functions as follows,

$$u_0(x,y) = \sum_{j=1}^{nCP} u_j R_j(x(\xi,\eta), y(\xi,\eta)); v_0(x,y) = \sum_{j=1}^{nCP} v_j R_j(x(\xi,\eta), y(\xi,\eta))$$

$$w_0(x,y) = \sum_{j=1}^{nCP} w_j R_j(x(\xi,\eta), y(\xi,\eta)) \tag{4.16}$$

$$\phi_x(x,y) = \sum_{j=1}^{nCP} \phi_{xj} R_j(x(\xi,\eta), y(\xi,\eta)); \phi_y(x,y) = \sum_{j=1}^{nCP} \phi_{yj} R_j(x(\xi,\eta), y(\xi,\eta))$$

where nCP are the number of control points per element and R_j are $2D$ Nurbs basis.

Substituting the displacement field approximation into the weak form, we obtain element stiffness matrix and load vector. For instance, the size of a sub-matrix, K^{11}, in element stiffness matrix, is $(nCP) \times (nCP)$ and the size of element load vector, F, is $(nCP \times dof, 1)$. nCP stands for control points per element, dof are the no. of degrees of freedom /control point and $(\alpha, \beta = 1, 2, ...5)$.

$$\left[K^{\alpha\beta}\right] = \begin{bmatrix} [K^{11}] & [K^{12}] & [K^{13}] & [K^{14}] & [K^{15}] \\ [K^{21}] & [K^{22}] & [K^{23}] & [K^{24}] & [K^{25}] \\ [K^{31}] & [K^{32}] & [K^{33}] & [K^{34}] & [K^{35}] \\ [K^{41}] & [K^{43}] & [K^{43}] & [K^{44}] & [K^{45}] \\ [K^{51}] & [K^{52}] & [K^{53}] & [K^{54}] & [K^{55}] \end{bmatrix} \tag{4.17}$$

$$F_i^{\alpha=3} = \int_{\Omega^e} qR_i^p dxdy \tag{4.18}$$

From the element stiffness matrix, the expression for K^{11}, a sub-matrix of element stiffness matrix, K, is as follows,

$$K_{ij}^{11} = \int_{\Omega^e} \left[A_{11} \frac{\partial R_i^p}{\partial x} \frac{\partial R_j^p}{\partial x} + A_{66} \frac{\partial R_i^p}{\partial y} \frac{\partial R_j^p}{\partial y} + A_{16} \left(\frac{\partial R_i^p}{\partial x} \frac{\partial R_j^p}{\partial y} + \frac{\partial R_i^p}{\partial y} \frac{\partial R_j^p}{\partial x} \right) \right] dxdy \tag{4.19}$$

The equation of motion can be written in the matrix form as,

$$[K]\{\Delta\} = \{F\} \tag{4.20}$$

4.2.2 Nurbs Basis

This subsection details bspline and rational basis generation and describes the transformation from physical to parametric to parent domain. The p and k-refined Nurbs elements are

constructed by modifying the knot vector by knot-insertion. Last part of this subsection describes the construction of various elements.

B-spline Basis

A knot vector in one dimension is a set of co-ordinates in the parametric space, $\Xi = \{\xi_1, \xi_2, ..., \xi_{n+p+1}\}$, where ξ_i is the i^{th} knot, i is the knot index where $i = 1, 2, ..., n + p + 1$, p is the order of the polynomial and n is the number of basis functions. The order of the polynomial, $p = 0, 1, 2, 3....$, refer to the constant, linear, quadratic, cubic piecewise polynomials, respectively. If more than one knot is located at the same parametric co-ordinate, these are termed as repeated knots. In case of the open knot vector, first and last knots are repeated $p + 1$ times. Basis function formed using the open knot vector are interpolatory at the beginning and end of the parametric space interval, *i.e.* $[\xi_1, \xi_{n+p+1}]$. This distinguishes the knots from the nodes in the finite element analysis as all the nodes are interpolatory. As a starting point, bspline basis functions are defined recursively using Cox-Deboor algorithm, starting with piecewise constants ($p = 0$).

$$N_i^p(\xi) = \begin{cases} 1 & if\ \xi_i \leq \xi < \xi_{i+1}, \\ 0 & otherwise \end{cases} \tag{4.21}$$

And, subsequently, basis functions for orders $p = 1, 2, 3, ...$, are defined as follows,

$$N_i^p(\xi) = \frac{\xi - \xi_i}{\xi_{i+p} - \xi_i} N_i^{p-1}(\xi) + \frac{\xi_{i+p+1} - \xi}{\xi_{i+p+1} - \xi_{i+1}} N_{i+1}^{p-1}(\xi) \tag{4.22}$$

Rational B-spline (Nurbs) Basis

2D Nurbs basis are formed by tensor product of B-spline basis in ξ and η direction and using projective weights associated with the control points. Rational basis are very similar to B-spline basis and derive the continuity and support for the function from the knot vector. Also, Nurbs basis form a partition of unity and are pointwise non-negative. These properties result in a strong convex hull property. Rational basis are formed as follows,

$$R_{i,j}^{p,q}(\xi,\eta) = \frac{N_i^p(\xi)M_j^q(\eta)W_{i,j}}{\sum_{i=1}^{CPw}\sum_{i=1}^{CPu} N_i^p(\xi)M_j^q(\eta)W_{i,j}} \tag{4.23}$$

Nurbs surface is defined as,

$$S(x,y) = \sum_{j=1}^{CPw}\sum_{i=1}^{CPu} R_{i,j}^{p,q}(\xi,\eta)B_{i,j} \tag{4.24}$$

where $N_i^p(\xi)$ and $M_j^q(\eta)$ are the B-spline basis in ξ and η directions respectively and $R_{i,j}^{p,q}$ denote $2D$ Nurbs basis function. CPw and CPu are the number of control points in ξ and η directions respectively and $nCP = CPu \times CPw$ is the total number of control points per element. $W_{i,j}$s are the weights associated with the control points, $B_{i,j}$ and weights are the vertical coordinates of the corresponding control points.

4.2.3 Numerical Integration

A multi-element patch, a tensor product of knot vectors in ξ and η directions, i.e. $\{0\ \ 0\ \ 0.5\ \ 1\ \ 1\}\times$ $\{0\ \ 0\ \ 0.5\ \ 1\ \ 1\}$, creates a 2×2 plate mesh in physical domain. Nurbs basis multiplied with respective control points constructs a geometric model of plate. In order to perform numerical integration, Guass quadrature is employed. The integration on physical domain is performed by transformation from physical to parametric and from parametric to parent domain. Mapping between physical and parametric domain is performed as follows,

$$\begin{Bmatrix} x \\ y \end{Bmatrix} = \sum_{k=1}^{nCP} R_k^1(\xi,\eta) \begin{Bmatrix} Bx_k \\ By_k \end{Bmatrix}$$

$$\begin{Bmatrix} \frac{\partial R_k^p}{\partial x} \\ \frac{\partial R_k^p}{\partial y} \end{Bmatrix} = [J^{-1}] \begin{Bmatrix} \frac{\partial R_k^p(\xi,\eta)}{\partial \xi} \\ \frac{\partial R_k^p(\xi,\eta)}{\partial \eta} \end{Bmatrix} \tag{4.25}$$

$$[J] = \begin{bmatrix} \frac{\partial x}{\partial \xi} & \frac{\partial y}{\partial \xi} \\ \frac{\partial x}{\partial \eta} & \frac{\partial y}{\partial \eta} \end{bmatrix}$$

Bx_k and By_k are control point coordinates and $J_{x\xi y\eta}$ is the mapping from physical to parametric domain. The Mapping from parametric to parent domain is the standard mapping as is done in finite element. Figure 6.3 shows schematic of Isogeometric framework.

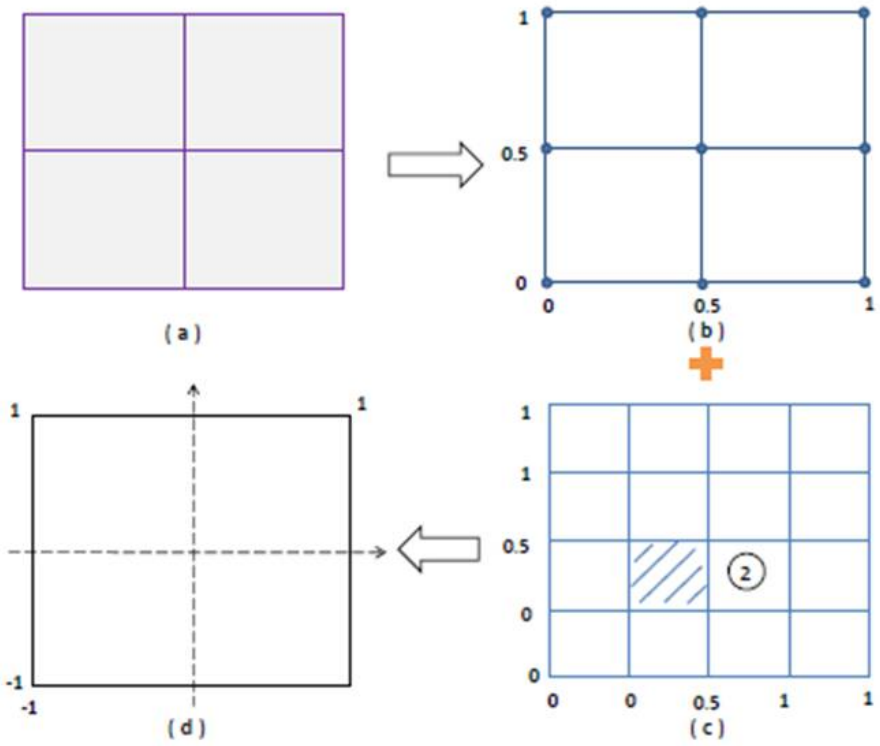

Figure 4.3: Mapping between physical and parent domain: a framework for Isogeometric finite element analysis

4.2.4 Nurbs Elements

Various lower and higher order Nurbs elements are constructed by utilizing various refinement techniques. Linear Nurbs element, 9LinNurbs/F, with 9 control point (i.e. with a knot insertion at locations such as { 0 }, { 0.25 } or { 0.5 } in knot vector), quadratic Nurbs element, 9QuadNurbs/(F/R), with 9 control points and k-refined, quadratic Nurbs element, 16QuadNurbsKR/F, with 16 control point are developed. Element notation is as follows: number in the front denotes the number of control points/element, KR denotes the k-refined

element. A few Nurbs elements construction is detailed here.

Quadratic Nurbs Element (9QuadNurbs))

A tensor product of knot vector $\{-1\ -1\ -1\ 1\ 1\ 1\}$ in $\hat{\xi}$ and $\hat{\eta}$ direction results in a bi-quadratic Nurbs element in the parent domain. $\hat{\xi}_i$ denote the i^{th} knot value in the knot vector. The element consists of 9 control points. The shape function in $\hat{\xi}$ direction can be written as follows,

$$\begin{aligned} M_1^2(\hat{\xi}) &= \left(\frac{\hat{\xi}_4 - \hat{\xi}}{\hat{\xi}_4 - \hat{\xi}_2}\right)\left(\frac{\hat{\xi}_4 - \hat{\xi}}{\hat{\xi}_4 - \hat{\xi}_3}\right) \\ M_2^2(\hat{\xi}) &= \left(\frac{\hat{\xi} - \hat{\xi}_2}{\hat{\xi}_4 - \hat{\xi}_2}\right)\left(\frac{\hat{\xi}_4 - \hat{\xi}}{\hat{\xi}_4 - \hat{\xi}_3}\right) + \left(\frac{\hat{\xi}_5 - \hat{\xi}}{\hat{\xi}_5 - \hat{\xi}_3}\right)\left(\frac{\hat{\xi} - \hat{\xi}_3}{\hat{\xi}_4 - \hat{\xi}3}\right) \qquad \hat{\xi}_3 \le \hat{\xi} < \hat{\xi}_4 \\ M_3^2(\hat{\xi}) &= \left(\frac{\hat{\xi} - \hat{\xi}_3}{\hat{\xi}_5 - \hat{\xi}_3}\right)\left(\frac{\hat{\xi} - \hat{\xi}}{\hat{\xi}_4 - \hat{\xi}3}\right) \end{aligned} \tag{4.26}$$

Similarly, the shape functions in $\hat{\eta}$ direction are obtained. The product rule yields the following bi-quadratic shape functions,

$$\begin{aligned} &R_1^2(\hat{\xi},\hat{\eta}) = M_1^2(\hat{\xi})N_1^2(\hat{\eta}) \quad R_2^2(\hat{\xi},\hat{\eta}) = M_1^2(\hat{\xi})N_2^2(\hat{\eta}) \quad R_3^2(\hat{\xi},\hat{\eta}) = M_1^2(\hat{\xi})N_3^2(\hat{\eta}) \\ &R_4^2(\hat{\xi},\hat{\eta}) = M_2^2(\hat{\xi})N_1^2(\hat{\eta}) \quad R_5^2(\hat{\xi},\hat{\eta}) = M_2^2(\hat{\xi})N_2^2(\hat{\eta}) \quad R_6^2(\hat{\xi},\hat{\eta}) = M_2^2(\hat{\xi})N_3^2(\hat{\eta}) \\ &R_7^2(\hat{\xi},\hat{\eta}) = M_3^2(\hat{\xi})N_1^2(\hat{\eta}) \quad R_8^2(\hat{\xi},\hat{\eta}) = M_3^2(\hat{\xi})N_2^2(\hat{\eta}) \quad R_9^2(\hat{\xi},\hat{\eta}) = M_3^2(\hat{\xi})N_3^2(\hat{\eta}) \end{aligned} \tag{4.27}$$

k-refined Quadratic Nurbs element I(16QuadNurbsKR)

A tensor product of knot vector $\{-1\ -1\ -1\ 0\ 1\ 1\ 1\}$ in $\hat{\xi}$ and $\hat{\eta}$ direction results in a bi-quadratic Nurbs element, 16QuadNurbsKR[1](F/R). The knot vector is divided into two intervals and shape functions have unique value over each interval. $\hat{\xi}_i$ denote the i^{th} knot value in the knot vector. The shape functions in $\hat{\xi}$ direction over each interval are derived as follows,

$$\begin{aligned}
M_1^2(\hat{\xi}) &= \left(\frac{\hat{\xi}_4-\hat{\xi}}{\hat{\xi}_4-\hat{\xi}_2}\right)\left(\frac{\hat{\xi}_4-\hat{\xi}}{\hat{\xi}_4-\hat{\xi}_3}\right) \\
M_2^2(\hat{\xi}) &= \left(\frac{\hat{\xi}-\hat{\xi}_2}{\hat{\xi}_4-\hat{\xi}_2}\right)\left(\frac{\hat{\xi}4-\hat{\xi}}{\hat{\xi}_4-\hat{\xi}_3}\right)+\left(\frac{\hat{\xi}_5-\hat{\xi}}{\hat{\xi}_5-\hat{\xi}_3}\right)\left(\frac{\hat{\xi}-\hat{\xi}_3}{\hat{\xi}_4-\hat{\xi}3}\right) \qquad \hat{\xi}_3 \le \hat{\xi} < \hat{\xi}_4 \\
M_3^2(\hat{\xi}) &= \left(\frac{\hat{\xi}-\hat{\xi}_3}{\hat{\xi}_5-\hat{\xi}_3}\right)\left(\frac{\hat{\xi}-\hat{\xi}}{\hat{\xi}_4-\hat{\xi}3}\right) \\
M_4^2(\hat{\xi}) &= 0
\end{aligned} \tag{4.28}$$

$$\begin{aligned}
M_1^2(\hat{\xi}) &= 0 \\
M_2^2(\hat{\xi}) &= \left(\frac{\hat{\xi}_5-\hat{\xi}}{\hat{\xi}_5-\hat{\xi}_3}\right)\left(\frac{\hat{\xi}_5-\hat{\xi}}{\hat{\xi}_5-\hat{\xi}_4}\right) \\
M_3^2(\hat{\xi}) &= \left(\frac{\hat{\xi}-\hat{\xi}_3}{\hat{\xi}_5-\hat{\xi}_3}\right)\left(\frac{\hat{\xi}-\hat{\xi}}{\hat{\xi}_4-\hat{\xi}3}\right)+\left(\frac{\hat{\xi}-\hat{\xi}_3}{\hat{\xi}_5-\hat{\xi}_3}\right)\left(\frac{\hat{\xi}_5-\hat{\xi}}{\hat{\xi}_5-\hat{\xi}_3}\right) \qquad \hat{\xi}_4 \le \hat{\xi} < \hat{\xi}_5 \\
M_4^2(\hat{\xi}) &= \left(\frac{\hat{\xi}-\hat{\xi}_4}{\hat{\xi}_6-\hat{\xi}_4}\right)\left(\frac{\hat{\xi}_4-\hat{\xi}}{\hat{\xi}_5-\hat{\xi}_4}\right)
\end{aligned} \tag{4.29}$$

Similarly, the shape functions in $\hat{\eta}$ direction are obtained. The product rule yields 16 bi-quadratic shape functions, R_k^2, requiring 4×4 Gauss points. In k-refinement process, the order of the existing knot vector from base model is elevated first and then, a knot is inserted

instead of elevating the order after knot insertion. This results in $q-1$ continuous derivatives instead of $p-1$ continuous derivatives, where p and q are the order of the knot vector before and after order elevation respectively.

For interlaminar stress calculation, two other modifications of k-refined quadratic Nurbs elements, 16quadNURBKR, are formulated by a single knot insertion in the knot vector at different locations. 16QuadNurbsKR[2] and 16QuudNUUBSKR[3] Nurbs elements are formed by a tensor product of knot vectors, $\{-1\ -1\ -1\ 0.25\ 1\ 1\ 1\}$ and $\{1\ 1\ 1\ 0.5\ 1\ 1\ 1\}$ in $\hat{\xi}$ and $\hat{\eta}$ directions, respectively.

4.3 Calculation of Interlaminar Stresses

The evaluation of transverse stresses τ_{xz} and σ_{zz} from the stress-strain constitutive relations leads to discontinuity at the interface of the two adjacent layers of the laminate. Three-dimensional analysis is very complex due to variation in constitutive laws in the thickness direction and continuity requirement of transverse stresses and displacement across the interface. Therefore, 3D elasticity equilibrium equations are used to calculate the transverse stresses in the k^{th} lamina and the equations are given as,

$$\begin{aligned} \frac{\partial \sigma^k_{xx}}{\partial x} + \frac{\partial \sigma^k_{xy}}{\partial y} + \frac{\partial \tau^k_{xz}}{\partial z} &= 0 \\ \frac{\partial \sigma^k_{xyx}}{\partial x} + \frac{\partial \sigma^k_{yy}}{\partial y} + \frac{\partial \tau^k_{yz}}{\partial z} &= 0 \\ \frac{\partial \tau^k_{xz}}{\partial x} + \frac{\partial \tau^k_{yz}}{\partial y} + \frac{\partial \sigma^k_{zz}}{\partial z} &= 0 \end{aligned} \tag{4.30}$$

The stresses are calculated using the direct integration method. It can be seen that the equations for transverse shear stress, τ_{xz} and τ_{yz} are a first-order equation. Since, in general, the transverse shear stresses are known at the top and bottom of the laminate, one can only obtain a non-unique solution as both the traction boundary conditions can not be enforced simultaneously. However, for the transverse normal stresses, a second-order equation is derived and requires double integration through the thickness.

The transverse stress can be computed directly as follows,

$$\begin{aligned} \tau_{xz} &= -\int_{z_k}^{z} \left(\frac{\partial \sigma_{xx}}{\partial x} + \frac{\partial \sigma_{xy}}{\partial y} \right) dz + C_1 \\ \tau_{yz} &= -\int_{z_k}^{z} \left(\frac{\partial \sigma_{xy}}{\partial x} + \frac{\partial \sigma_{yy}}{\partial y} \right) dz + C_2 \\ \sigma_{zz} &= \int_{z_k}^{z} \left(\int_{z} \left(\frac{\partial^2 \sigma_{xx}}{\partial x^2} + \frac{\partial^2 \sigma_{yy}}{\partial y^2} + 2\frac{\partial^2 \tau_{xy}}{\partial x \partial y} \right) dz \right) dz + zC_3 + C_4 \end{aligned} \tag{4.31}$$

where C_1, C_2, C_3 and C_4 are the constants of integration and are obtained by satisfaction of traction boundary and interface continuity conditions.

4.4 Numerical Testing

Laminated composite and sandwich plates are studied for validation purposes. Different boundary conditions, plate to thickness ratios and anti-symmetric angle ply composite lam-

inated plate are considered. Due to bi-axial symmetry, only a quadrant of the plate is modeled and deflection and interlaminar stresses are computed at nearest Gauss points of specific location.

4.4.1 Simply supported, four layer, cross-ply (0/90/90/0) square plate

In this analysis, a simply-supported, square, cross-ply (0/90/90/0) laminated composite plate with $a/h = 10$ ratio, under sinusoidal loading condition is studied. Material for each lamina is considered as homogeneous, elastic and orthotropic. Material properties used are as follows: $E_1 = 25E_2$, $G_{12} = G_{13} = 0.5E_2$, $G_{13} = 0.2E_2$, $\nu_{12} = 0.25$, and $K_s = 5/6$. 9QuadNurbs with 3×3 mesh and 2×2 Gauss integration scheme and family of k-refined quadratic Nurbs elements, 16QuadNurbsKR, with 2×2 mesh and 4×4 Gauss integration scheme are used for computing in-plane and interlaminar stresses. The in-plane stresses are obtained using constitutive equations with smoother displacement gradients. Interlaminar stresses are computed from 3D equilibrium equations by direct integration and without any recovery procedure and are computed from in-plane stress/strain gradients.

The computed stresses are compared with 3D elasticity solution^{Pagano} and 4Q8Reddy/FE i.e. 4×4 mesh of 8 node quadratic Lagrange element. Interlaminar stresses are found to be in close proximity to 3D elasticity solution for k-refined quadratic Nurbs elements. k-refinement provide smoother in-plane stress gradients and thus, resulting in smoother in-

terlaminar stresses computation for the coarsest mesh. Figure 4.4 and 4.5 show comparison of interlaminar shear stresses τ_{xz} and τ_{yz} for family of Nurbs elements with 3D elasticity solution. Table 4.1 shows the comparison of stresses computed using Nurbs post-processor with 3D elasticity solution.

a/h	Source	$\overline{\sigma}_{xx}^{(0,0,-h/2)}$	$\overline{\sigma}_{yy}^{(0,0,-h/4)}$	$\overline{\sigma}_{xy}^{(a/2,b/2,-h/2)}$	$\overline{\sigma}_{xz}^{(a/2,0,0)}$	$\overline{\sigma}_{yz}^{(0,b/2,0)}$
10	ELS/Pagano	0.5590	0.4010	0.0276	0.301	0.196
	9QuadReddyFE	0.4954	0.3589	0.0240	0.318	0.181
	9QuadNurbs	0.5197	0.4029*	0.0263	0.2980*	0.1812
	16QuadNurbsKR[1]	0.5703	0.3959	0.0307	0.4211	0.2606
	16QuadNurbsKR[2]	0.5365	0.4142	0.0283	0.3194	0.2127
	16QuadNurbsKR[3]	0.5478*	0.4193	0.0274*	0.2976*	0.2057*

Table 4.1: Comparison of non-dimensionalized stresses $\overline{\sigma}$ of a simply supported (SS1), cross-ply (0/90/90/0) square plate under sinusoidal loading with 3D elasticity solution^{Pagano}

4.4.2 Simply-supported, three layer, cross-ply (0/90/0) square plate

In this analysis, a simply-supported, square, cross-ply (0/90/0) laminated composite plate with various length to thickness ratios, $a/h = 10, 20, 100$, subjected to sinusoidal loading is studied. Material for each lamina is considered as homogeneous, elastic and orthotropic. Material properties used are as follows: $E_1 = 1.72369 \times 10^{11}\ N/m^2$, $E_2 = 6.894757 \times 10^9\ N/m^2$, $G_{12} = G_{13} = 3.447378 \times 10^9\ N/m^2$, $G_{23} = 1.378951 \times 10^9\ N/m^2$, $\nu_{12} = 0.25$, and $K_s = 5/6$. A family of k-refined quadratic Nurbs elements, 16QuadNurbsKR with 2×2

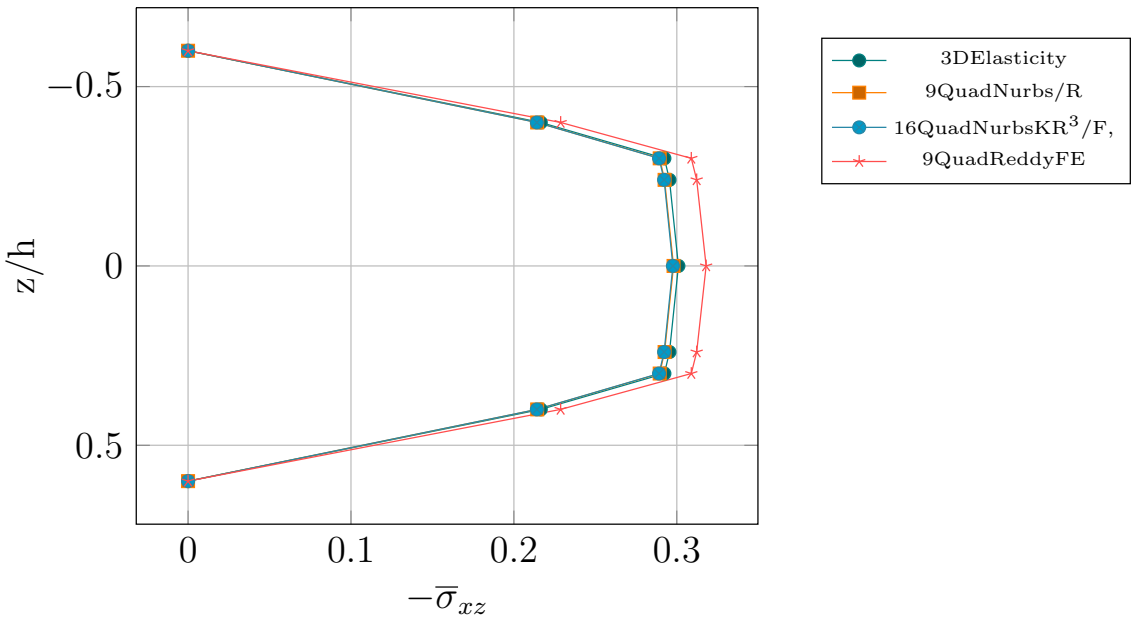

Figure 4.4: Small Interlaminar Shear Stress $-\overline{\sigma}_{xz}$(a/2,0,z) in, a simply supported (SS1), cross-ply (0/90/90/0) square plate under sinusoidal loading

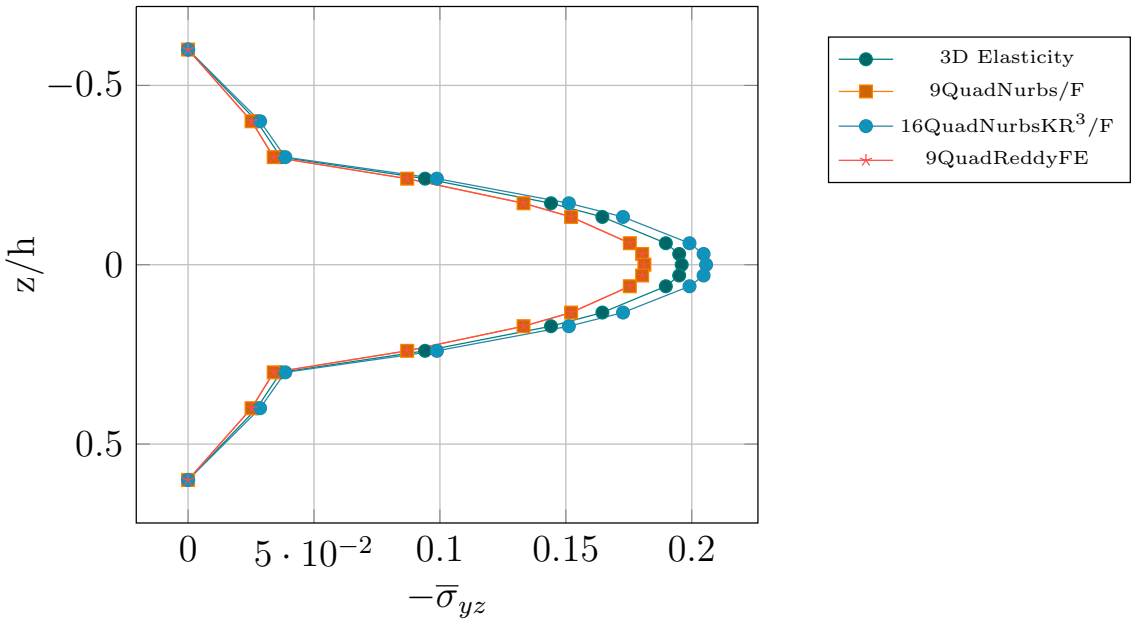

Figure 4.5: Interlaminar shear stress $-\overline{\sigma}_{yz}(0, b/2, z)$ in a simply supported (SS1), cross-ply (0/90/90/0) square plate under sinusoidal loading

mesh and two Gauss integration schemes i.e. 3×3 and 4×4, are used.

Interlaminar stresses are computed from direct integration of 3D equilibrium equations, without any recovery procedure. Computed stresses are compared with 3D elasticity solution^{Pagano}, Byun and Kapania(7×7 mesh of 9 node quadratic Lagrange element with stress recovery procedure) and 4Q8Reddy/FE (4×4 mesh of 8 node quadratic Lagrange element). Tables 4.2, 4.3, 4.4 provide the comparison of in-plane and interlaminar stresses with 3D elasticity solution, Byun and Kapania's and Reddy's results.

Stresses are found to be in an excellent agreement with 3D elasticity solution for at least one of the elements in the family of k-refined quadratic Nurbs elements when compared with 3D elasticity solution and Byun and Kapania's results. However, to obtain the most accurate interlaminar stresses, a single **knot** in the knot vector of a particular element of the family of k-refined quadratic Nurbs elements, for which the most accurate interlaminar stress is obtained, is replaced by a **new knot** at a slightly perturbed position. This procedure produces the most accurate interlaminar stresses which are almost exact to 3D elasticity solution. This **new knot** seems to produce most smoothed in-plane stress gradients and thus, interlaminar stresses. This trend is seen for all the length to thickness ratios and for both integration schemes. In Tables 4.2, 4.3, 4.4, these stress values are provided with the new knot location and the knot location are shown as superscript.

a/h	Source	$\overline{\sigma}_{xx}$	$\overline{\sigma}_{yy}$	$\overline{\sigma}_{xy}$	$\overline{\sigma}_{xz}$	$\overline{\sigma}_{yz}$	
10	16QuadNurbsKR[1]	0.4658	0.2466	0.0237	0.5109	0.1564	4×4
	16QuadNurbsKR[1]	0.5928*	0.3118	0.0319	0.1755	0.0559	3×3
	16QuadNurbsKR[2]	0.5571	0.2859	0.0295	0.3995	0.1345*	4×4
	16QuadNurbsKR[2]	0.5294	0.2738	0.0257	0.3204*	0.1107*	3×3
	16QuadNurbsKR[3]	0.5664	0.2873*	0.0287*	0.3587*	0.1378	4×4
	16QuadNurbsKR[3]	0.4816	0.2470	0.0227	0.7397	0.2348	3×3
	16QuadNurbsKR^{OP}	-	-	-	$0.3571^{(0.4985)}$	$0.1246^{(0.275)}$	4×4
	16QuadNurbsKR^{OP}	-	-	-	$0.3575^{(0.29)}$	$0.1259^{(0.30)}$	3×3
	Elasticity^{Pagano}	0.590	0.288	0.0290	0.357	0.1228	
	Byun and Kapania	0.513	0.254	0.0252	0.380	0.1106	
	Reddy/FE	0.5098	0.2518	0.0250	0.4060	0.0908	

Table 4.2: Non-dimensionalized stress $\overline{\sigma}$ in a simply supported (SS1), cross-ply (0/90/0) square plate under sinusoidal loading for a/h = 10

a/h	Source	$\overline{\sigma}_{xx}$	$\overline{\sigma}_{yy}$	$\overline{\sigma}_{xy}$	$\overline{\sigma}_{xz}$	$\overline{\sigma}_{yz}$	
20	16QuadNurbsKR[1]	0.4883	0.1959	0.0221	0.5246	0.1164	4×4
	16QuadNurbsKR[1]	0.6179	0.2390	0.0263	0.1764	0.0443	3×3
	16QuadNurbsKR[2]	0.5786	0.2156	0.0250	0.4191	0.1160*	4×4
	16QuadNurbsKR[2]	0.5513*	0.2088*	0.0231*	0.3305*	0.0880*	3×3
	16QuadNurbsKR[3]	0.5006	0.2166	0.0253	0.3839*	0.1333	4×4
	16QuadNurbsKR[3]	0.5890	0.1864	0.0229	0.7641	0.1768	3×3
	16QuadNurbsKR^{OP}	-	-	-	$0.3851^{(0.501)}$	$0.0935^{(0.31)}$	4×4
	16QuadNurbsKR^{OP}	-	-	-	$0.3847^{(0.304)}$	$0.0935^{(0.275)}$	3×3
	Elasticity^{Pagano}	0.552	0.210	0.0234	0.385	0.0938	
	Byun and Kapania	0.532	0.200	0.0223	0.390	0.0899	
	Reddy/FE	0.5281	0.198	0.0222	0.4176	0.0754	

Table 4.3: Non-dimensionalized stress $\overline{\sigma}$ in a simply supported (SS1), cross-ply (0/90/0) square plate under sinusoidal loading for a/h = 20

4.4.3 Simply-supported, two layer, cross-ply (0/90), square laminate

A simply supported, two layered (0/90), square laminate with a/h ratio = 4, subjected to sinusoidal loading is considered. The material properties used here are as follows:$E_1/E_2 = 25$;

a/h	Source	$\overline{\sigma}_{xx}$	$\overline{\sigma}_{yy}$	$\overline{\sigma}_{xy}$	$\overline{\sigma}_{xz}$	$\overline{\sigma}_{yz}$	
100	16QuadNurbsKR[1]	0.5371*	0.1903	0.0217*	0.4463*	0.0886*	4×4
	16QuadNurbsKR[1]	0.6256	0.2118	0.0224	0.1750	0.0415	3×3
	16QuadNurbsKR[2]	0.55668	0.1821*	0.0232	0.5722	0.1459	4×4
	16QuadNurbsKR[2]	0.5594	0.1853	0.0225	0.3346*	0.0781*	3×3
	16QuadNurbsKR[3]	0.5788	0.1846	0.0246	0.6651	0.2055	4×4
	16QuadNurbsKR[3]	0.5069	0.1647	0.0242	0.7754	0.1496	3×3
	16QuadNurbsKR^{OP}	-	$0.181^{(0.268)}$	-	$0.3957^{(-0.0407)}$	$0.0827^{(-0.02)}$	4×4
	16QuadNurbsKR^{OP}	-	-	-	$0.3954^{(0.309)}$	$0.0826^{(0.275)}$	3×3
	Elasticity^{Pagano}	0.539	0.181	0.0213	0.395	0.0828	
	Chansup Byun	0.539	0.181	0.0213	0.394	0.0825	
	Reddy/FE	0.5346	0.1791	0.0212	0.4215	0.0699	

Table 4.4: Non-dimensionalized stress $\overline{\sigma}$ in a simply supported (SS1), cross-ply (0/90/0) square plate under sinusoidal loading for a/h = 100

$G_{12}/E_2 = 0.50$; $G_{23}/E_2 = 0.20$; $G_{13} = G_{12}$; $E_2 = E_3$; $\nu_{12} = \nu_{23} = \nu_{13} = 0.25$.Computed interlaminar stresses are compared with Kant's[77] and 3D elasticity[116] solution. Kant uses various techniques such as finite difference and exact surface fitting to compute interlaminar stresses from in-plane stresses along with HSDT. Cubic and k-refined quadratic Nurbs elements are developed to compute interlaminar shear stresses. In the k-refinement procedure, a single knot is inserted between -1 and 1 and an analysis is run for different knot insertions to obtain the most accurate stresses. Table 4.6 compares the interlaminar shear and normal stresses with 3D elasticity, Kant's and Ren's[64] solution.

From Table 4.6, for cubic Nurbs element, the computed σ_{yz} is found to be within 9% and for k-refined Nurbs element, computed σ_{yz} is found to be within 1% w.r.t the 3D elasticity solution. In the k-refinement procedure, a knot insertion at a location 0.515 in the knot vector of k-refined quadratic Nurbs element along with a 2×2 mesh computes the value of σ_{yz} as

0.3161 when compared to the value of σ_{yz} 0.3188 obtained from the 3D elasticity's solution, 0.319233 obtained from Kant's HOST11(16N)(direct integration(DI)) element, which is a cubic, 16 node element with 11 degrees of freedom per node, and 0.32580 computed from Ren's higher order shear deformation theory model. Figure 4.6 shows the comparison of through the thickness distribution of σ_{xz} with 3D elasticity solution. Similarly, σ_{yz} is computed using cubic and quadratic Nurbs element. Figure 4.7 shows the comparison of interlaminar shear stress, σ_{yz}, with the 3D elasticity solution.

However, σ_{zz} requires calculation of third-order displacement derivatives and thus, require higher order polynomial approximation of solution space. Cubic and quartic Nurbs elements are constructed for computing σ_{zz}. From Table 4.6, it is observed that Nurbs elements produce better estimate of through thickness distribution of σ_{zz} as compared to Kant's solution. The k-refinement procedure seems to enhance the smoothness of strain gradients and thus, 3D elasticity equivalent interlaminar normal stresses are obtained for various single knot insertion values. Figure 4.8 shows the comparison of through the thickness distribution of interlaminar normal stress with the 3D elasticity and Kant's solutions.

4.4.4 Simply supported, anti-symmetric, angle-ply, square laminate

A simply supported (SS2), 2 and 10 layered, (45 -45), anti-symmetric square laminate for various a/h ratios, subjected to sinusoidal loading is analyzed here. The material properties

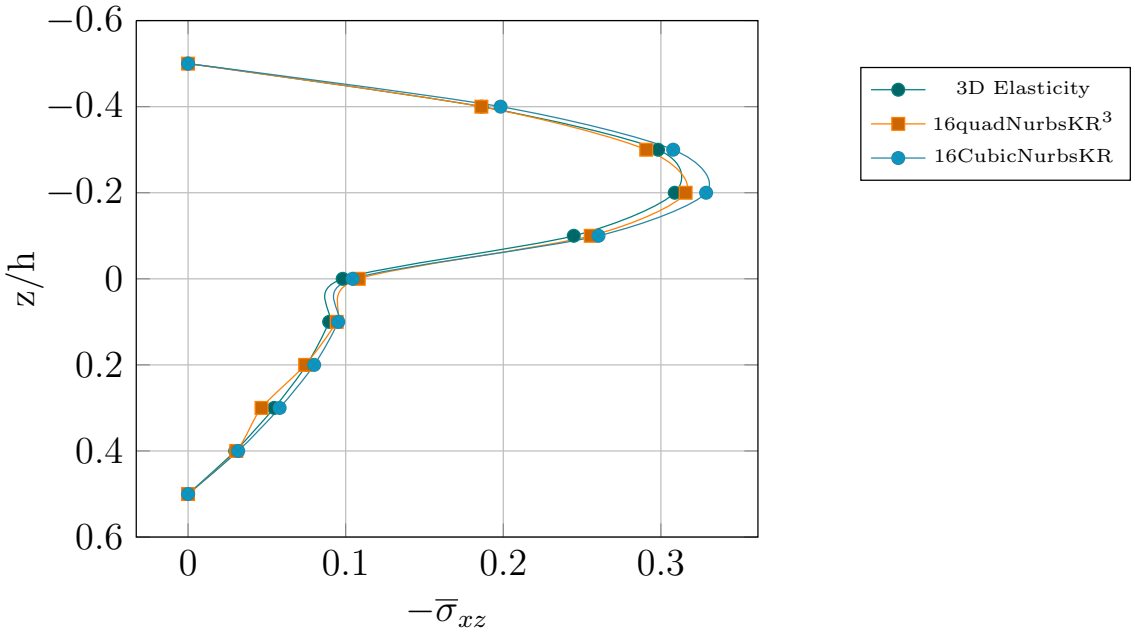

Figure 4.6: Interlaminar Shear Stress $-\overline{\sigma}_{xz}(a/2, 0, z)$ in a simply supported (SS1), cross-ply (0/90) square plate under sinusoidal loading

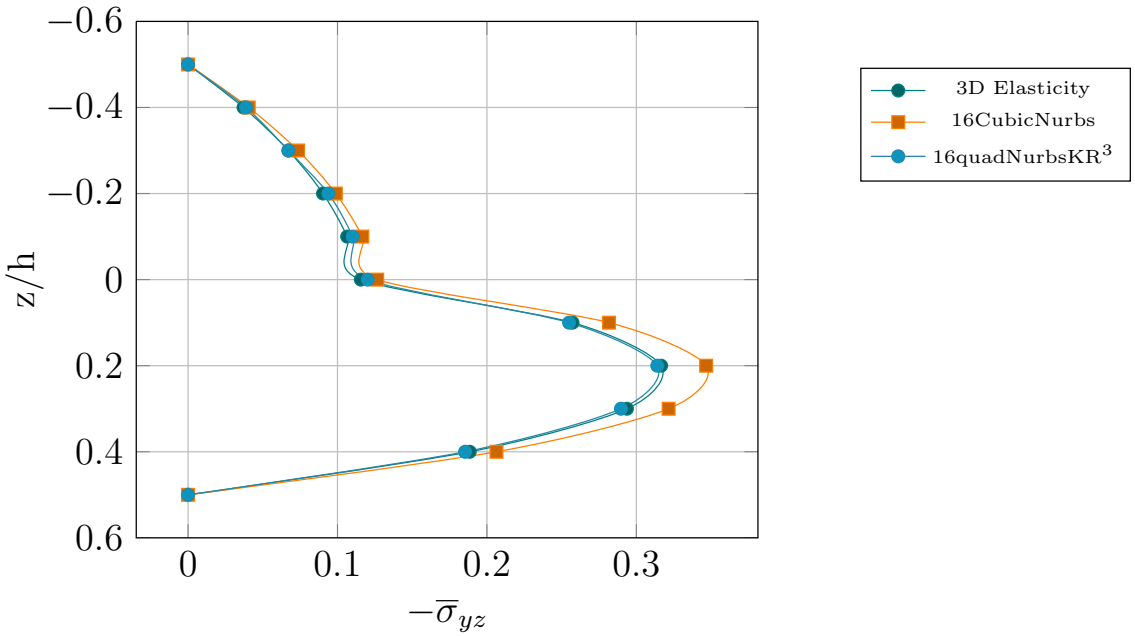

Figure 4.7: Interlaminar Shear Stress $-\overline{\sigma}_{yz}(0, b/2, z)$ in a simply supported (SS1), cross-ply (0/90) square plate under sinusoidal loading

a/h	Source	$\overline{\sigma}_{xz}$	$\overline{\sigma}_{yz}$	Mesh
4	16QuadNurbsKR[1]	-	-	2×2
	16QuadNurbsKR[2]	-	-	2×2
	16QuadNurbsKR[3]	-	0.3541	2×2
	16QuadNurbsKR^{OP}	$0.3157^{(0.515)}$	$0.3161^{(0.515)}$	2×2
	16CubicNurbs	0.3403	0.3688	2×2
	16QuadNurbsKR^{OP}	$0.3137^{(0.515)}$	$0.3151^{(0.515)}$	3×3
	16CubicNurbs	0.3316	0.3489	3×3
	$Elasticity^{Pagano}$	0.3127	0.3188	
	Ren[64]	0.32450	0.32580	
	HOST7A(9N)(FD)[77]	0.313515	0.294540	
	HOST12(16N)(FD)[77]	0.316315	0.319463	

Table 4.5: Non-dimensionalized interlaminar shear stresses $\overline{\sigma}_{xz,yz}$ in a simply supported (SS1), cross-ply (0/90) square plate under sinusoidal loading for a/h = 4

z/h	3D Elasticity	HOST11(16N)(DI)	16CubicNurbs	25CubicNurbsKR	25QuarticNurbs	36QuarticNurbsKR
-0.5	1	1	1	1	1	1
-0.4	0.973684	0.924730	0.9011	$0.9725^{(0.775,0.775)}$	0.9051	0.9233
-0.3	0.960526	0.817625	0.8023	$0.9646^{(0.7765,0.7765)}$	0.8102	0.84659
-0.2	0.921053	0.698580	0.7034	$0.9260^{(0.7755,0.7755)}$	0.7152	0.76988
-0.1	0.868421	0.58460	0.6046	$0.8654^{(0.774,0.774)}$	0.6204	0.6932
0.0	0.789474	0.491027	0.5057	$0.78832^{(0.7725,0.7725)}$	0.5255	0.6165
0.1	0.671050	0.399094	0.3954	$0.67387^{(0.75,0.175)}$	0.3796	0.4427
0.2	0.460526	0.287604	0.2966	$0.5053^{(0.75,0.175)}$	0.2847	0.3321
0.3	0.25	0.171356	0.1977	$0.2568^{(0.75,-0.045)}$	0.1898	0.2241
0.4	0.07899	0.072587	0.0989	$0.07815^{(0.768,0.75)}$	0.0949	0.0767
0.5	0.0	0.0	0.0	0.0	0.0	0.0

Table 4.6: Non-dimensionalized interlaminar normal stress $\overline{\sigma}_{zz}$ in a simply supported (SS1), cross-ply (0/90) square plate under sinusoidal loading for a/h = 4

used here are as follows: $E_1/E_2 = 40$; $G_{12}/E_2 = 0.60$; $G_{23}/E_2 = 0.5$; $G_{13} = G_{12}$; $E_2 = E_3$; $\nu_{12} = \nu_{23} = \nu_{13} = 0.25$. Center deflection and in-plane stresses are computed using linear and quadratic Nurbs element and are compared with closed form solution. For this particular angle, in-plane stresses do not vary with increasing a/h ratios. Table 4.7 shows comparison of

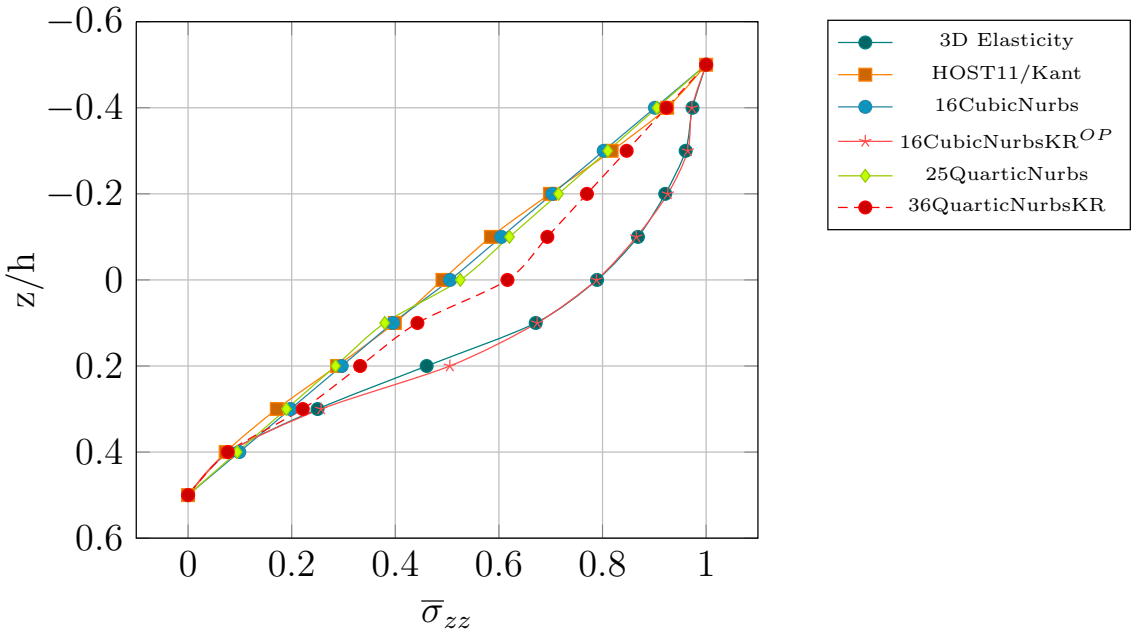

Figure 4.8: Interlaminar normal stress $\overline{\sigma}_{zz}(0, 0, z)$ in a simply supported (SS1), cross-ply (0/90) square plate under sinusoidal loading

both the center deflection and the in-plane stresses with the closed form solution. Solutions from 9QuadNurbs and 9LinNurbs elements, with 2×2 mesh, compares well with the closed form solution. Here, $(\theta, -\theta)_n$ (n stands for no of layers in anti-symmetric angle ply laminates.

Next, the interlaminar shear and normal stresses are computed for antisymmetric, two layered, (45/-45), angle-ply laminate using quadratic, higher-order Nurbs elements. In case of quadratic Nurbs element, 2×2 and 4×4 meshes are considered while for higher order Nurbs elements, 2×2 mesh is considered. Figure 4.9 shows through the thickness distribution of $\overline{\sigma}_{xz}$ for quadratic and higher order Nurbs elements. Figures 4.10, 4.11 and 4.12 show through the thickness distribution of $\overline{\sigma}_{zz}$ for higher order Nurbs elements for various a/h ratios.

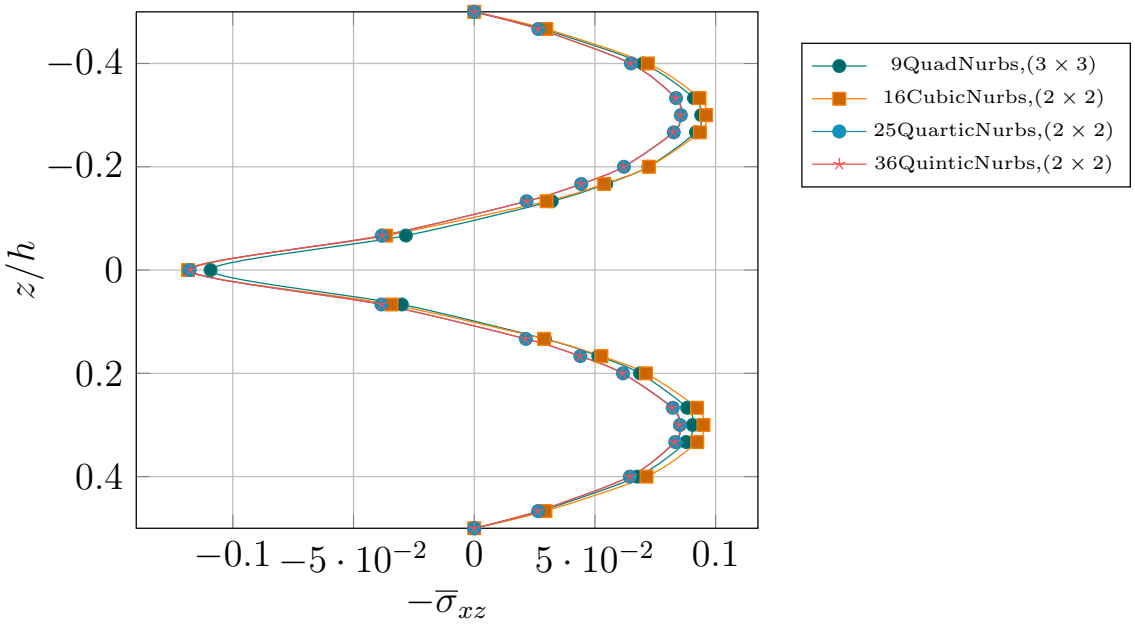

Figure 4.9: Through the thickness distribution of interlaminar shear stress, $-\overline{\sigma}_{xz}(a/2, 0, z)$, in a simply supported (SS2), anti-symmetric (45/-45) square laminated plate, a/h=4

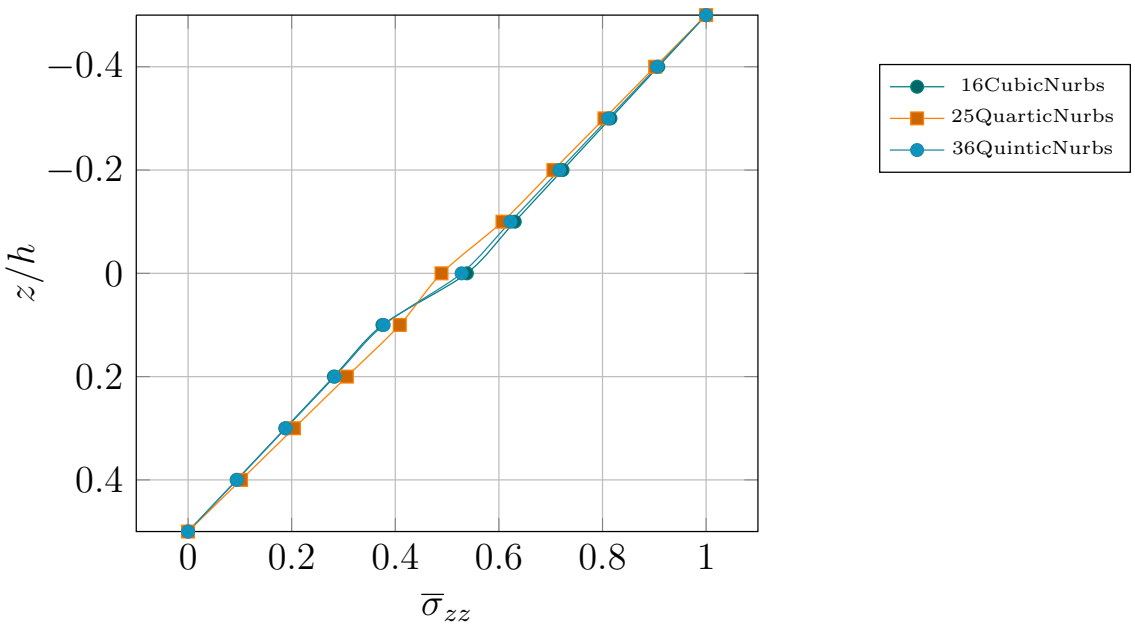

Figure 4.10: Through the thickness distribution of interlaminar shear stress, $\overline{\sigma}_{zz}(0, 0, z)$, in a simply supported (SS2), antisymmetric (45/-45) square laminated plate, a/h=4

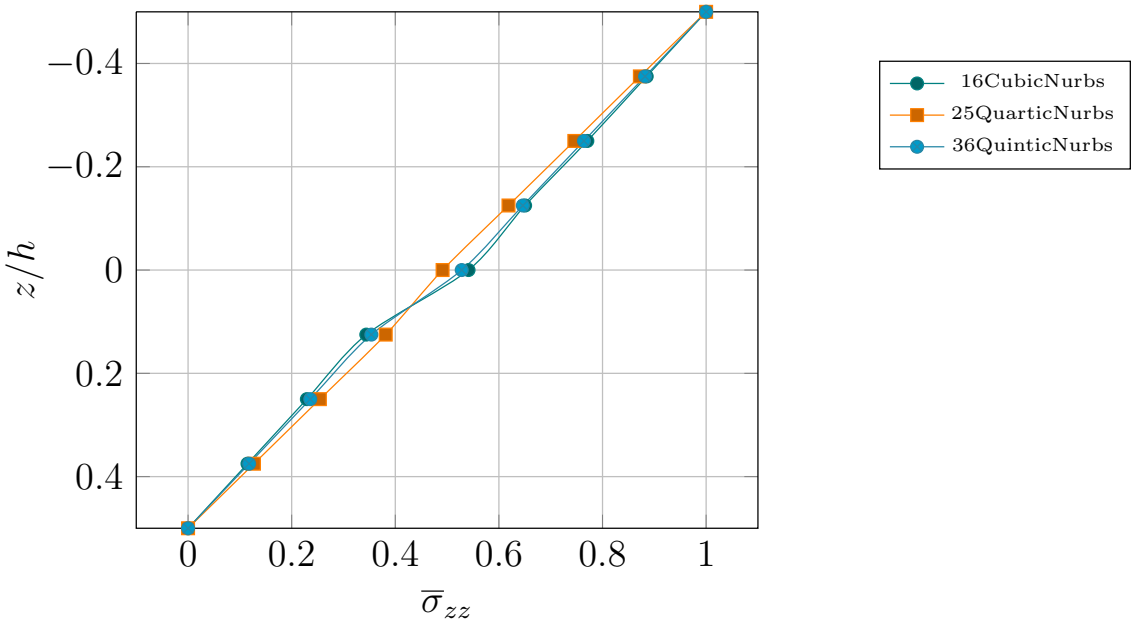

Figure 4.11: Through the thickness distribution of interlaminar normal stress, $\overline{\sigma}_{zz}(0, 0, z)$, in a simply supported (SS2), antisymmetric (45/-45) square laminated plate, a/h=10

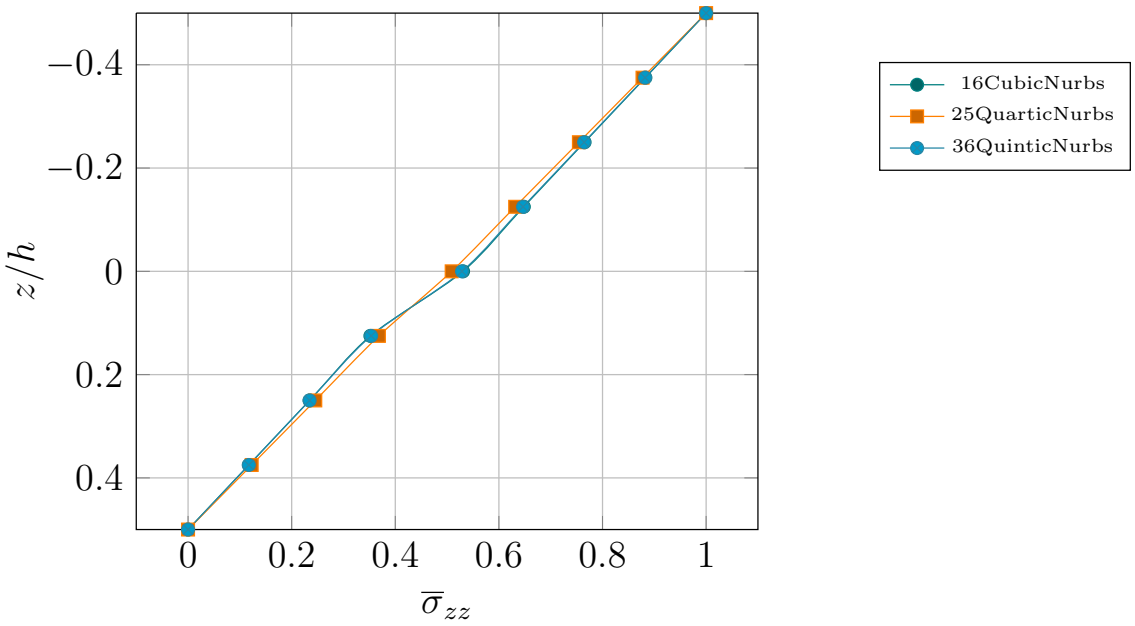

Figure 4.12: Through the thickness distribution of interlaminar normal stress, $\overline{\sigma}_{zz}(0, 0, z)$, in a simply supported (SS2), antisymmetric (45/-45) square laminated plate, a/h=50

a/h	Source	$\overline{w} * 10^2$ $(n = 2)$	$\overline{w} * 10^2$ $(n = 10)$	$\overline{\sigma}_{xx}$ $(n = 10)$	$\overline{\sigma}_{xy}$ $(n = 10)$
4	9QuadNurbs	1.1850	0.8645	0.14377	0.14016
	9LinNurbs	1.18038	0.8654	0.1386	0.1349
	Closed Form	1.1576	0.8450	0.1430	0.1392
10	9QuadNurbs	0.5907	0.27098	0.14377	0.1402
	9LinNurbs	0.58395	0.2690	0.1386	0.1350
	Closed Form	0.5773	0.2647	0.1430	0.1392
20	9QuadNurbs	0.5053	0.1860	0.14379	0.1403
	9LinNurbs	0.4987	0.1838	0.13865	0.1350
	Closed Form	0.4944	0.1818	0.1430	0.1392
100	9QuadNurbs	0.4757	0.1565	0.14379	0.1403
	9LinNurbs	0.4713	0.1581	0.13883	0.135368
	Closed Form	0.4678	0.1553	0.1430	0.1392

Table 4.7: Non-dimensionalized displacement and in-plane stresses in a simply supported (SS2), cross-ply (45/-45) square plate under sinusoidal loading

4.4.5 Simply-supported, sandwich plate

A simply supported (SS1), sandwich plate subjected to sinusoidal distributed transverse loading is analyzed here. The face sheet's material (orthotropic) properties used here are as follows: $E_1 = 25E_2$; $E_2 = 1E6$; $G_{12} = 0.50E_2$; $G_{23} = 0.2$; $G_{13} = G_{12}$; $\nu_{12} = \nu_{13} = 0.25$ the core material properties are as follows, $E_1 = E_2 = 1e6$; $G_{13} = G_{23} = 0.06E6$; $G_{12} = 0.16E6$; and $\nu_{12} = 0.25$. Each face sheet is assumed to have one tenth of the total thickness of the sandwich plate. In-plane stresses are computed using 9QuadNurbs and 9LinNurbs elements with 2×2 mesh and 2×2 and 3×3 Gauss integration schemes (GIS). Linear Nurbs element with $\{0\}$ as single knot insertion computes in-plane stresses which are very close to 3D elasticity solution. While the 9QuadNurbs element behaves similar to 9QuadLagrange finite

element with slightly better in-plane stresses. For example, 9LinNurbs element with $\{0\}$ as single knot insertion and with 3×3 Gauss integration scheme computes value of $\overline{\sigma}_{xx}(0,0,h/2)$ as 1.5896 as compared to 1.556 computed using the 3D elasticity solution, 0.8918 computed using Reddy's 4×4 mesh of 9QuadLagrange finite element and 0.9522 computed using 9QuadNurbs element with 2×2 mesh and 3×3 Gauss integration scheme. Similar results are obtained for $\overline{\sigma}_{yy}(0,0,h/2)$ as well. However, in case of $\overline{\sigma}_{xy}(a/2,b/2,-h/2)$, LinearNurbs element with knot insertion at $\{0.2\}$ and with 3×3 Gauss integration scheme produces the 3D elasticity equivalent in-plane shear stress.

Interlaminar shear stresses are computed using 9QuadNurbs, 16QuadNurbsKR and 16CubicNurbs elements with 2×2 mesh and 3×3 and 4×4 Gauss integration schemes. The k-refined Nurbs element produces interlaminar shear stresses which are closer to the 3D elasticity solution than the 9QuadNurbs and the 16CubicNurbs elements. Table 4.8 shows the comparison of in-plane and interlaminar shear stresses with 3D elasticity and 4×4 mesh of the 9QuadLagrange finite element.

4.5 Conclusions

This chapter describes the development of Nurbs post-processor for computation of interlaminar stresses in laminated composite and sandwich plates. First-order, shear-deformable laminate composite plate theory is utilized in deriving the governing equations using a variational formulation. Linear, quadratic, higher order and k-refined Nurbs elements are con-

a/h	Source	$\overline{\sigma}_{xx}$	$\overline{\sigma}_{yy}$	$\overline{\sigma}_{xy}$	$\overline{\sigma}_{xz}$	$\overline{\sigma}_{yz}$	GIS
4	9LinNurbs	$0.8714^{(0)}$	$0.15587^{(0)}$	$0.1157^{(-0.5)}$	-	-	2×2
	9LinNurbs	$1.5896^{(0)}$	$0.2651^{(0)}$	$0.14397^{(0.2)}$		-	3×3
	9QuadNurbs	0.9167	0.16191	0.0939	0.26094	0.0682	2×2
	9QuadNurbs	0.9522	0.1679	0.0977	0.2645	0.0683	3×3
	16QuadNurbsKR	-	-	-	$0.2396^{(0.25)}$	$0.1078^{(0.4)}$	3×3
	16QuadNurbsKR	-	-	-	$0.2343^{(0.45)}$	$0.1078^{(0.625)}$	4×4
	16CubicNurbsKR	-	-	-	0.2929	0.0781	3×3
	16CubicNurbsKR	-	-	-	0.2127	0.0789	4×4
	9QuadFEM/Reddy	0.8918	0.1551	0.0901	0.2808	0.0746	3×3
	3D Elasticity	1.556	0.2595	0.1481	0.239	0.1072	

Table 4.8: Non-dimensionalized in-plane and interlaminar shear stresses in a simply supported (SS1), sandwich square plate under sinusoidal loading

structed. Lagrange finite element suffers from higher- order strain gradient oscillations due to Gibbs phenomenon and require alternative stress recovery procedures. In this chapter, a Nurbs based post-processor is developed which computes interlaminar shear and normal stresses directly from higher order gradients of Nurbs basis in a single step procedure. Numerical examples tested include symmetric, anti-symmetric composite and sandwich plates. In addition, it is observed that smoothed linear Nurbs with knot insertion at optimal point and k-refined Nurbs elements compute 3D elasticity equivalent in-plane and interlaminar stresses for coarsest meshes.

Chapter 5

Stress analysis of Composite Plate with Hole using Nurbs Isogeometric Finite Element Analysis

This chapter presents the stress analysis of laminated composite plate with a hole using Nurbs Isogeometric finite element analysis, especifically, developed to study stress concentration problem. Geometry is modeled exactly in Isogeometric framework and iso-parametric finite element representation is invoked for field variable defination. The h-refinement process is performed internally by inserting a single knot in the knot vector and corresponding control net is obtained from the algorithm. The control net forms the scaffold over the physical mesh and is interpolatory only at the end points. Isotropic, $(90/0)_s$ and $(-45/45)_s$

laminates are studied under remote loading and one-forth model is considered due to symmetry. Convergence study is performed for various Isogeometric meshes. The streses are found to be in good agreement with the literature.

5.1 Plate with a Circular Hole Nurbs geometry

This subsection describes the generation of circular hole plate geometry, by construction of Nurbs basis and Nurbs surface generation. A h-refinement process is then described which is used for subsequent mesh refinements.

5.1.1 B-spline Basis

A knot vector in one dimension is a set of co-ordinates in the parametric space, $\Xi = \{\xi_1, \xi_2, ..., \xi_{n+p+1}\}$, where ξ_i is the i^{th} knot, i is the knot index where $i = 1, 2, ..., n + p + 1$, p is the order of the polynomial and n is the number of basis functions. The order of the polynomial, $p = 0, 1, 2, 3....$, refers to the constant, linear, quadratic, cubic piecewise polynomials, respectively. If more than one knot is located at the same parametric co-ordinate, these are termed as repeated knots. In case of the open knot vector, first and last knots are repeated $p + 1$ times. Basis function formed using the open knot vector are interpolatory at the beginning and end of the parametric space interval, *i.e.* $[\xi_1, \xi_{n+p+1}]$. This distinguishes the knots from the nodes in the finite element analysis as all the nodes are interpolatory. As a starting point, B-spline basis functions are defined recursively using

Cox-Deboor algorithm, starting with piecewise constants ($p = 0$).

$$N_i^p(\xi) = \begin{cases} 1 & if\ \xi_i \leq \xi < \xi_{i+1}, \\ 0 & otherwise \end{cases} \tag{5.1}$$

And, subsequently, basis functions for orders $p = 1, 2, 3, ...$, are defined as follows,

$$N_i^p(\xi) = \frac{\xi - \xi_i}{\xi_{i+p} - \xi_i} N_i^{p-1}(\xi) + \frac{\xi_{i+p+1} - \xi}{\xi_{i+p+1} - \xi_{i+1}} N_{i+1}^{p-1}(\xi) \tag{5.2}$$

5.1.2 Non-uniform Rational B-spline (Nurbs) Basis

2D Nurbs basis are formed by tensor product of B-spline basis in ξ and η direction and using projective weights associated with the control points. Rational basis functions are very similar to B-spline basis and derive the continuity and support for the function from the knot vector. Also, Nurbs basis form a partition of unity and are pointwise non-negative. These properties result in a strong convex hull property. Rational basis are formed as follows,

$$R_{i,j}^{p,q}(\xi, \eta) = \frac{N_i^p(\xi) M_j^q(\eta) W_{i,j}}{\sum_{i=1}^{CPw} \sum_{i=1}^{CPu} N_i^p(\xi) M_j^q(\eta) W_{i,j}} \approx R_k^p \tag{5.3}$$

Nurbs surface is defined as,

$$S(x, y) = \sum_{j=1}^{CPw} \sum_{i=1}^{CPu} R_{i,j}^{p,q}(\xi, \eta) B_{i,j} \tag{5.4}$$

where $N_i^p(\xi)$ and $M_j^q(\eta)$ are the B-spline basis in ξ and η direction and $R_{i,j}^{p,q}$ denotes a 2D Nurbs basis function. CPw and CPu are the number of control points in ξ and η directions and $nCP = CPu \times CPw$ is the total number of control points per element. $W_{i,j}$s are the weights associated with the control points, $B_{i,j}$ and weights are the vertical coordinates of the corresponding control points. Here, weights, Ws considered are equal to one.

5.1.3 h-refinement: Knot Insertion

h-refinement is the process of single knot insertion in the knot vector. Given a knot vector $\xi = \{\xi_1, \xi_2, ..., \xi_{n+p+1}\}$, let $\overline{\xi} - > [\xi_k, \xi_{k+1}]$ be a desired new knot. The new $n+1$ basis functions are formed recursively and new knot vector generated is as follows; $\xi = \left\{\xi_1, \xi_2, ...\xi_k, \overline{\xi}, \xi_{k+1}...., \xi_{n+p+1}\right\}$. The new $n+1$ control points, $\left\{\overline{B}_1, \overline{B}_2, ...\overline{B}_{n+1}\right\}$ are formed from the original control points, $\{B_1, B_2, ..., B_n\}$ by

$$\overline{B}_i = \alpha_i B_i + (1 - \alpha_i) * B_{i-1} \tag{5.5}$$

where

$$\alpha_i = \begin{cases} 1 & 1 \leq ik - p \\ \frac{\overline{\xi}_i - \xi_i}{\xi_{i+p} - \xi_i} & k - p + 1 \leq ik \\ 0 & k + 1 \leq i \leq n + p + 2 \end{cases} \tag{5.6}$$

Continuity of the curve is preserved by choosing the control points using above equations.

5.1.4 Circular hole plate geometry

A plate with a circular hole geometry is modeled here in Isogeometric framework. one-eightth of plate with open-hole is modeled due to symmetry. The h and p-refinement processes are applied for increasing mesh density. The coarsest mesh is defined by the knot vectors, $\xi = \{0, 0, 0, 0.5, 1, 1, 1\}$ and $\eta = \{0, 0, 0, 1, 1, 1\}$. Figures 5.1($a$) and ($b$) show the physical meshes and the control net for the plate with a circular hole. Two control points on the upper left corner creates the corner for the plate. Figures 5.2(a) and (b) show the parametric domain and the index space respectively. Exact geometry is represented by two elements ($Mesh^0$). Figures 5.3$(a) - (d)$ show various h-refined physical meshes. Physical mesh shown in 5.3(a) consists of 8 elements and 120 linear equations ($Mesh^2$), mesh in 5.3(b) consist of 32elements and 300 equations ($Mesh^3$), mesh in 5.3(c) consists of 128 elements and 900 equations ($Mesh^4$) and mesh in 5.3(d) consists of 512 elements and 3060 linear equations ($Mesh^5$) and $Mesh^6$ consists of 2048 elements and 11220 equations.

5.2 Numerical Validation

Stress concentration plays an important role in the design of layered structures. A plate with a circular hole is an important concentration problem under far-field tension loading. Symmetry boundary condition is applied at quarter symmetry. Isotropic, $(0, 90)_s$ and $(-45, 45)_s$ laminates are considered for analysis. In-plane stresses are computed at the free

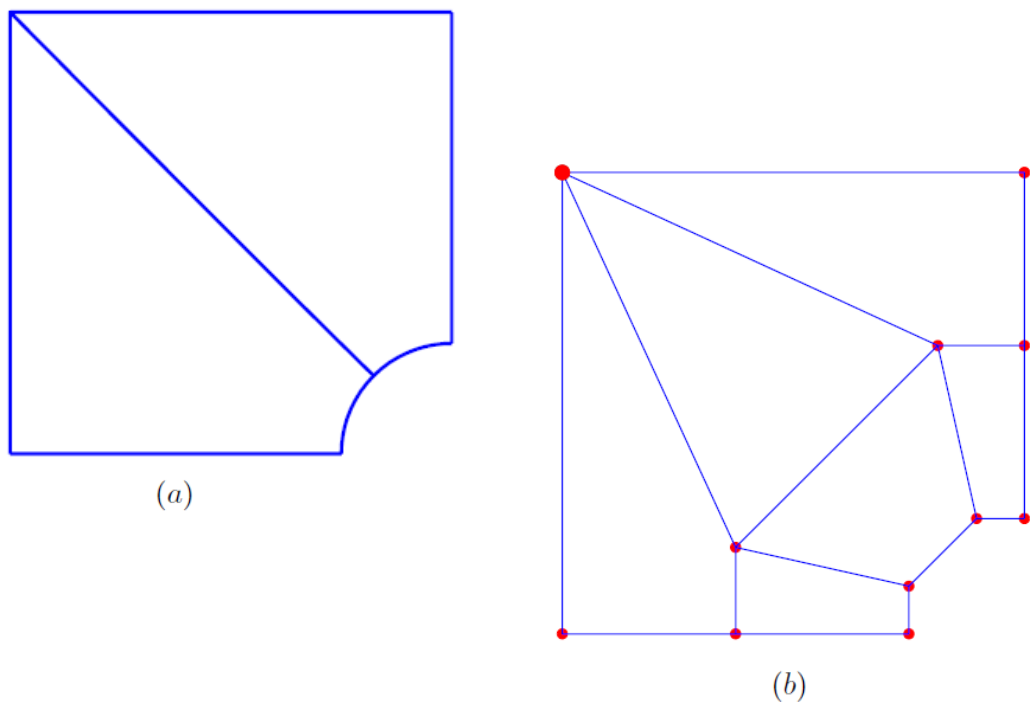

Figure 5.1: 2 element physical mesh and control net for plate with circular hole geometry

edge boundary and mesh convergence study is presented.

5.2.1 Stress analysis of isotropic plate with open hole

This example studies the circular hole problem in infinite plate under uniaxial loading. Material considered is homogeneous, elastic and isotropic and the properties are as follows; $E_1 = E_2$; $G_{12} = 0.5E_2 = G_{23} = G_{13}$; $\nu_{12} = 0.3$. Normalized hoop-stress is computed along the hole's free edge under remote tensle loading. Table 5.1 shows the hoop stress distribution for 90^0 angle around the hole. Maximum hoop stress $(\sigma_{\theta\theta}/\sigma_0)$ is obtained at

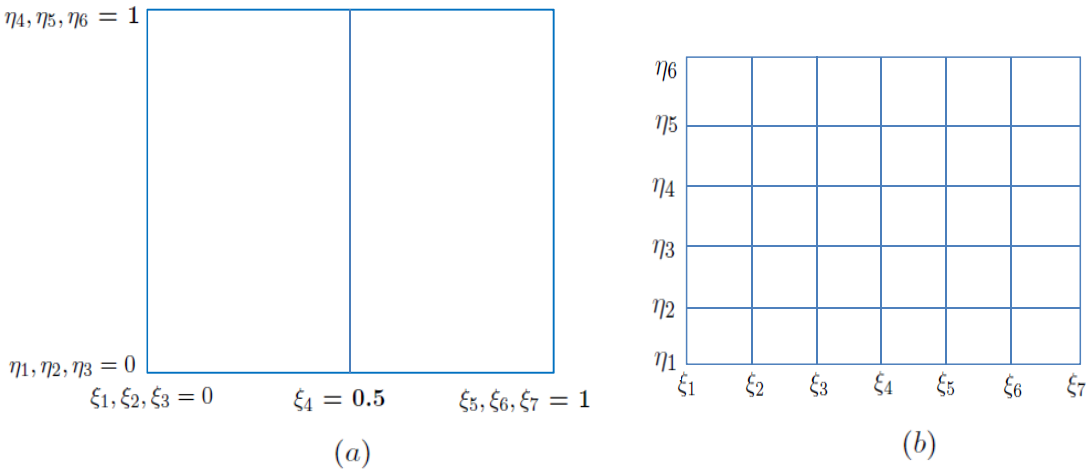

Figure 5.2: Two element parametric mesh and index space for plate with a circular hole geometry

hole's free edge and stress concentration factor is found to be 3 which is in agreement with analytical solution. Next, convergence study for increased mesh density is presented. With $Mesh^2$, $Mesh^3$ and $Mesh^4$, stresses are found to converge within 1% difference as compared with previous mesh.

Source	$\sigma_{\theta\theta}/\sigma_0(90^0)$
NurbsIso^0	3.0334
NurbsIso^2	2.9978
NurbsIso^3	3.0226
NurbsIso^4	3.0226
Analytical	3.0

Table 5.1: Stress convergence test for $\sigma_{\theta\theta}/\sigma_0$ at 90 degree angle i.e. hole edge in the mid-plane of isotropic plate

5.2.2 Stress analysis of $(90, 0)_s$ laminated composite plate with open hole

Material considered is homogeneous, elastic and orthotropic. The properties are as follows; $E_1 = 138\ GPa$; $E_2 = 14\ GPa$; $G_{12} = 5.86\ GPa$; $G_{23} = 3.43\ GPa$; $G_{13} = G_{12}$; $\nu_{12} = \nu_{13} = 0.3$. Normalized hoop-stress is computed along the hole-edge in the middle of 90^0 ($z = -3h/8$) and 0^0 ($z = -h/8$) plies. Figures 5.6 and 5.7 shows the hoop stress distribution for various angles around the hole and convergence study with increasing mesh density is presented. With $Mesh^3$ and $Mesh^4$, stresses are found to converge within $3-5\%$ difference as compared with previous mesh. Stress concentration increases with the angle along the circumference and reaches extremum at 90^0 along the hole's other edge.

For validation purposes, analysis was carried out with different orthotropic material prop-

erties which are as follows, $E_1 = 206.84GPa$; $E_2 = 20.684GPa$; $G_{12} = 6.895GPa = G_{23}$ =G_{13};$\nu_{12} = \nu_{13} = 0.336$. Table 5.1 compares the non-dimensionalized hoop stress values at 90^0 angle on the hole edge with Atluri [92] and Pan [97]'s analysis. Streses are found to be in close agreement with the literature.

Source	$\sigma_{\theta\theta}/\sigma_0(0^0)$	$\sigma_{\theta\theta}/\sigma_0(90^0)$
NurbsIso^{128}	9.57	-0.948
NurbsIso^{512}	10.22	-1.09
Nishioka	10.8	-1.0
Pan	10.7	-0.95

Table 5.2: Comparison of $\sigma_{\theta\theta}/\sigma_0$ at 90 degree angle i.e. hole edge in the mid-plane of 0 and 90 layers in $(90/s)_s$ lay up with Pan's result

5.2.3 Stress analysis of $(-45/45)_s$ laminated composite plate with open hole

Material considered is homogeneous, elastic and orthotropic. The properties are as follows; $E_1 = 138GPa$; $E_2 = 14GPa$; $G_{12} = 5.86GPa$; $G_{23} = 3.43GPa$; $G_{13} = G_{12}$; $\nu_{12} = \nu_{13} = 0.3$. Normalized in-plane stresses are computed along the hole-edge in the middle of -45^0 ($z = -3h/8$) and 45^0 ($z = -h/8$) plies. Figure 5.6 shows the in-plane stress distribution for various angles around the hole in the middle of -45^0 ply. Similarly, figure 5.7 shows normalized in-

plane stress distribution at various angles along the hole edge in the middle of 45^0 ply. These stresses are plotted using $Mesh^5$ which shows stress convergence within $2-3\%$ difference from one level less refined mesh.

5.3 Conclusions

This research presents the stress analysis around a hole's free edge in a laminated composite plate using Nurbs Isogeometric finite element, specifically developed to study stress concentration problem. Geometry is modeled exactly in Isogeometric framework and isoparametric finite element representation is invoked for solution space. Various refined Isogeometric meshes are generated for convergence study using the h-refinement process. The h-refinement process is performed internally by inserting a single knot in the knot vector and the corresponding control net is obtained from the algorithm. The control net forms the scaffold over the physical mesh and is interpolatory only at the end points. Exactly the same basis functions are used for field variable representation as are used for geometric representation. Isotropic, $(90/0)_s$ and $(-45/45)_s$ laminates are studied under remote in-plane loading and one-quater of the model is considered due to symmetry. In isotropic case, all the meshes converges to the analytical solution. For other cases, convergence study is performed for various Isogeometric meshes and good agreement is found with literature as well.

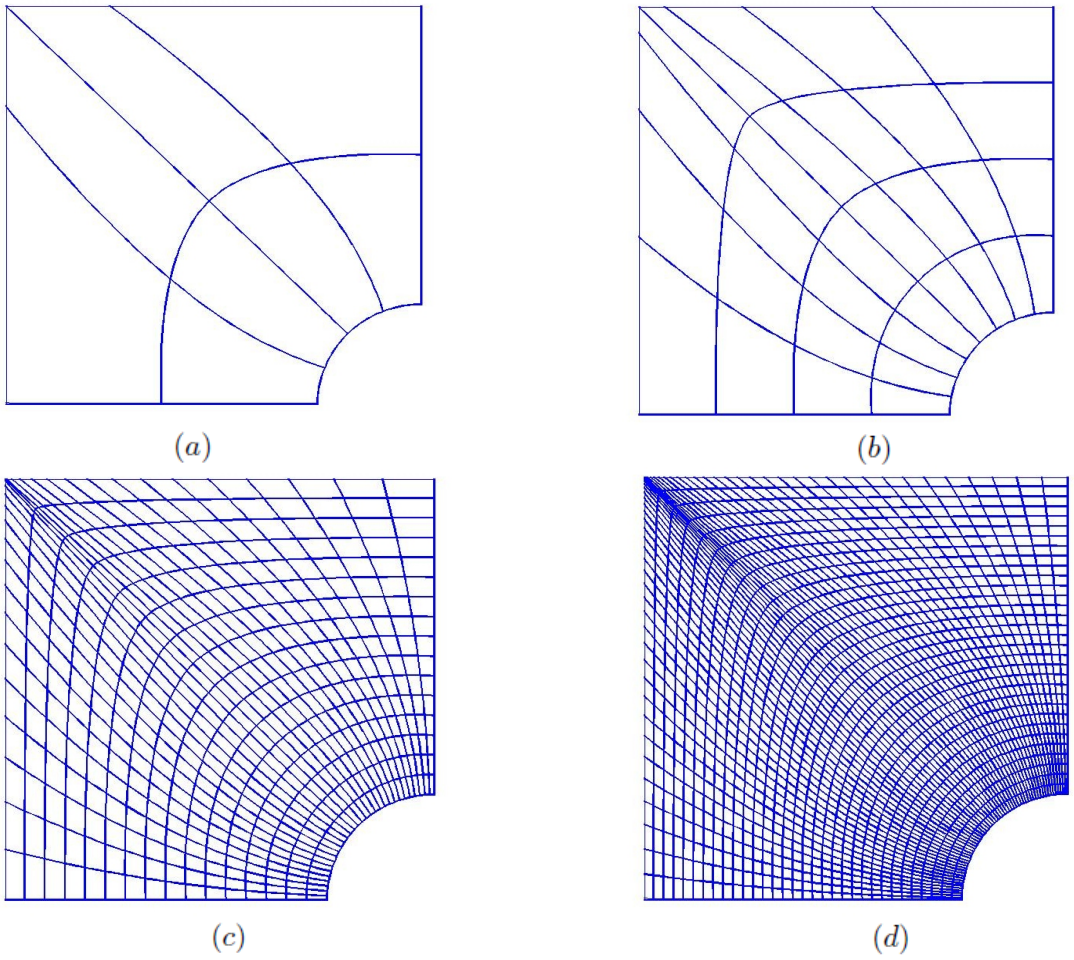

Figure 5.3: Various refined physical meshes for circular hole plate geometry

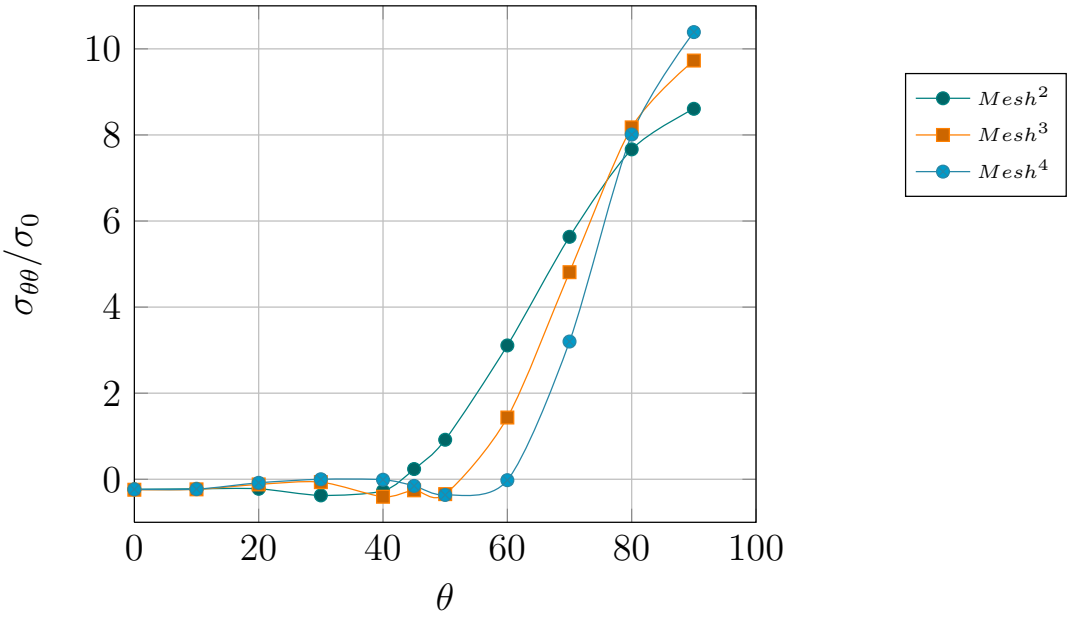

Figure 5.4: Variation of $\sigma_{\theta\theta}/\sigma_0$ around the hole edge in the middle of 0 layer in $(0/90)_s$ composite plate with a circular hole

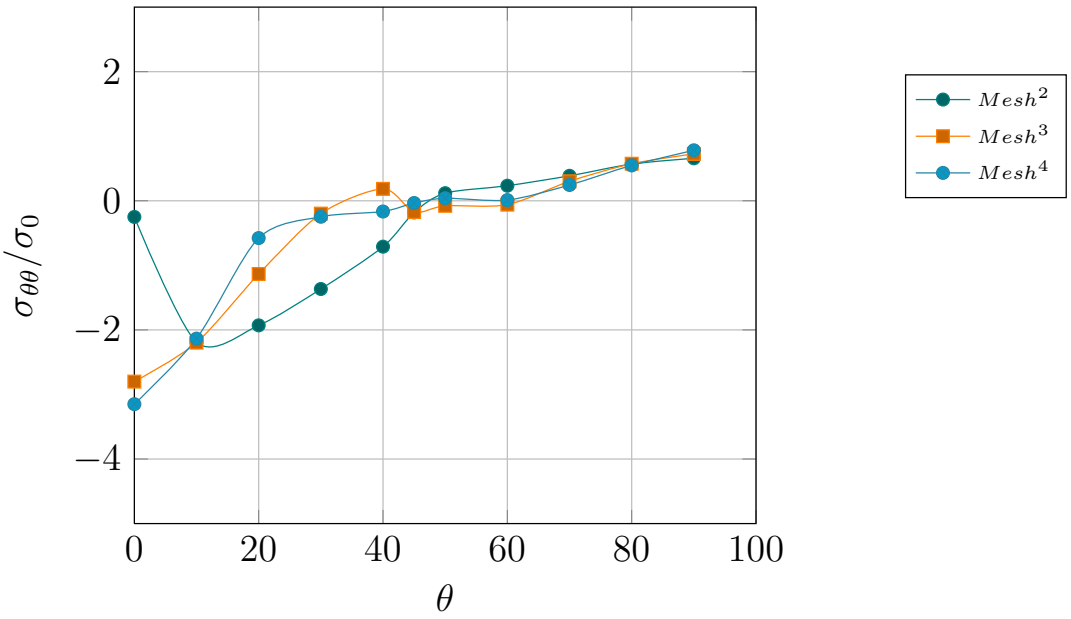

Figure 5.5: Variation of $\sigma_{\theta\theta}/\sigma_0$ around the hole edge in the middle of 90 layer in $(0/90)_s$ composite plate with a circular hole

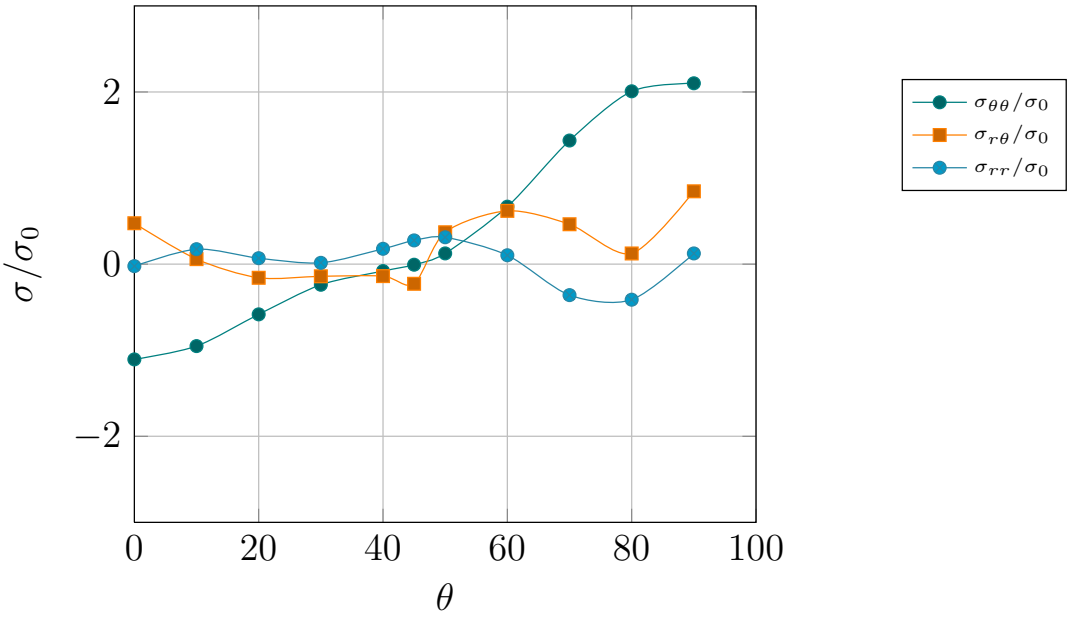

Figure 5.6: Variation of stresses around the hole edge in the middle of -45 layer in $(-45/45)_s$ laminate at refinement level 5

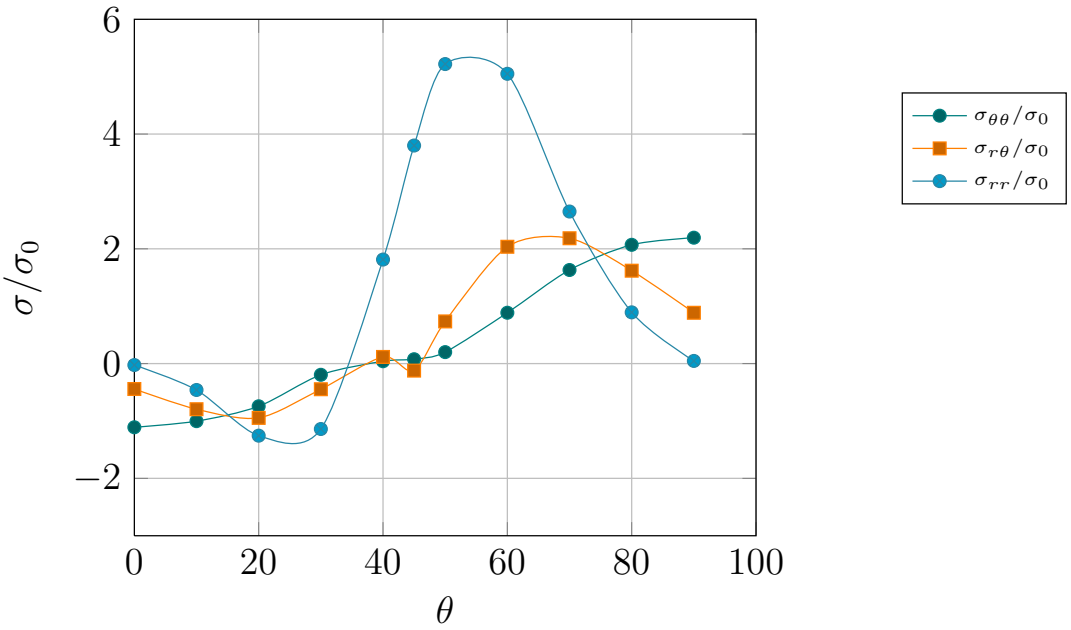

Figure 5.7: Variation of normalised stresses around the hole edge in the middle of 45 layer in $(-45/45)_s$ laminate with refinement level 5

Chapter 6

Free Vibration and Linear Dynamics Analysis

This chapter describes the development of Nurbs Isogeometric finite element analysis code for free vibration and linear dynamics analysis of composite plates. First-order, shear-deformable laminate composite plate theory is utilized in deriving the governing equations using a variational formulation. Linear, quadratic, higher order and k-refined Nurbs elements are constructed and numerical validation is performed for orthotropic and laminated composite plates. Different ply to thickness ratios, modulus ratios and ply-angles are considered.

6.1 First-order shear deformation plate theory for Laminated Composite Plates

6.1.1 Governing Equations

The origin of material coordinate system is considered to be the mid-plane of the laminate and Kirchhoff assumption that the transverse normal remain perpendicular to the mid-surface after deformation is relaxed. However, transverse strain, ϵ_z, and out-of plane normal stress, σ_z are considered negeligible. Layers are assumed to be perfectly bonded. Figure 6.1 shows the coordinate system and layer numbering of a laminated composite plate. Figure 6.2 shows the undeformed and deformed configuration of first order shear-deformable laminated composite plate. The displacement field is defined as,

$$\begin{aligned} u(x,y,z,t) &= u_0(x,y,t) + z\phi_x(x,y,t) \\ v(x,y,z,t) &= v_0(x,y,t) + z\phi_y(x,y,t) \\ w(x,y,z,t) &= w_0(x,y,t) \end{aligned} \tag{6.1}$$

where u_0, v_0, w_0, are the displacement along the x, y and z-axis and ϕ_x, ϕ_y are the rotation of transverse normal of the mid-plane about the y and x-axis respectively and t is the time variable.

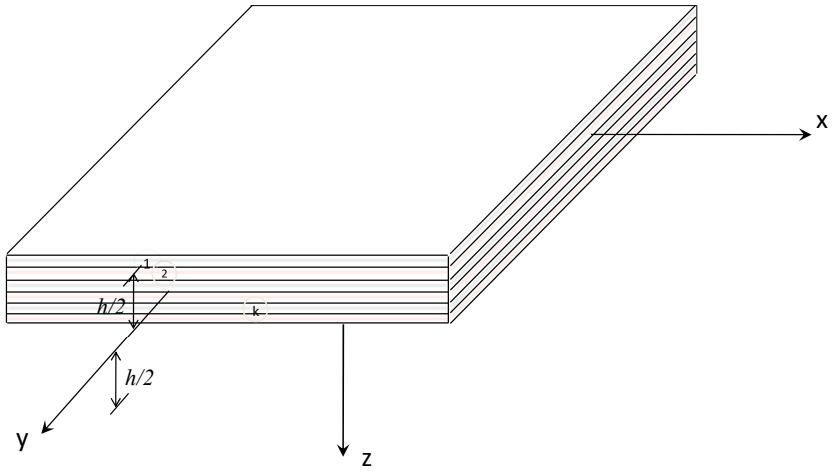

Figure 6.1: Coordinate system and layer numbering used for a laminate plate

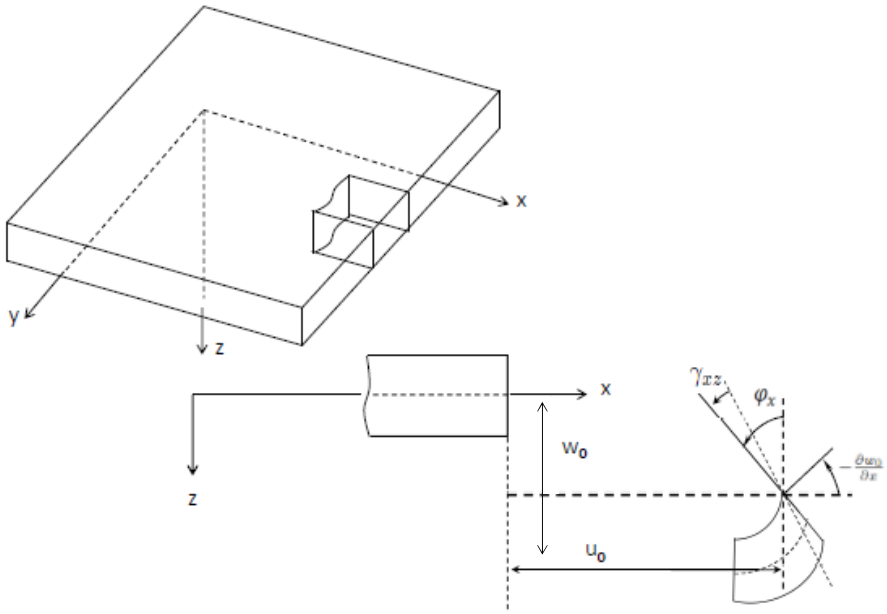

Figure 6.2: Undeformed and deformed configuration of first order shear-deformable plate

Total in-plane strain ϵ is decomposed into membrane and bending strains.

$$\epsilon = \epsilon^m + z\epsilon^b \tag{6.2}$$

ϵ^m, the membrane strain can be written as follows,

$$\epsilon^m = \left\{ \begin{array}{c} \epsilon_x^m \\ \epsilon_y^m \\ \gamma_{xy}^m \end{array} \right\} = \left\{ \begin{array}{c} \frac{\partial u_0}{\partial x} \\ \frac{\partial v_0}{\partial y} \\ \frac{\partial u_0}{\partial y} + \frac{\partial v_0}{\partial x} \end{array} \right\} \tag{6.3}$$

ϵ^b, the bending strain can be written as follows,

$$\epsilon^b = \left\{ \begin{array}{c} \epsilon_x^b \\ \epsilon_y^b \\ \gamma_{xy}^b \end{array} \right\} = \left\{ \begin{array}{c} \frac{\partial \phi_y}{\partial y} \\ \frac{\partial \phi_y}{\partial y} \\ \frac{\partial \phi_x}{\partial y} + \frac{\partial \phi_y}{\partial x} \end{array} \right\} \tag{6.4}$$

The transverse shear strain can be written as follows,

$$\left\{ \begin{array}{c} \gamma_{yz} \\ \gamma_{xz} \end{array} \right\} = \left\{ \begin{array}{c} \frac{\partial w_0}{\partial x} + \phi_x \\ \frac{\partial w_0}{\partial y} + \phi_y \end{array} \right\} \tag{6.5}$$

The stress strain relation w.r.t principal material co-ordinate system of a lamina can be

written as,

$$\begin{Bmatrix} \sigma_{xx} \\ \sigma_{yy} \\ \sigma_{xy} \end{Bmatrix}^{(k)} = \begin{bmatrix} \overline{Q}_{11} & \overline{Q}_{12} & \overline{Q}_{16} \\ \overline{Q}_{12} & \overline{Q}_{22} & \overline{Q}_{26} \\ \overline{Q}_{16} & \overline{Q}_{26} & \overline{Q}_{66} \end{bmatrix}^{(k)} \begin{Bmatrix} \epsilon_{xx} \\ \epsilon_{yy} \\ \gamma_{xy} \end{Bmatrix} \tag{6.6}$$

$$\begin{Bmatrix} \tau_{yz} \\ \tau_{xz} \end{Bmatrix}^{(k)} = \begin{bmatrix} \overline{Q}_{44} & \overline{Q}_{45} \\ \overline{Q}_{45} & \overline{Q}_{55} \end{bmatrix}^{(k)} \begin{Bmatrix} \gamma_{yz} \\ \gamma_{xz} \end{Bmatrix} \tag{6.7}$$

The equilibrium equations are developed from stress resultants by considering balance of force and moment on an infinitesimal area of the laminate. The strong form of the governing equation of motion can, then, be written as,

$$\begin{aligned} \frac{\partial N_{xx}}{\partial x} + \frac{\partial N_{xy}}{\partial y} &= I_0 \frac{\partial^2 w_o}{\partial t^2} + I_1 \frac{\partial^2 \phi_x}{\partial t^2} \\ \frac{\partial N_{xy}}{\partial x} + \frac{\partial N_{yy}}{\partial y} &= I_0 \frac{\partial^2 v_o}{\partial t^2} + I_1 \frac{\partial^2 \phi_y}{\partial t^2} \\ \frac{\partial Q_x}{\partial x} + \frac{\partial Q_y}{\partial y} + q &= I_0 \frac{\partial^2 w_0}{\partial t^2} \\ \frac{\partial M_{xx}}{\partial x} + \frac{\partial M_{xy}}{\partial y} - Q_x &= I_2 \frac{\partial^2 \phi_x}{\partial t^2} + I_1 \frac{\partial^2 u_0}{\partial t^2} \\ \frac{\partial M_{xy}}{\partial x} + \frac{\partial M_{yy}}{\partial y} - Q_y &= I_2 \frac{\partial^2 \phi_y}{\partial t^2} + I_1 \frac{\partial^2 v_0}{\partial t^2} \end{aligned} \tag{6.8}$$

where $N = \{N_{xx}, N_{yy}, N_{xy}\}$ are the force resultants, $M = \{M_{xx}, M_{xy}, M_{yy}\}$ are the moment resultants and $Q = \{Q_x, Q_y\}$ are the shear force resultants. These resultants acting per unit

length can be written as,

$$\begin{Bmatrix} N_{xx} \\ N_{yy} \\ N_{xy} \end{Bmatrix} = \int_{-h/2}^{h/2} \begin{Bmatrix} \sigma_{xx} \\ \sigma_{yy} \\ \sigma_{xy} \end{Bmatrix} dz$$
$$\begin{Bmatrix} M_{xx} \\ M_{yy} \\ M_{xy} \end{Bmatrix} = \int_{-h/2}^{h/2} \begin{Bmatrix} \sigma_{xx} \\ \sigma_{yy} \\ \sigma_{xy} \end{Bmatrix} z dz \tag{6.9}$$
$$\begin{Bmatrix} Q_x \\ Q_y \end{Bmatrix} = \int_{-h/2}^{h/2} \begin{Bmatrix} \tau_{xz} \\ \tau_{yz} \end{Bmatrix} dz$$

The laminate constitutive equations relate the force and moment resultant to strains in laminate coordinate system through ABD matrix.

$$\begin{Bmatrix} N_{xx} \\ N_{yy} \\ N_{xy} \end{Bmatrix} = \begin{bmatrix} A_{11} & A_{12} & A_{16} \\ A_{12} & A_{22} & A_{26} \\ A_{16} & A_{26} & A_{66} \end{bmatrix} \begin{Bmatrix} \epsilon_x^m \\ \epsilon_y^m \\ \epsilon_{xy}^m \end{Bmatrix} + \begin{bmatrix} B_{11} & B_{12} & B_{16} \\ B_{12} & B_{22} & B_{26} \\ B_{16} & B_{26} & B_{66} \end{bmatrix} \begin{Bmatrix} \epsilon_x^b \\ \epsilon_y^b \\ \epsilon_{xy}^b \end{Bmatrix} \tag{6.10}$$

$$\left\{ \begin{array}{c} M_{xx} \\ M_{yy} \\ M_{xy} \end{array} \right\} = \left[\begin{array}{ccc} B_{11} & B_{12} & B_{16} \\ B_{12} & B_{22} & B_{26} \\ B_{16} & B_{26} & B_{66} \end{array} \right] \left\{ \begin{array}{c} \epsilon_x^m \\ \epsilon_y^m \\ \epsilon_{xy}^m \end{array} \right\} + \left[\begin{array}{ccc} D_{11} & D_{12} & D_{16} \\ D_{12} & D_{22} & D_{26} \\ D_{16} & D_{26} & D_{66} \end{array} \right] \left\{ \begin{array}{c} \epsilon_x^b \\ \epsilon_y^b \\ \epsilon_{xy}^b \end{array} \right\} \tag{6.11}$$

$$\left\{ \begin{array}{c} Q_y \\ Q_x \end{array} \right\} = K \left[\begin{array}{cc} A_{44} & A_{45} \\ A_{45} & A_{55} \end{array} \right] \left\{ \begin{array}{c} \gamma_{yz} \\ \gamma_{xz} \end{array} \right\} \tag{6.12}$$

$$(A_{ij}, B_{ij}, D_{ij}) = \sum_{k=1}^{N} \left(\overline{Q}_{ij}^k \left(z_{k+1} - z_k \right), \frac{1}{2} \overline{Q}_{ij}^k \left(z_{k+1}^2 - z_k^2 \right), \frac{1}{3} \overline{Q}_{ij}^k \left(z_{k+1}^3 - z_k^3 \right) \right) \tag{6.13}$$

$$(A_{44}, A_{45}, A_{55}) = \sum_{k=1}^{N} \left(\overline{Q}_{44}^k, \overline{Q}_{45}^k, \overline{Q}_{55}^k \right) \left(z_{k+1} - z_k \right) \tag{6.14}$$

In the ABD matrix, A_{ij}, B_{ij} and D_{ij} terms represent extensional and shear, extensional-bending coupling and bending stiffness terms and $\overline{Q}_{ij}^{k}$s are plane-stress reduced stiffness terms. K is the shear correction factor.

Weak form of the governing equations is obtained by pre-multipying the equation of motion with δu_0, δv_0, δw_0, $\delta \phi_x$ and $\delta \phi_y$ respectively and integrating by parts over the element domain. Substituting the in-plane force, moment and shear force resultant,

$$\begin{aligned} 0 &= \int_{\Omega^e} \left(\frac{\partial \delta u_0}{\partial x} N_{xx} + \frac{\partial \delta u_0}{\partial y} N_{yy} + I_0 \delta u_0 \frac{\partial^2 u_o}{\partial t^2} + I_1 \delta u_0 \frac{\partial^2 \phi_x}{\partial t^2} \right) dxdy \\ &\quad - \oint_{\Gamma^e} P_x \delta u_0 ds \end{aligned}$$

$$\begin{aligned} 0 &= \int_{\Omega^e} \left(\frac{\partial \delta v_0}{\partial x} N_{xy} + \frac{\partial \delta v_0}{\partial y} N_{yy} + I_0 \delta v_0 \frac{\partial^2 v_o}{\partial t^2} + I_1 \delta v_0 \frac{\partial^2 \phi_y}{\partial t^2} \right) dxdy \\ &\quad - \oint_{\Gamma^e} P_y \delta u_0 ds \end{aligned}$$

$$\begin{aligned} 0 &= \int_{\Omega^e} \left[\frac{\partial \delta w_0}{\partial x} Q_x + \frac{\partial \delta W_0}{\partial y} Q_y - \delta w_0 q + I_0 \delta w_0 \frac{\partial^2 w_0}{\partial t^2} + \right. \\ &\quad \left. \frac{\partial \delta w_0}{\partial x} \left(\hat{N}_{xx} \frac{\partial \delta w_0}{\partial x} + \hat{N}_{xy} \frac{\partial \delta w_0}{\partial y} \right) + \frac{\partial \delta w_0}{\partial y} \left(\hat{N}_{xy} \frac{\partial \delta w_0}{\partial x} + \hat{N}_{yy} \frac{\partial \delta w_0}{\partial y} \right) \right] dxdy - \\ &\quad \oint_{\Gamma^e} \left[\left(Q_x + \hat{N}_{xx} \frac{\partial \delta w_0}{\partial x} + \hat{N}_{xy} \frac{\partial \delta w_0}{\partial y} \right) n_x + \left(Q_y + \hat{N}_{xy} \frac{\partial \delta w_0}{\partial x} \right. \right. \\ &\quad \left. \left. + \hat{N}_{yy} \frac{\partial \delta w_0}{\partial y} \right) n_y \delta w_0 ds \right. \end{aligned}$$

$$
\begin{aligned}
0 &= \int_{\Omega^e} \left(\frac{\partial \delta\phi_x}{\partial x} M_{xx} + \frac{\partial \delta\phi_x}{\partial y} M_{xy} + \delta\phi_x Q_x + I_2 \delta\phi_x \frac{\partial^2 \phi_x}{\partial t^2} + \right. \\
&\quad \left. I_1 \delta\phi_x \frac{\partial^2 u_0}{\partial t^2} \right) dxdy - \oint_{\Gamma^e} T_x \delta\phi_x ds
\end{aligned} \tag{6.16}
$$

$$
\begin{aligned}
0 &= \int_{\Omega^e} \left(\frac{\partial \delta\phi_y}{\partial x} M_{xy} + \frac{\partial \delta\phi_y}{\partial y} M_{yy} + \delta\phi_y Q_y + I_2 \delta\phi_y \frac{\partial^2 \phi_y}{\partial t^2} + \right. \\
&\quad \left. I_1 \delta\phi_y \frac{\partial^2 v_0}{\partial t^2} \right) dxdy - \oint_{\Gamma^e} T_y \delta\phi_y ds
\end{aligned}
$$

6.2 Linear Nurbs Isogeometric Finite Element Formulation / Dynamics

6.2.1 Finite Element Model

The dependent displacement field variables are approximated by Nurbs basis as follows,

$$
u_0(x,y) = \sum_{j=1}^{nCP} u_j R_j(x(\xi,\eta), y(\xi,\eta)), v_0(x,y) = \sum_{j=1}^{nCP} v_j R_j(x(\xi,\eta), y(\xi,\eta))
$$

$$
w_0(x,y) = \sum_{j=1}^{nCP} w_j R_j(x(\xi,\eta), y(\xi,\eta)) \tag{6.17}
$$

$$
\phi_x(x,y) = \sum_{j=1}^{nCP} \phi_{xj} R_j(x(\xi,\eta), y(\xi,\eta)), \phi_y(x,y) = \sum_{j=1}^{nCP} \phi_{yj} R_j(x(\xi,\eta), y(\xi,\eta))
$$

where nCP are the number of control points per element and R_j are $2D$ Nurbs basis.

Substituting the displacement field approximation into the weak form, we obtain element

stiffness matrix, mass matrix and load vector. I_0, I_1, I_2 are mass inertia terms. For instance, the size of a sub-matrix, K_{ij}^{11} and M_{ij}, in element stiffness matrix, is $(nCP) \times (nCP)$ and the size of element load vector, F, is $(nCP \times dof, 1)$. nCP stands for control points per element, dof are the no. of degrees of freedom /control point and $(\alpha, \beta = 1, 2, ...5)$.

$$\left[K^{\alpha\beta}\right] = \begin{bmatrix} [K^{11}] & [K^{12}] & [K^{13}] & [K^{14}] & [K^{15}] \\ [K^{21}] & [K^{22}] & [K^{23}] & [K^{24}] & [K^{25}] \\ [K^{31}] & [K^{32}] & [K^{33}] & [K^{34}] & [K^{35}] \\ [K^{41}] & [K^{43}] & [K^{43}] & [K^{44}] & [K^{45}] \\ [K^{51}] & [K^{52}] & [K^{53}] & [K^{54}] & [K^{55}] \end{bmatrix} \tag{6.18}$$

$$[M] = \begin{bmatrix} I_0\,[M] & [0] & [0] & I_1\,[M] & [0] \\ [0] & I_0\,[M] & [0] & [0] & I_1\,[M] \\ [0] & [0] & I_0\,[M] & [0] & [0] \\ I_1\,[M] & [0] & [0] & I_2\,[M] & [0] \\ [0] & I_1\,[M] & [0] & [0] & I_2\,[M] \end{bmatrix} \tag{6.19}$$

$$F_i^{\alpha=3} = \int_{\Omega^e} qR_i^p dxdy \tag{6.20}$$

From the element stiffness matrix, the expression for K^{11}, a sub-matrix of element stiffness

matrix, K, and M_{ij} of M, matrix are as follows,

$$K_{ij}^{11} = \int_{\Omega^e} \left[A_{11} \frac{\partial R_i^p}{\partial x} \frac{\partial R_j^p}{\partial x} + A_{66} \frac{\partial R_i^p}{\partial y} \frac{\partial R_j^p}{\partial y} + A_{16} \left(\frac{\partial R_i^p}{\partial x} \frac{\partial R_j^p}{\partial y} + \frac{\partial R_i^p}{\partial y} \frac{\partial R_j^p}{\partial x} \right) \right] dxdy \tag{6.21}$$

$$M_{ij} = \int_{\Omega^e} R_i^p R_j^p dxdy \tag{6.22}$$

Free Vibration and Linear Dynamics Analysis

For natural vibration, we obtain the following equation:

$$0 = [K] - \omega^2 [M] \tag{6.23}$$

In this analysis, Singular Value Decomposition (SVD) method is used for eigenvalue analysis. The steps are as follows,

$$RM = \sqrt{M}; \qquad InvM = RM^{-1}; \qquad \lambda = svd(InvM * K * InvM) \tag{6.24}$$

The transient analysis equations can be written as follows,

$$[K^e] \{\Delta^e\} + [M^e] \left\{\ddot{\Delta}^e\right\} = \{F^e\} \tag{6.25}$$

All the symbolic notations have the usual meaning. Newmark method is used for time integration and constant average acceleration method is used as it is unconditionally stable.

6.2.2 Nurbs Basis Formulation

This subsection details B-spline and rational basis generation and describes the transformation from physical to parametric to parent domain. The p and k-refined Nurbs elements are constructed by modifying the knot vector. Last part of this subsection describes the construction of various elements.

B-spline Basis

A knot vector in one dimension is a set of co-ordinates in the parametric space, $\Xi = \{\xi_1, \xi_2, ..., \xi_{n+p+1}\}$, where ξ_i is the i^{th} knot, i is the knot index where $i = 1, 2, ..., n + p + 1$, p is the order of the polynomial and n is the number of basis functions. The order of the polynomial, $p = 0, 1, 2, 3....$, refer to the constant, linear, quadratic, cubic piecewise polynomials, respectively. If more than one knot is located at the same parametric co-ordinate, these are termed as repeated knots. In case of the open knot vector, first and last knots are repeated $p + 1$ times. Basis function formed using the open knot vector are interpolatory at the beginning and end of the parametric space interval, *i.e.* $[\xi_1, \xi_{n+p+1}]$. This distinguishes the knots from the nodes in the finite element analysis as all the nodes are interpolatory. As a starting point, bspline basis functions are defined recursively using Cox-Deboor algorithm, starting with piecewise constants ($p = 0$).

$$N_i^p(\xi) = \begin{cases} 1 & if\ \xi_i \leq \xi < \xi_{i+1}, \\ 0 & otherwise \end{cases} \tag{6.26}$$

And, subsequently, basis functions for orders $p = 1, 2, 3, ...$, are defined as follows,

$$N_i^p(\xi) = \frac{\xi - \xi_i}{\xi_{i+p} - \xi_i} N_i^{p-1}(\xi) + \frac{\xi_{i+p+1} - \xi}{\xi_{i+p+1} - \xi_{i+1}} N_{i+1}^{p-1}(\xi) \tag{6.27}$$

Rational B-spline (Nurbs) Basis

2D Nurbs basis are formed by tensor product of B-spline basis in ξ and η direction and using projective weights associated with the control points. Rational basis are very similar to B-spline basis and derive the continuity and support for the function from the knot vector. Also, Nurbs basis form a partition of unity and are pointwise non-negative. These properties result in a strong convex hull property. Rational basis are formed as follows,

$$R_{i,j}^{p,q}(\xi, \eta) = \frac{N_i^p(\xi) M_j^q(\eta) W_{i,j}}{\sum_{i=1}^{CPw} \sum_{i=1}^{CPu} N_i^p(\xi) M_j^q(\eta) W_{i,j}} \tag{6.28}$$

Nurbs surface is defined as,

$$S(x, y) = \sum_{j=1}^{CPw} \sum_{i=1}^{CPu} R_{i,j}^{p,q}(\xi, \eta) B_{i,j} \tag{6.29}$$

where $N_i^p(\xi)$ and $M_j^q(\eta)$ are the B-spline basis in ξ and η direction and $R_{i,j}^{p,q}$ denotes a 2D Nurbs basis function. CPw and CPu are the number of control points in ξ and η directions and $nCP = CPu \times CPw$ is the total number of control points per element. $W_{i,j}$s are the weights associated with the control points, $B_{i,j}$ and weights are the vertical coordinates of the corresponding control points. Here, weights, Ws considered are equal to one.

6.2.3 Nurbs Isogeometric Meshes

Various Nurbs Isogeometric meshes are developed using linear, quadratic and cubic Nurbs basis functions constructed above. Exact (linear) and various higher-order Nurbs Isogeometric meshes are developed using the knot vector manuplation. Linear mesh requires a tensor product of knot vector, [0 0 1 1], in ξ and η directions. Similarly, quadratic, [0 0 0 1 1 1], cubic, [0 0 0 0 1 1 1 1], and k-refined quadratic knot vector, [0 0 0 0.5 1 1 1], forms various Nurbs Isogeometric meshes. Figures show 8×8 meshes constructed using above knot vectors. From figure (c) and (d) one can see the variation in mesh

6.2.4 Numerical Integration

A multi-element patch, a tensor product of knot vectors in ξ and η directions, i.e. $\{0 \;\; 0 \;\; 0.5 \;\; 1 \;\; 1\} \times \{0 \;\; 0 \;\; 0.5 \;\; 1 \;\; 1\}$, creates a 2×2 plate mesh in physical domain. A linear combination of Nurbs basis with respective control points constructs a geometric model of plate. In order to perform numerical integration, Gauss quadrature is employed. The integration on physical domain is performed by transformation from physical to parametric and from parametric to parent domain. Mapping between physical and parametric domain is performed as follows,

$$\left\{ \begin{array}{c} x \\ \\ y \end{array} \right\} = \sum_{k=1}^{nCP} R_k^1(\xi, \eta) \left\{ \begin{array}{c} Bx_k \\ \\ By_k \end{array} \right\}$$

$$\left\{ \begin{array}{c} \frac{\partial R_k^p}{\partial x} \\ \\ \frac{\partial R_k^p}{\partial y} \end{array} \right\} = [J^{-1}] \left\{ \begin{array}{c} \frac{\partial R_k^p(\xi,\eta)}{\partial \xi} \\ \\ \frac{\partial R_k^p(\xi,\eta)}{\partial \eta} \end{array} \right\} \tag{6.30}$$

$$[J] = \left[\begin{array}{cc} \frac{\partial x}{\partial \xi} & \frac{\partial y}{\partial \xi} \\ \\ \frac{\partial x}{\partial \eta} & \frac{\partial y}{\partial \eta} \end{array} \right]$$

Bx_k and By_k are control point coordinates and $J_{x\xi y\eta}$ is the mapping from physical to parametric domain. The Mapping from parametric to parent domain is the standard mapping as is done in finite element. Figure 6.3 shows schematic of Isogeometric framework.

6.2.5 Nurbs Elements

Various lower and higher order Nurbs elements are constructed by utilizing various refinement techniques. Linear Nurbs element, 9LinNurbs, with 9 control point (with a knot insertion at locations such as { 0 }, 2×2 Guass integration scheme), quadratic Nurbs element, 9QuadNurbs/(F/R), with 9 control points and k-refined, quadratic Nurbs element, 16QuadNurbsKR/F, with 16 control points are developed. Element notation is as follows: number in the front denotes the number of control points/element, KR denotes the k-refined element. A few Nurbs elements construction is detailed here.

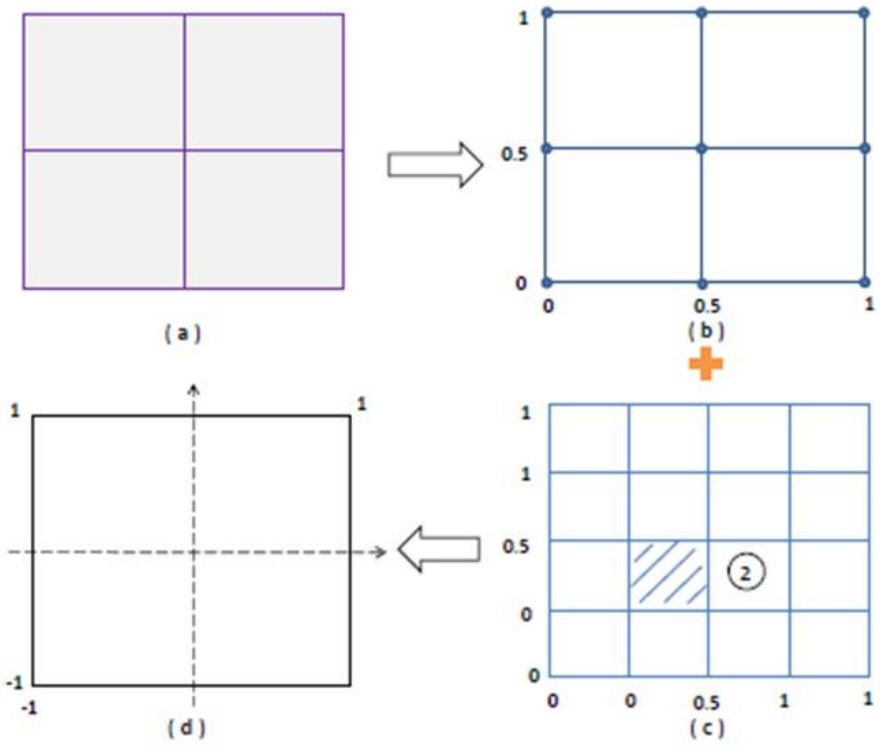

Figure 6.3: Mapping between physical and parent domain: a framework for Isogeometric finite element analysis

Quadratic Nurbs Element (9QuadNurbs))

A tensor product of knot vector $\{-1\ -1\ -1\ 1\ 1\ 1\}$ in $\hat{\xi}$ and $\hat{\eta}$ direction results in a bi-quadratic Nurbs element in the parent domain. $\hat{\xi}_i$ denote the i^{th} knot value in the knot vector. The element consists of 9 control points. The shape function in $\hat{\xi}$ direction can be written as follows,

$$M_1^2(\hat{\xi}) = \left(\frac{\hat{\xi}_4 - \hat{\xi}}{\hat{\xi}_4 - \hat{\xi}_2}\right)\left(\frac{\hat{\xi}_4 - \hat{\xi}}{\hat{\xi}_4 - \hat{\xi}_3}\right)$$

$$
\begin{aligned}
M_2^2(\hat{\xi}) &= \left(\frac{\hat{\xi}-\hat{\xi}_2}{\hat{\xi}_4-\hat{\xi}_2}\right)\left(\frac{\hat{\xi}_4-\hat{\xi}}{\hat{\xi}_4-\hat{\xi}_3}\right)+\left(\frac{\hat{\xi}_5-\hat{\xi}}{\hat{\xi}_5-\hat{\xi}_3}\right)\left(\frac{\hat{\xi}-\hat{\xi}_3}{\hat{\xi}_4-\hat{\xi}3}\right) \qquad \hat{\xi}_3 \le \hat{\xi} < \hat{\xi}_4 \\
M_3^2(\hat{\xi}) &= \left(\frac{\hat{\xi}-\hat{\xi}_3}{\hat{\xi}_5-\hat{\xi}_3}\right)\left(\frac{\hat{\xi}-\hat{\xi}}{\hat{\xi}_4-\hat{\xi}3}\right)
\end{aligned} \tag{6.31}
$$

k-refined Quadratic Nurbs element I(16QuadNurbsKR)

A tensor product of knot vector $\{-1\ -1\ -1\ 0\ 1\ 1\ 1\}$ in $\hat{\xi}$ and $\hat{\eta}$ direction results in a quadratic Nurbs element, 16QuadNurbsKR[1](F/R). The knot vector is divided into two intervals and shape functions have unique value over each interval. $\hat{\xi}_i$ denote the i^{th} knot value in the knot vector. The shape functions in $\hat{\xi}$ direction over each interval are derived as follows,

$$
\begin{aligned}
M_1^2(\hat{\xi}) &= \left(\frac{\hat{\xi}_4-\hat{\xi}}{\hat{\xi}_4-\hat{\xi}_2}\right)\left(\frac{\hat{\xi}_4-\hat{\xi}}{\hat{\xi}_4-\hat{\xi}_3}\right) \\
M_2^2(\hat{\xi}) &= \left(\frac{\hat{\xi}-\hat{\xi}_2}{\hat{\xi}_4-\hat{\xi}_2}\right)\left(\frac{\hat{\xi}4-\hat{\xi}}{\hat{\xi}_4-\hat{\xi}_3}\right)+\left(\frac{\hat{\xi}_5-\hat{\xi}}{\hat{\xi}_5-\hat{\xi}_3}\right)\left(\frac{\hat{\xi}-\hat{\xi}_3}{\hat{\xi}_4-\hat{\xi}3}\right) \qquad \hat{\xi}_3 \le \hat{\xi} < \hat{\xi}_4 \\
M_3^2(\hat{\xi}) &= \left(\frac{\hat{\xi}-\hat{\xi}_3}{\hat{\xi}_5-\hat{\xi}_3}\right)\left(\frac{\hat{\xi}-\hat{\xi}}{\hat{\xi}_4-\hat{\xi}3}\right) \\
M_4^2(\hat{\xi}) &= 0
\end{aligned} \tag{6.32}
$$

$$
\begin{aligned}
M_1^2(\hat{\xi}) &= 0 \\
M_2^2(\hat{\xi}) &= \left(\frac{\hat{\xi}_5-\hat{\xi}}{\hat{\xi}_5-\hat{\xi}_3}\right)\left(\frac{\hat{\xi}_5-\hat{\xi}}{\hat{\xi}_5-\hat{\xi}_4}\right) \\
M_3^2(\hat{\xi}) &= \left(\frac{\hat{\xi}-\hat{\xi}_3}{\hat{\xi}_5-\hat{\xi}_3}\right)\left(\frac{\hat{\xi}-\hat{\xi}}{\hat{\xi}_4-\hat{\xi}3}\right)+\left(\frac{\hat{\xi}-\hat{\xi}_3}{\hat{\xi}_5-\hat{\xi}_3}\right)\left(\frac{\hat{\xi}_5-\hat{\xi}}{\hat{\xi}_5-\hat{\xi}_3}\right) \qquad \hat{\xi}_4 \le \hat{\xi} < \hat{\xi}_5 \\
M_4^2(\hat{\xi}) &= \left(\frac{\hat{\xi}-\hat{\xi}_4}{\hat{\xi}_6-\hat{\xi}_4}\right)\left(\frac{\hat{\xi}_4-\hat{\xi}}{\hat{\xi}_5-\hat{\xi}_4}\right)
\end{aligned} \tag{6.33}
$$

Similarly, the shape functions in $\hat{\eta}$ direction are obtained. The product rule yields 16 bi-quadratic shape functions, R_k^2, requiring 4×4 Gauss points. In k-refinement process, the order of the existing knot vector from base model is elevated first and then, a knot is inserted instead of elevating the order after knot insertion. This results in $q-1$ continuous derivatives instead of $p-1$ continuous derivatives, where p and q are the order of the knot vector before and after the order elevation, respectively.

6.3 Numerical Testing

Laminated composite plates with various orientation and thickness ratios are studied for validation purposes. Cross-ply and anti-symmetric angle ply composite laminated plate are studied. Due to bi-axial symmetry, only a quadrant of the plate is modeled and fundamental frequency and center deflection are plotted.

6.3.1 Simply supported, cross-ply (0/90/90/0), square plate

In this analysis, a simply-supported, square, laminated cross-ply plate is studied. Material for each lamina is considered as homogeneous, elastic and orthotropic. Material properties used are as follows: $E_1 = 25E_2$, $G_{12} = G_{13} = 0.5E_2$, $G_{13} = 0.2E_2$, $\nu_{12} = 0.25$, and $K_s = 5/6$. $9QuadNurbs$ with 3×3 Gauss integration scheme and 9LinNurbs with 2×2 Gauss integration schemes are considered. 2×2, 4×4 and 8×8 physical meshes are used in the analysis. Effect of modulus in fiber direction on natural frequency is studied and compared with the

existing literature. Fundamental frequency for different elements is compared with exact solution [116], [113], MLSDQ's solution by Liew et al.[114] and RBF's results [115] for the coarsest mesh. Table 6.1 shows the fundamental frequency comparison for these elements.

Element	Mesh	E_2/E_1 10	20	30	40
9quadNurbs	2×2	8.54	9.37	9.99	10.29
9quadNurbs	3×3	8.42	9.45	9.92	10.36
9LinNurbs	2×2	9.144	10.01	10.52	10.86
9LinNurbs	3×3	8.72	9.64	10.18	10.54
LinIsoNurbs	4×4	8.88	9.79	10.32	10.68
LinIsoNurbs	8×8	8.53	9.49	-	-
LinIsoNurbs	16×16	8.376	-	-	-
MLSDQ		8.2924	9.5613	10.32	10.849
RBF		8.3101	9.5801	10.349	10.864
Exact		8.2982	9.5671	10.326	10.854

Table 6.1: Comparison of natural frequency of a simply supported, cross-ply (0/90/90/0) square plate for various E_2/E_1

6.3.2 Effect of span-to-thickness ratio on simply-supported, laminated cross-ply $(0/90/90/0)$, square plate

In this analysis, a simply-supported, square, cross-ply (0/90/90/0), laminated composite plate with various span to thickness ratios, $a/h = 5, 10, 20, 25, 50, 100$, are analyzed. Material for each lamina is considered as homogeneous, elastic and orthotropic. Material properties used are as follows: $E_2/E_1 = 40, G_{12} = G_{13} = 0.5E_2, G_{23} = 0.2E_2, \nu_{12} = 0.25$, and $K_s = 5/6$. $9QuadNurbs$ element with 3×3 Guass integration and $9LinNurbs$ element with 2×2 Guass integration scheme are used. Table 6.2 shows the fundamental frequency comparison for these elements with 2×2 and 4×4 meshes. Comparisons are made with Reddy and Phan [112], $p - Ritz$ solution [114], RBF-pseudospectral method [115]. Table 6.2 shows the comparison of fundamental frequency for various Nurbs elements. It is observed that lower span to thickness ratio has considerable effect on natural frequency, however, the effect dies down for higher a/h ratios.

6.3.3 Effect of Layup Sequence and Fiber Orientation

A simply supported, cross-ply (0/90/90/0), square laminate with $a/h = 100$, is studied for free vibration analysis. The material properties used here are as follows : $E_1/E_2 = 25$; $G_{12}/E_2 = 0.50$; $G_{23}/E_2 = 0.20$; $G_{13} = G_{12}$; $E_2 = E_3$; $\nu_{12} = \nu_{23} = \nu_{13} = 0.25$. This example investigates the effect of layup sequence and fiber orientation for $[\theta/0/0/\theta]$ and $[0/\theta/\theta/0]$ plies under simply-supported boundary conditions. Span to thickness ratio of $a/h = 100$

Element	Mesh	a/h 10	20	50	100
9quadNurbs	3×3	14.40	17.50	18.61	19.03
9LinNurbs	3×3	14.52	17.33	18.81	18.90
LinIsoNurbs	4×4	16.27	18.99	21.37	22.52
LinIsoNurbs	8×8	15.4865	18.20	19.84	20.37
LinIsoNurbs	16×16	15.177	17.92	19.39	19.74
HSDT		15.2689	17.6669	18.4624	18.7561
p-Ritz		15.1434	17.6583	18.6734	18.8359
RBF		15.1007	17.6338	18.6586	18.8223

Table 6.2: Comparison of natural frequency of a simply supported, cross-ply (0/90/90/0) square plate for various a/h ratios with the literature ($\omega^* = (\omega * a^2/h)\sqrt{\rho/E_2}$)

and modulus ratio, $E_1/E_2 = 10$ is used in computation. Figures 6.4 and 6.5 shows the effect of lay-up sequence and fiber orientation on natural frequency.

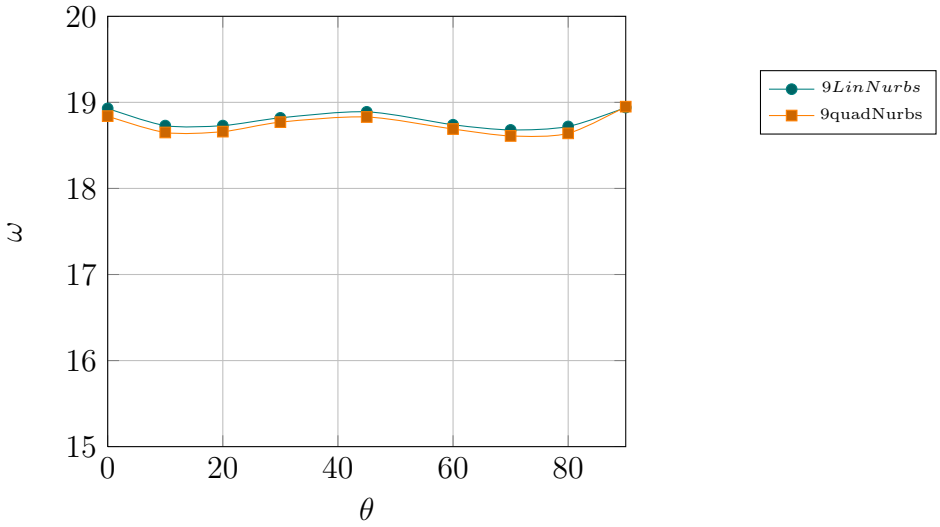

Figure 6.4: Effect of fiber orientation and stacking sequence $[0, \theta, \theta, 0]$ on natural frequency of square laminated plate

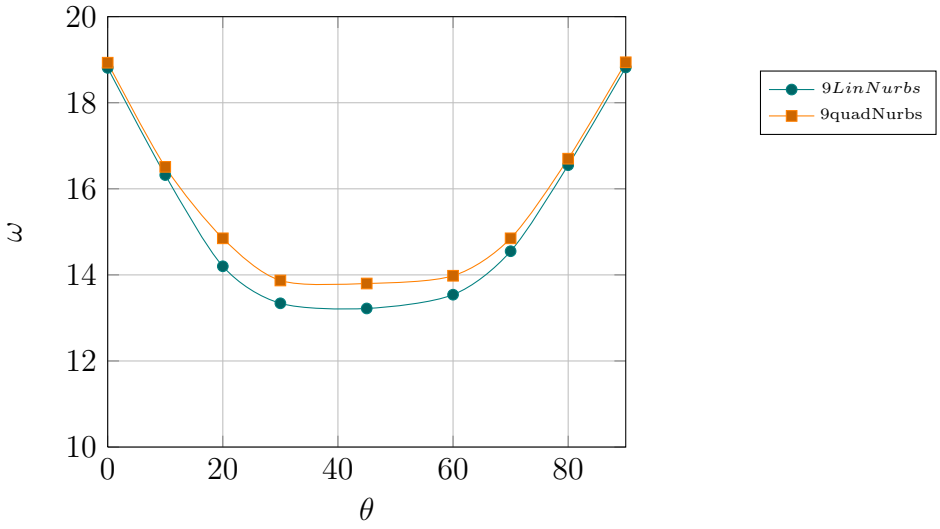

Figure 6.5: Effect of fiber orientation and stacking sequence $[\theta, 0, 0, \theta]$ on natural frequency of square laminated plate

6.3.4 Higher frequencies using higher order Nurbs elements

A simply supported ($SS1$), cross-ply laminate is studied here. The material properties used here are as follows : $E_1/E_2 = 40$; $G_{12}/E_2 = 0.60$; $G_{23}/E_2 = 0.5$;$G_{13} = G_{12}$; $E_2 = E_3$; $\nu_{12} = \nu_{23} = \nu_{13} = 0.25$. First five natural frequencies are computed in Table 6.3 for $a/h = 10$. 9QuadNurbs, 9LinNurbs and 16CubicNurbs and 16QuadNurbsKR elements are considered. 2×2, 4×4 and 8×8 meshes are used for analysis. It is observed that $9LinNurbs$ element computes lower frequencies than other elements considered.

Element	Mesh	ω_1^*	ω_2^*	ω_3^*	ω_4^*	ω_5^*
9quadNurbs	4×4	14.48	44.07	53.65	68.17	86.15
9quadNurbs	8×8	14.48	43.88	53.55	67.97	84.94
9LinNurbs	4×4	13.295	40.05	50.03	63.49	82.23
9LinNurbs	8×8	13.185	40.26	49.33	67.97	84.94
16CubicNurbs	2×2	14.47	43.82	53.48	67.88	85.30
16quadNurbsKR	2×2	14.32	45.03	54.48	69.46	93.5

Table 6.3: Comparison of first five natural frequencies of a simply supported, cross-ply (0/90/90/0) square plate for $a/h = 10$ for various Nurbs elements, $(\omega^* = (\omega * a^2/h)\sqrt{\rho/E_2})$

6.3.5 Orthotropic Plate under step loading

A simply-supported ($SS1$), orthotropic plate is studied. The material properties used are as follows:$E_1 = 525000$; $E_2 = 21000\ N/mm^2$; $G_{12}/E_2 = 0.60$; $G_{23}/E_2 = 0.5$; $G_{13} = G_{12}$;

$E_2 = E_3$; $\nu_{12} = \nu_{23} = \nu_{13} = 0.25$. Orthotropic plate is subjected to uniform step loading and center delfection is computed. $9LinNurbs$ and $9quadNurbs$ element are constructed and span to thickness ratios of $50, 10$, are considered for analysis respectively. Maximum center deflection for $a/h = 50$ was compared with Chen[84]'s analysis. Chen's analysis, (6×6 mesh), computed the maximum normalized center deflection as 0.435 as compared to 0.41 obtained using $9quadNurbs$ element and 0.45 obtained using $9LinNurbs$ element. Figures 6.6 and 6.7 show center deflection vs time response for above elements.

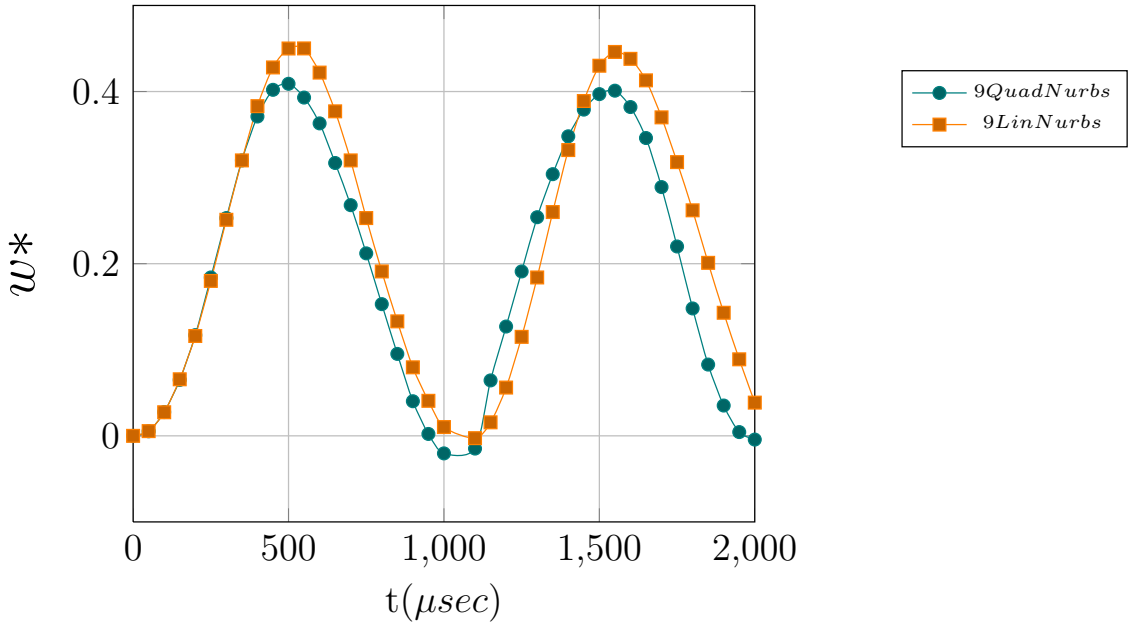

Figure 6.6: Transient response of orthotropic plate for $a/h = 50$

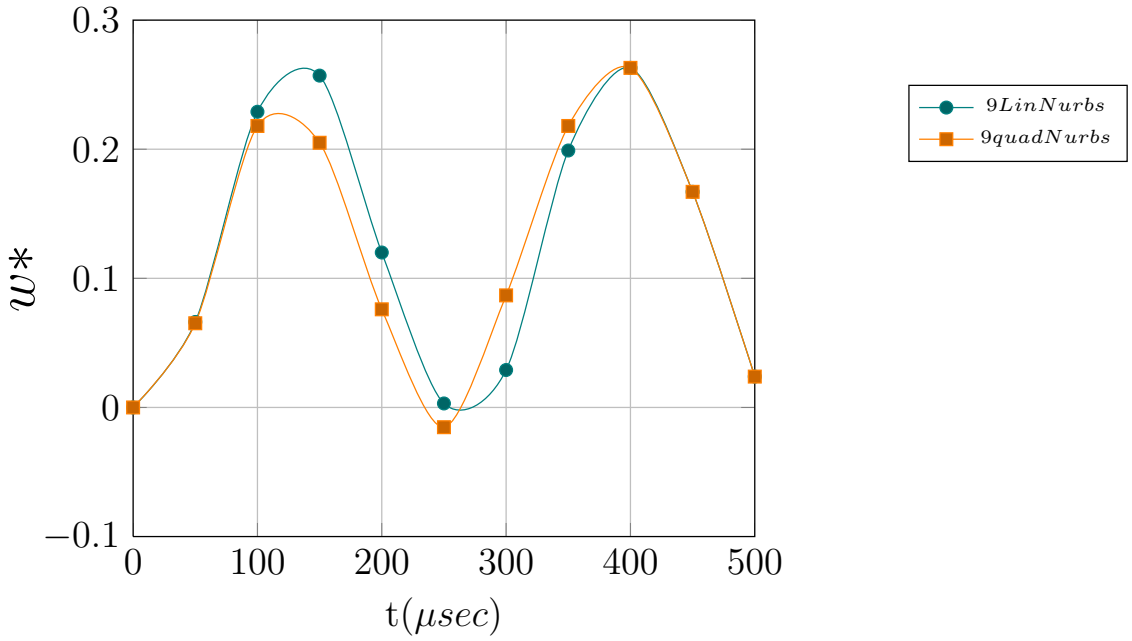

Figure 6.7: Transient response of orthotropic plate for $a/h = 10$

6.3.6 Four layer cross-ply and anti-symmetric angle-ply plates under step loading

A simply-supported ($SS1$), cross-ply 0/90/90/0), composite plate is studied here. The foloowing material properties were used here, $E_1 = 40E_2$; $E_2 = 21000\ N/mm^2$; $G_{12}/E_2 = 0.60$; $G_{23}/E_2 = 0.5$; $G_{13} = G_{12}$; $E_2 = E_3$; $\nu_{12} = \nu_{23} = \nu_{13} = 0.25$. Transient analysis is performed for span to thickness ratio, $a/h = 50$ and $9LinNurbs$ and $9quadNurbs$ are considered in this analysis. In Fig. 6.8, the center deflection vs time is plotted for the coarsest mesh.

Anti-symmetric angle-ply layup introduces B_{16} and B_{26} coupling coefficients. Effect of these coupling coeffcients are explored in this analysis. Transient analysis is performed for [45/ −

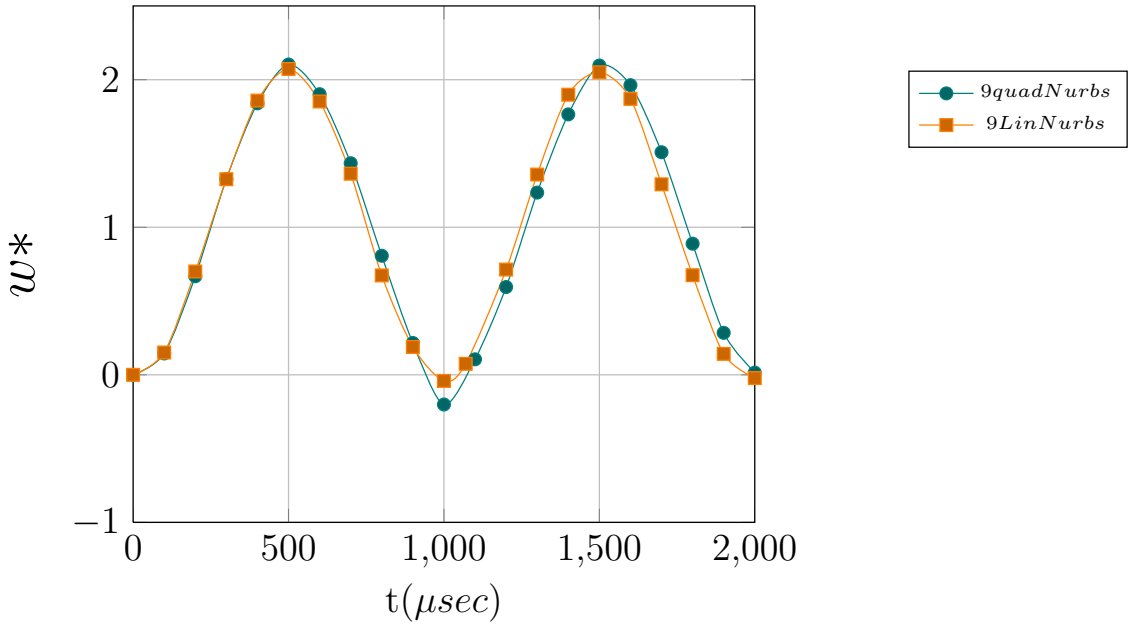

Figure 6.8: Transient response of laminated composite lay up (0/90/90/0) sequence for $a/h = 50$

$45/45/-45]$ angle-ply layup for $a/h = 50$. $9LinNurbs$ and $9quadNurbs$ elements are considered in this analysis. In Fig. 6.9, center deflection vs time response is plotted for the coarsest mesh. It is observed that the center deflections are reduced in this case when compared with the [0/90/90/0] lay-up. This is due to coupling coefficient contribution to the stiffness matrix.

6.4 Conclusions

This chapter details the development of Nurbs Isogeometric finite element analysis code for free vibration and linear dynamics analysis of composite plates. First-order, shear-deformable laminate composite plate theory is utilized in deriving the governing equations

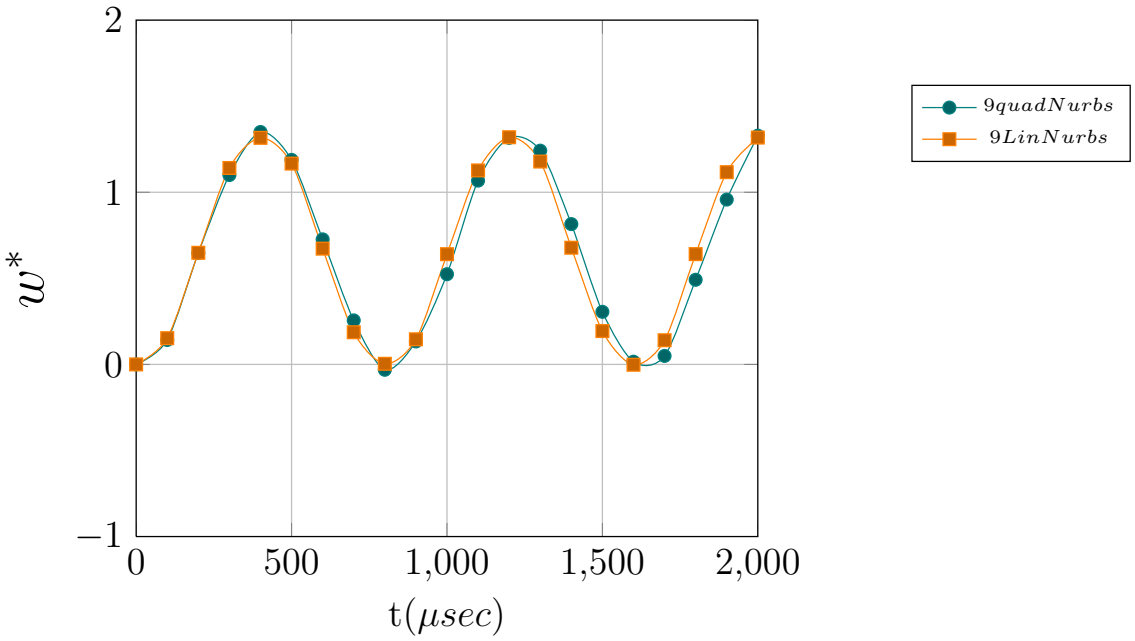

Figure 6.9: Transient response of laminated composite lay up $(45/-45/45/-45)$ sequence for $a/h = 50$

using a variational formulation. Linear, quadratic, higher order and k-refined Nurbs elements are constructed and numerical validation is performed for orthotropic, laminated composite plates. Different ply to thickness ratios, modulus ratios and ply-angles are considered.

Chapter 7

Conclusion and Future Work

Inspite of the extensive use of finite element methods, the barriers between engineering design and analysis still exist and the way to bridge gap is use the same model for analysis as used in CAD. The idea, introduced by T.J.R. Hughes, to use the same CAD basis for analysis purpose as used for geometry representation is known as Isogeometric analysis. There are several CAD functions which can be used for Isogeometric analysis. Of most widely used CAD basis in engineering design process are Nurbs (non-uniform rational B-splines) as presented by Piegle and tiller[20], Farin[21], Cohen et al.[22] and Rogers[23]. The CAD industry widely uses Nurbs to describe the smooth lines and surfaces. The curve or surface generated using Nurbs depends on control points which are associated with unique basis function. Thus, each vertex effects the shape of the curve over a range of parametric values where the basis function is non-zero.

The CAD based functions such as bezier basis have been used for solving computational mechanics problems. They offers advantage over the regular finite element due to their piecewise form, smoothness and higher-order continuity. Besides that, these functions offer computational efficiency, good accuracy and convergence characteristics. Nurbs basis possess useful mathematical property of refinement through knot insertion and variational diminishing property of convex hull i.e. curve does not oscillate about any straight line more than its control polygon oscillates about the line.

Most finite element are still performed with low-order elements for which geometric errors are largest. Isogeometric analysis entirely removes the finite element polynomial approximation of geometry. Besides this, Nurbs basis are generated using recursion algorithm which tends to improve the computational efficiency. Equation systems are more homogeneous as basis have same shape on both ends. Nurbs basis are non negative and therefore, the mass matrix is non-negative.

This research endevour develops Isogeometric approach for analysis of composite structures and take advantage of higher order continuity, smoothness and variation dimishing properties of Nurbs basis for interlaminar stress analysis of composite and sandwich structures. Nurbs Isogeometric finite element analysis code is developed for analysis of composite plates in (geometrically) nonlinear and linear range and for static and dynamic analysis. Besides that, newer parent elements are also developed using refinement techonology of knot vector. various Nurbs elements such as 9 control point linear (utilizing h-refinement), quadratic, cubic and k-refined quadratic, cubic, quartic Nurbs element are constructed and validated

with numerical tesing. It is found that 9 control point linear Nurbs element removes shear locking in linear and nonlinear ranges contrary to Nurbs quadratic and quadratic Lagrange elements. Though, reduced integration removes shear locking, it accompanies with hourglass instability or mesh distortion due to rank deficiency. 9 control point linear Nurbs element and k-refined element technology removes this deficienicy without reducing the order of integration, especially in nonlinear range.

Next, Nurbs post-processor for in-plane and interlaminar stress calculation in laminated composite and sandwich plates is developed. Lagrange finite element suffers from higher order stress gradient oscillations due to Gibbs phenomenon and require alternative stress recovery procedures for accurate interlaminar stress calculations, especially interlaminar normal stress. Researchers have developed higher order shear defromation theories and zig-zag theories for accurate prediction of interlaminar stresses. Here, direct Nurbs based post-processing is performed which computes in-plane and interlaminar shear and normal stresses from higher order gradients of Nurbs basis in a single step procedure. The stresses are found to be in an excellent agreement with 3D elasticity solution and better than Lagrange finite element and higher order shear deformation theory. Some of the elements perform exactly w.r.t 3D elasticity solution which is due to higher order smoothness properties of Nurbs basis. **In beam analysis, B-spline basis developed using Cox-Deboor recursion algorithm are found to be better than basis constructed using old form of B-splines in terms of computational efficiency**.

Next, stress analysis of laminated composite plate with open-hole using Nurbs Isogeometric

finite element analysis is developed. Geometry is modeled exactly in Isogeometric framework and iso-parametric finite element representation is invoked for field variable defination. Various refined Isogeometric meshes are generated for convergence study using h-refinement process. h-refinement process is performed internally by inserting a single knot in the knot vector and corresponding control net is obtained from the algorithm. Isotropic plate with hole, $(0/90)_s$ and $(-45/45)_s$ composite laminates are studied under in-plane loading. Stress concentration factor plays an important role in design consideration for composite structures and free edge calculations are important. Here, stress concentration factor is computed along the hole edge and compared with the literature. Convergence study is performed for various Isogeometric meshes and stress convergence is obtained with increased mesh density. In isotropic example, all the meshes converge to the same solution which matches the analytical solution.

Next, Nurbs Isogeometric finite element code for free-vibration and linear dynamics analysis of laminated composite plates is developed. First-order, shear-deformable laminate composite plate theory is utilized in deriving the governing equations using a variational formulation. Linear, quadratic, higher order and k-refined Nurbs elements are constructed and numerical validation is performed for orthotropic and laminated composite plates. Different ply to thickness ratios, modulus ratios and ply-angles are considered. The results are found to be in good agreement with the literature. Linear Nurbs Isogeometric analysis with one Gauss integration point converges well, however, 9 control point linear Nurbs and quadratic Nurbs elements perform better in terms of mesh refinement.

For future direction, the applications of the Nurbs based Isogeometric analysis are numerous. Further direction can be to extend this code for analysis of plate with straight and curved stiffners, buckling analysis, crack propagation analysis with XFEM, impact and crashworthiness analysis, elastic-plastic analysis and for wave propagation in complex geometries like pi-joints.

Bibliography

[1] Courant, R.,"Variational methods in solution of equilibrium and vibration," of American Mathematical Society, Vol. 49, 1-43, 1943

[2] Zeinkeiwicz, O. C. and Cheung, Y. K.,*The finite element method in structural and continuum mechanics*, McGraw-Hill

[3] Taig, I. C.,*Structural analysis by matrix displacement method*, Technical report, English Electric Aviation

[4] Zeinkeiwicz, O. C., Taylor, R. L. and Too, J. M.,"Reduced integration technique in general analysis of plates and shells,"*International Journal of Numerical Methods in Engineering*, Vol. 3, 275-290, 1971

[5] Schoenberg, I. J.,"Contributions to the problems of approximation of equidistant data by analytical functions," *Quart. Appl. Math.*, Vol. 4, 112-141, 1946

[6] DeBoor, C. R., "A Practical Guide to Splines ," *Springer-Verlag*, 1978

[7] Gontier, C. and Vollmer, C.,"A large displacement analysis of a beam using a CAD geometric definition," *Computers and Structures*, Vol. 57, No. 6, 981-989, 1995

[8] Kagan, P., Fischer, A. and Yoseph, P. B.,"New B-spline finite element approach for geometrical design and mechanical analysis," *International Journal of Numerical methods in Engineering*, Vo. 41, 435-458, 1998

[9] Kagan, P., Fischer, A. and Yoseph, P. B.,"Mechanically based model: Adaptive refinement of B-spline finite element," *International Journal of Numerical methods in Engineering*, Vo. 57, 1145-1175, 2003

[10] Ganapathi, M., Patel, B. P., Saravanam, J., and Tousatier, M.,"Shear-flexible Curved beam element for static analysis," *Finite Element in Analysis and Design*, Vol. 32, pp. 181 - 202, 1999

[11] Chen, J. S., Han, W. and Meng, X.,"A reproducing kernel method with nodal interpolation property," *International Journal of Numerical Methods in Engineering*, Vol. 56, pp. 935-960, 2003

[12] Atluri, S. N. and Shen, S. P., "The meshfree local Petrov-Galerkin (MLPG) method ," *Tech Science Press Encino*, USA, 2002

[13] Atluri, S. N. and Zhu, T., "A meshfree local Petroc-Galerkin (MLPG) approach to computational mechnics," *Computational Mechanics*, Vol. 22, pp. 117-127, 1998

[14] Melenk, J. M. and Babuska, I."The partition of unity finite element method: basic theory and application ," *Computer Methods in Applied Mechanics and Engineering*, Vol. 139, pp. 289-314, 1996

[15] Babuska, I. and Melenk, J. M. "Partition of unity method," *International Journal of Numerical Methods in Engineering*, Vol. 40, pp. 727-758, 1997

[16] Rao, B. N. and Rahman, S.,"An element-free Galerkin method for probabilistic mechanics and reliability," *International Journal of Solids and Structures*, Vol. 38, no. 50-51, pp. 9313-9330, 2001

[17] Belytschko, T., Organ, D. and Gerlach, C.,"Element-free Galerkin methods for dynamic fracture in concrete," *Computer Methods in Applied Mechanics and Engineering*, Vol. 48, no. 11, pp. 385-399, 2000

[18] Dolbow, J. and Belytschko, T.,"An introduction to programming the meshless element-free Galerkin method," *Archives of Computational Methods in Engineering*, Vol. 5, no. 3, pp. 207-241, 1998

[19] Liu, G. R., Yan, L. and Wang, J. G.,"A point integration method based on local residual formulation using radial functions ," *Structural Engineering And Mechanics*, Vol. 14, no. 6, pp. 713-732, 2002

[20] Piegl, L., and Tiller, W.,*The Nurbs book (Monograph in visual communication)*, 2nd Edition, Springer-Verleg

[21] Farin, G.,*Curves and Surfaces, A practical guide*, 5th Edition, Morgan aufmann Publishers, 1950

[22] Cohen, E., Lyche, T., and Reisenfield, R.,"Discrete b-splines and subdivision techniques in computer aided geometric design and computer graphics," *Computer graphics and Image processing*, Vol. 14, pp. 87-111, 1980

[23] Rogers, D. F.,"Introdution to Nurbs with historic prospective,"*Academic Press*, 1955

[24] Peters, J., and Reif, U.,"Subdivision surface,"*Springer-Verlag*

[25] Warren, J., and Weimer, H.,"Introdution to Nurbs with historic prospectiveSubdivision methods for Geometric Design,"*Morgan Kaufmann Publishers*

[26] Gordon, W.,"Spline-blended interpolation through curve networks,"*Journal of Methamatics and Mechanics*, Vol. 18, 931-952, 1969

[27] Gregory, J. A.,*n-sided surface patches*, N. Gregory, j. A. editor, Mathematics of Surfaces,Clarendon Press

[28] Loop, C. T., and DeRose, T. D.,"A multisided generalization of Bezier surfaces," *ACM Transaction on Graphics*, Vol. 8, 204-234, 1989

[29] Bajaj, C., Chen, J. and Xu, G.,"Modeling with cubic A-patches,"*ACT Transactions on Graphics*, vol. 14, 103-133, 1995

[30] Hughes, T.J.R., Cottrell, J.A. and Bazilevs, Y.,"Isogeometric analysis: CAD, Finite elements, Nurbs, exact geometry and mesh refinement," *Computer Methods in Applied Mechanics and Engineering*, Vol. 194 , 4135-4195, 2005

[31] Hughes, T.J.R, Reali, A. and Sangali, G.,"Duality and unified analysis of discrete approximation in structural dynamics and wave propagation: comparison of p-method finite elements with k-method Nurbs," *Comput. Meth. Appl. Mech. Engng.*, Vol. 197, 4104-4124, 2008

[32] Bazilevs, Y., Calo, V. M., Hughes, T.J.R. and Zhang, Y.,"Isogeometric fluid-structure inreaction: theory, algorithm and computations, *Comput. Mech.*, Vol. 38, 310-322, 2006

[33] Cottrel, J.A., Hughes, T.J.R. and Reali, A.,"Isogeometric analysis of structural vibration," *Computer Aided Geometric Design*, Vol. 27, 644-655, 2010

[34] Vuong, A. V., Heinrich, Ch. and Simeon, B.,"ISOGAT: A 2D tutorial MATLAB code for Isogeometric Analysis," *Comput. Meth. Appl. Mech. Eng.*, Vol. 196, 4160-4183, 2010

[35] Reissner, E.,"On the theory of bending of elastic plates," *Journal of Mathematical Physics*, 23, 184-191, 1944

[36] Reissner, E.,"Effect of transverse shear deformation on the bending of elastic plates," *Journal of Applied Mechanics*, 12, 69-77, 1945

[37] Mindlin, R.,"Influence of rotatory inertia and shear on flexural motions of isotropic, elastic plates," *Journal of applied mechanics*, 18, 31-38, 1951

[38] Whitney, J. and Pagano, N.,"Shear deformation in heterogeneous anisotropic plates," *Journal of Applied Mechanics*, Vol. 37, 1031-1036, 1970

[39] Urthaler, Y. and Reddy, J. N.,"A mixed finite element for the nonlinear bending analysis of laminated composite plates based on FSDT," *Mechanics of Advanced Materials and Structures*, Vol. 15, 335-354, 2008

[40] Putcha N. S. and Reddy, J. N.,"A refined mixed shear flexible finite element for the nonlinear analysis of laminated plates," *Computer Structure*, Vol. 22, 529-38, 1986

[41] Kant, T. and Kommineni, J. R.,"C^0 finite element geometrically nonlinear analysis of fibre reinforced composite and sandwich laminates based on a higher-order theory," *Computers & Structures* , Vol. 45, 511-520, 1992

[42] Polit, O. and Touratier, M.,"A multilayered/Sandwich triangular finite element applied to linear and non-linear analyses," *Composite Structures*, 121-128, 2002

[43] Reddy, J. N. and Robbins, DH. Jr,"Theories and computational models for composite laminates," *Appl. Mech. Rev.*, Vol. 47, no. 6, 147 - 169, 1994

[44] Wang, C. M. and Reddy, J. N."Shear deformable beams and plates: Relationship with classical solutions," *Elsevier, Oxford, U. K.*, 2000

[45] Reddy, J. N. and Sandidge, D.,"Mixed finite element models for laminated composite plates," *Journal of Engineering for Industry*, Vol. 109, 39-45, 1986

[46] Zienkeiwicz, O. C., Taylor, R. L. and Too, J. M.,"Reduced integration technique in general analysis of plates and shells," *International Journal for Numerical Methods in Engineering*, Vol. 3, pp. 275-290, 1971

[47] Hughes, T. J. R., Taylor, R. L. and Kanoknukuchai, W.,"A simple and efficient finite element for plate bending," *International Journal for Numerical Methods in Engineering*, Vol. 11, pp. 1529-1543, 1977

[48] MacNeal, R. H.,"Derivation of element stiffness matrices by assumed strain distribution," *Nuclear Engineering and Design*, Vol. 70, pp. 3-12, 1982

[49] Bathe, K. J., and Dvorkin, E. N.,"A four-node plate bending element based on Mindlin/Reissner plate theory and a mixed interpolation," *International Journal for Numerical Methods in Engineering*, Vol. 21, pp. 367-383, 1983

[50] Batoz, J. L. and Katili, I.,"On a simple triangular nine d.o.f element based on incompatible modes and discrete constraints," *International Journal for Numerical Methods in Engineering*, Vol. 35, pp. 1603-1632, 1992

[51] Zienkeiwicz, O. C., Zeng, L. F., Samuelsson, A., and Wiberg, N. E.,"Linked Interpolation for Reissner-Mindlin Plate element: Part I- a simple quadrilateral.," *International Journal for Numerical Methods in Engineering*, Vol. 36, pp. 3043-3056, 1993

[52] Shi, Z. C., Ming, P. and Braess, D.,"Shear locking in a plane elasticity prolem and the enhanced assumed strain method," *Siam J. Numer. Anal.*, Vol. 47, No. 9, 4479-4491, 2010

[53] Echer, R. and Bischoff, M.,"Numerical efficiency, locking and unlocking of Nurbs finite elements,*Comput. Meth. Appl. Mech. Eng.*, Vol. 199, 374-382, 2010

[54] Zhang, Y. X. and Kim, K. S.,"Geometrically nonlinear analysis of laminated composite plates by two new displacement-based quadrilateral plate elements," *Composite Structures*, Vol. 72, 301 - 310, 2006

[55] Minghini, F., Tullini, N., and Laudiero, F.,"Locking-free finite element for shear deformable orthotropic thin-walled beams," *International Journal for Numerical Methods in Engineering*, Vol. 72, 808-834, 2007

[56] Nguyen-Xuan, H., Rabczuk, T., Bordas, S., and Debongnie, J. F.,"A Smoothed Finite Element for Plate Analysis," *Computational Methods for Applied Mechanics Engineering*, Vol. 197, pp. 1184-1203, 2008

[57] Cai, Y. C., Tian, L. G., and Atluri, S. N.,"A Simple Locking Free Discrete Shear Triangular Plate Element," *CMES*, Vol. 77, no. 4, pp. 221-238, 2011

[58] Bathe, K. J."The Finite Element Methods," *Prentice-Hall*, Englewood Cliffs, NNJ/MA, 1987

[59] Bathe, K. J.,*A Finite Element Procedures*, Prentice-Hall/MIT ,Englewood Cliffs, NNJ/MA, 1996

[60] Zienkiewicz, O. C., Taylor, R. L.,"The Finite Element Methods, fifth ed.," *Oxford*, Butterworht-Heinemann, 2000

[61] Flanagan, T. P., and Belytschko, T.,"A uniform strain hexahedron and quadrilateral with orthogonal hourglass control," *Int. j. Numer. Methods Engng.*, Vol. 17, 679-706, 1981

[62] Tessler, A. and Hughes, T.J.R.,"An improved treatment of transverse shear in the Mindlin-type four node quadrilateral element," *Comput. Methods Appl. Mech. Engng.*, Vol. 39, 311-335, 1983

[63] Phan, ND. and Reddy, J. N.,"Analysis of laminated composite plate using a higher order shear deformation theory," *International Journal for Numerical Methods in Engineering*, Vol. 21(12), 2201-19, 1985

[64] Ren, J. G. and Hinton, E.,"The finite element analysis of homogeneous and laminated composite plates using a simple higher order theory. *Communications in Applied Numerical methods*, Vol. 2(2), 217-28, 1986

[65] Codina, R.,"On stabilized finite element methods for linear systems of convection-diffusion-reaction equations," *Comput. Methods Appli. Mech. Engng.*, Vol. 188, 61-82, 2000

[66] Lyly, M. and Stenberg, R.,"On the connection between some linear triangular Riessener-Mindlin plate bending elements," *Numer. Math.*, Vol. 85, 77-107, 2000

[67] Tessler, A.,"Accurate interlaminar stress recovery from finite element analysis," *NASA Technical Memorandum*, NASA-TM-109149, Sept. 1994

[68] Reddy, J. N.,"A simple higher order theory for laminated composite plates," *Journal of Applied Mechanics*, Vol. 51, pp. 745-752, Dec. 1984

[69] Byun, C., and Kapania, R. K.,"Prediction of interlaminar stresses in laminated plates using the global orthogonal interpolation polynomials," *AIAA Journal*, Vol. 30, No. 11, Nov. 1992

[70] Lee, K., and Lee, S.,"A post-processing approach to determine transverse stresses in geometrically nonlinear composite and sandwich structures", *Journal of Composite Materials*, Vol. 37, pp. 2207 - 2224, 1996

[71] Park, J. W., and Kim, Y. H.,"Displacement, stresses and their sensitivity coefficients in composite panels," *Journal of Composite Materials*, Vol. 33, No. 13, pp. 1222 -1243, 1999

[72] Park, B. P., Park, J. W., and Kim, Y. H.,"Stress recovery in laminated composite and sandwich panels undergoing finite rotation," *Composite Structures*, vol. 59, pp. 227-235, 2003

[73] Noor, A. K., Kim, Y. H., and Peters, J. M.,"Transverse shear stresses and their sensitivity coefficients in multi-layered composite panels," *AIAA Journal*, Vol. 32, No. 6, pp. 1259-1269, 1994

[74] Matsunaga, H.,"Interlaminar stress analysis of laminated composite beams to global higher-order deformation theories," *Composite Structures*, Vol. 55, pp. 105-114, 2002

[75] Makeev, A., and Armanios, E. A.,"An iterative method for solving elasticity problems for composite laminates," *ASME Journal of Applied Mechanics*, Vol. 67, No. 1, March 2000

[76] Rolfes, R. and Rohwer, K.,"Improved transverse shear stresses in composite finite elements based on the first order shear deformation theory," *International Journal for Numerical Methods in Engineering*, Vol. 40, pp. 51 - 60, 1997

[77] Kant, T., and Manjunatha, B. S.,"On accurate estimation of transverse stresses in multilayer composites," *Computers and Structures*, Vol. 50, No. 3, pp. 3451 - 365, 1994

[78] Kant, T., Gupta, A. B., Pendhari, S. S., and Desai, Y. M.,"Elasticity solution of cross-ply composite and sandwich laminate," *Computers and Structures*, Vol. 83, No. 1, pp. 13-24, March, 2008

[79] Nosier, A., and Baharami, A.,"Interlaminar stresses in antisymmetric angle - ply laminates," *Composite Structures*, Vol. 78, pp. 18 - 33, 2007

[80] S. S. Vel, and Batra, R. C.,"Analytical solutions for rectangular thick laminated plates subjected to arbitrary boundary conditions," *AIAA Journal*, Vol. 37, pp. 1464-1473, 1999

[81] Barlow, J.,"Optimal stress locations in finite element models," *Int. J. Numer. Methods*, Vol. 10(2), pp. 243-251, 1976

[82] Oden, J. T., and Brachli, H. J.,"On the calculation of consistent stress distribution in finite element approximation,"*Int. J. Numer. Methods*, Vol. 10(2), pp. 243-251, 1971

[83] Hinton, J. S., and Cambell, E.,"Local and global smoothing of discontinuous finite element functions using a least square method,"*Int. J. Numer. Methods*, Vol. 8(3), pp. 461-480, 1974

[84] Chen, D. J., Shah, D. K., and Chan, W. S.,"Interfacial stress estimation using least-square extrapolation and local stress smoothing in a laminated composites,"*Computer Structures*, Vol. 58, pp. 765-774, 1996

[85] Zienkiewicz, O.C. and Zhu, J. Z.,"The super convergent patch recovery and a posteriori erro estimates. Part I: the recovery technique,"*Int. J. Numer. Methods Eng*, Vol. 33(7), pp. 1331-64, 1992

[86] Yuan, J., Saleeb, A., and Gendy,, A.,"Projection stress: layerwise- equivalent formulation for accurate prediction of transverse stresses in laminated plate and shells,"*Int. J. Computat. Eng. Sci*, Vol. 1(1), pp. 91-138, 1982

[87] Prathap, G., and Naganarayana, B. P.,"Consistent thermal stress evaluation in finite elements," *Comput. Struc*, Vol. 54(3), pp. 415-46, 1995

[88] Tang, S.,"Interlaminar stresses around circular cutouts in composite plates under tension," *AIAA Journal*, Vol. 15(11), pp. 1631-37, 1976

[89] Tang, S.,"A variational approach to edge stresses of circular cutouts in composites," *20th AIAA/ASME/ASCE/AHS, SDM Conference, St. Louis, MO*, AIAA Paper 79-0802, pp. 326-32, 1979

[90] RamKumar, R. L., Saether, E. S., and Cheng, D.,"Design guide for bolted joints in composite structures," *AFWAL-TR-86-3035*, 1986

[91] Soni, S. R.,"Stress and strength analysis of bolted joints in composite laminates," *Composite Structures*, Vol. 03, pp. 50-62, 1981

[92] Nishioka, T., and Atluri, S. N.,"Stress analysis of holes in angle-ply laminates: an efficient assumed stress special hole element approach and a simple estimation method," *Computer Structures*, Vol. 15(2), pp. 135-147, 1982

[93] Iarve, E. V., "Spline variational three dimensional stress analysis of laminated composite plates with open holes," *International Journal of Solid Structures*, Vol. 33(14), pp. 2095-2118, 1996

[94] Raju, I. S., and Crews, Jr.,"Three dimensional analysis of $[0/90]_s$ and $[90/0]_s$ laminates with a central circular hole," *Composite Technology Review* , Vol. 4(4), pp. 116-124, 1982

[95] Folias, E. S.,"Boundary layer effects of interlaminar stress analysis at free edges of composite laminate," *Computers Structure* , Vol. 29, pp. 171-186, 1992

[96] Bar Yoseph, P. and Avrashi, G."Interlaminar stress analysis of laminated plates containing a curvilinear hole," *Computers Structure* , Vol. 21, pp. 917-932, 1985

[97] Pan, E., Yang, B., Cai, G. and Yuan, F. G."Stress analysis around holes in composite laminates using boundary element method," *Engineering Analysis with Boundary Elements* , Vol. 25, pp. 31-40, 2001

[98] Rybivki, E. F., and Hopper, A. T."Analytical investigation of stress concentrations due to holes in fiber reinforced plastci laminated plates: three-dimensional models," *AFML-TR-73-100* , Battlelle, Columbus Labs, 1973

[99] Bert, C. W.,"Research on dynamics of composite sandwich plates," *Shock and Vibration Digets*, Vol. 14, pp. 17-34, 1982

[100] Mohammad, S. Q.,"Recent research advances in the dynamic behavior of shell: 1989-2000, Part 1: Laminated composite shells," *ASME Applied Mechanics Reviews*, Vol. 55(4), pp. 325-350, 2002

[101] Song, S., and Waas, A.,"Effects of shear deformation on buckling and free vibration of laminated composite beams," *Composite Structures*, Vol. 37(1), pp. 33-43, 1997

[102] Lim, S. p. Chen, X. L. and Liu, G. R.,"An element free Galerkin method for free vibration analysis of composite laminates," *Composite Structures*, Vol. 47, pp. 101-127, 2000

[103] Liew, K. M., Huang, Y. Q., and Reddy, J. N.,"Vibration analysis of symmetrically laminated plates based on FSDT using moving least square differential quadrature method," *Computer Methods in Applied Mechanics and Engineering*, Vol. 192, pp. 2203-2222, 2003

[104] Ferreira, A. J. M., and Roque, C. M. C.,"Free vibration analysis of symmetric laminated composite plates by FSDT and radial basis functions," *Computer Methods in Applied Mechanics and Engineering*, Vol. 194, pp. 4265-4278, 2005

[105] Liu, G. R., Dai, K. Y. and Nguyen, T. T.,"A smoothed finite element method for mechanics problems," *Computational Mechanics*, Vol. 39(6), pp. 859-877, 2007

[106] Liu, G. R., Nguyen, T. T., Dai, K. Y. and Lam, K. Y.,"Theoretical aspects of smoothed finite element method (SFEM)," *International Journal for Nimerical Methods in Engineering*, Vol. 71(8), pp. 902-930, 2006

[107] Kapania, R. K. and Raciti, S.,"Recent advances in Analysis of Laminated Beams and Plates, Part II : Vibrations and wave propagation'," *AIAA Journal*, Vol. 27, No. 7, July, 1989

[108] Kapania, R., K. and Raciti, S.,"Recent Advances in Analysis of Laminated Beams and Plates, Part I : Shear effects and Buckling'," *AIAA Journal*, Vol. 27, No. 7, July, 1989

[109] Reddy, J. N.,"Mechanics of Laminated composite plates and shells," *CRC Press*, 2000

[110] Levy, S.,"Square plate with clamped edges under normal pressure producing large deflection," *Tech. Report, National Advisory Committee for Aeronautics*, 1942

[111] Argyris, J., and Tanek, L.,"Linear and geometrically nonlinear bending of isotropic and multilayered composite plates by natural mode method," *Comput. Meth. Appl. Mech Eng*, Vol. 113, 207 - 51, 1994

[112] Reddy, J. N. and Phan, P. H.,"Stability and vibration of isotropic, orthotropic and laminated plates according to a higher order shear deformation theory," *Journal of Sound and Vibration*, Vol. 89, pp. 157-170, 1985

[113] Ferreira, A. J. M. and Fasshauer, G. E.,"Analysis of natural frequencies of composite plates by RBF-pseudospectral method," *Composite Structures*, Vol. 79(2), pp. 202-210, 2007

[114] Reddy, J. N.,"An introduction to nonlinear finite element analysis," *Oxford University Press*

[115] Khdeir, A. A. and Librescu, L.,"Analysis of symmetric cross-ply elastic plates using a higher-order theory. Part II: buckling and free vibration," *Composite Structures*, Vol. 9, pp. 259-277, 1988

[116] Liew, K. M., "Solving the vibration of thick symmetrric laminates by Reissner/Mindlin plate theory and p-Ritz method," *Journal of Sound and Vibration*, Vol. 198, pp. 343-360, 1996

-